AN ASSESSMENT OF
SEA SURFACE TEMPERATURE IN THE BAY OF BENGAL

Name : Al Jubaer
Exam Roll: 180760
Reg. No : 37846
Session : 2013-14

MASTER OF SCIENCE IN GEOGRAPHY AND ENVIRONMENT



DEPARTMENT OF GEOGRAPHY AND ENVIRONMENT
JAHANGIRNAGAR UNIVERSITY

December, 2019

AN ASSESSMENT OF
SEA SURFACE TEMPERATURE IN THE BAY OF BENGAL

Dissertation submitted to the Department of Geography and Environment, Under the Faculty Social sciences, Jahangirnagar University, Savar, Dhaka, in partial fulfillment of the requirements for the Masters of Science Degree

By

Name : Al Jubaer
Exam Roll : 140918
Reg. No : 37846
Session : 2013-14



DEPARTMENT OF GEOGRAPHY AND ENVIRONMENT
JAHANGIRNAGAR UNIVERSITY

December, 2019

CERTIFICATE OF APPROVAL

I am very pleased to approve the report title**"Assessment of Sea Surface Temperature"** by Al Jubaer to be submitted to the Department of Geography & Environment, Faculty of Social Sciences, Jahangirnagar University, in partial to the fulfillment of the Degree of Master of Science.

Supervisor,

.....

Dr. Sheikh Tawhidul Islam
Professor
Department of Geography and Environment
Jahangirnagar University
Savar, Dhaka-1342

DECLARATION

I hereby certify that the research work presented in this report has been completely performed by me and this work or any part of it has not been submitted elsewhere for any other purposes except for publication.

December 2019 **Al Jubaer**

Copyright © 2019

The copyright of this dissertation rests with the author. No quotation from it should be published without the author's prior written consent and information derived from it should be acknowledged.

DEDICATIONS

This report is dedicated to my parents. Their uninterrupted inspiration, support, guidance made this effort possible.

TABLE OF CONTENTS

TITLE	PAGE NO.
Declaration	v
Dedication	vi
Table of Content	viii
List of Table	ix
List of Figure	x
List of Photograph	xi
List of Abbreviation	xii
Acknowledgement	xiii
Abstract	xiv

SL	TITLE	PAGE
CHAPTER 1 : INTRODUCTION		
1.1	Introduction	1
1.2	Aim of the Research	2
1.3	Objective of the Research	2
1.4	Scope of the Research	3
1.5	Gape and Limitation of the Research	3
1.6	Organization of the Research	4
1.7	Conclusion	4
CHAPTER 2 : LITERATURE REVIEW		
2.1	Introduction	5
2.2	Literature Review	5
2.3	Remote Sensing	6
2.4	Satellite and Sensor	7
2.5	Space borne remote sensing	10
2.6	Electromagnetic spectrum (EMS)	11
2.7	Daytime SST Algorithms	13
2.8	Nighttime SST Algorithms	13
2.9	Sea Surface Temperature	14
2.10	Applications of SST	15
2.11	Special Variation	15
2.12	Temporal Variation	15
2.13	Conclusion	16

SL	TITLE	PAGE
CHAPTER 3 : STUDY AREA		
3.1	Introduction	17
3.2	Physical Features	19
3.3	Economic Aspects	21
3.8	Conclusion	23
CHAPTER 4 : DATA SOURCES AND METHODS		
4.1	Introduction	25
4.2	Data Sources	25
4.3	Methodology of the Study	26
4.4	Collection of Published Data	28
4.5	Scanning and Digitization	29
4.6	Data analysis	29
4.7	Data	30
4.8	Data on sea surface temperature	31
4.9	Ocean colour data	31
4.10	Temporal variability analysis	32
4.11	Singular spectrum analysis (SSA):	32
4.12	Data source	32
4.13	Data mapping and visualization	33
4.14	Conclusion	34
CHAPTER 5 : THE SPACE BORNE SATELLITE SENSORS AS TEMPERATURE DATA SOURCES FOR THE STUDY AND SST CALCULATION ASSESSMENT ALGORITHM		
5.1	Introduction	35
5.2	Remote Sensing	36
5.3	Remote Sensors	36
5.4	Development in Space borne remote sensing	40
5.5	Characteristics of materials in electromagnetic spectrum (EMS)	42
5.6	Electromagnetic spectrum	45
5.7	Objects and spectrum	46
5.8	Space borne sensors	46
5.9	Optical imaging sensors	47
5.10	Thermal IR imaging sensors	48
5.11	Radar imaging sensors	49
5.12	Non-imaging sensors	51
5.13	Commonly used remote sensing satellites	54
5.14	Types of Ocean Satellite and their Sensor	56
5.15	Ocean Satellite and Sensor	57
5.16	Ocean Microwave Satellite Sensor	59
5.17	18 Ocean Optical Satellite Sensor	60

SL	TITLE	PAGE
5.18	Ocean Sensor, Mission, Band, Swatch Area and their resolution.	61
5.19	Sea Surface Temperature Measurement Algorithm	62
5.20	AVHRR SST Algorithms	63
5.21	Fittest Algorithm	66
5.22	Conclusion	68
CHAPTER 6 : THE SPATIAL AND TEMPORAL DISTRIBUTION OF SEA SURFACE TEMPERATURE DURING LAST 20 YEARS IN THE BAY OF BENGAL.		
6.1	Introduction	69
6.2	Temporal distribution of SST	69
6.3	Sea Surface Temperature and Tropical Cyclone Intensity	89
6.4	Bay of Bengal Cyclone Track from 2006 to 2018	90
6.5	Conclusion	91
CHAPTER 7 : CONCLUSION, REFERENCE & APPENDIX		
7.1	Conclusion	92
7.2	Reference	93

LIST OF TABLE

TITLE	PAGE
Table 4.1 Research Methods	23
Table 5.1 Evolution and advancement in remote sensing satellites and sensors.	41
Table 5.3 Satellite optical imaging systems.	47
Table 5.5 Thermal IR sensors.	48
Table 5.6. Commonly used frequency and spectrum bands of radar imaging sensors	49
Table 5.7 Non-imaging sensors.	50
Table 5.8 Typical laser sources.	52
Table 5.9. Commonly used laser wavelength.	53
Table 5.10 Remote sensing satellites.	55
Table 5.11 Ocean satellites and Sensors.	58
Table 5.12 List of ocean satellites, Sensors, Band, Mission, Swatch, Resolution	61
Table: 5.13 Day time MC SST Split Algorithm data	62
Table: 5.14 Night time MC SST Split Algorithm data	63
Table: 5.15 Day time MC SST Dual Algorithm data	64
Table 6.1 BoB Pre-monsoon Average Minimum Temperature	71
Table 6.2: BoB Pre-monsoon Average Maximum Temperature	72
Table 6.3: BoB Monsoon Average Minimum Temperature	73
Table 6.4: BoB Monsoon Average Maximum Temperature	74
Figure 6.4: BoB Monsoon Average Maximum Temperature	75
Table 6.5: Post-monsoon Average Minimum Temperature	76
Table 6.6 Post-monsoon Average Maximum Temperature	77
Table 6.7: Winter Average Minimum Temperature	78
Table 6.8: Winter Average Maximum Temperature	79
Table 6.9: Bay of Bengal region and season wise average Min and Max temperature variation	80
Table 6.11: Seasonal Average temperature variation from 1999 to 2018	82
Table 6.12: Bay of Bengal Cyclone track, data, season, temperature, region, intensity and Levels.	90

LIST OF FIGURES

TITLE	PAGE
Figure 2.1 The electromagnetic spectrum.	12
Figure 4.1 : AVHRR Temperature Data	31
Figure 5.1 Active and Passive Sensor.	37
Figure 5.2 The electromagnetic spectrum.	44
Figure 5.3 Transmission spectrum of soda-lime glass with a 2-mm thickness	45
Figure 5.4 Examples of reflective materials. Image referenced from Wikimedia.	46
5.5 Space borne remote sensing sensors.	47
Figure 5.6 Types of Ocean Satellite and their Sensor	48
Figure 5.7 Ocean Sensor Applications	50
Figure 5.8 Types of Ocean Microwave Sensor	53
Figure 5.9 Types of Ocean Satellite Sensor	55
Figure 5.10 SST Algorithm Model.	59
Figure 6.1 BoB Pre-monsoon Average Minimum Temperature	72
Figure 6.2: BoB Pre-monsoon Average Maximum Temperature	73
Figure 6.3 BoB Monsoon Average Minimum Temperature	74
Figure 6.4: BoB Monsoon Average Maximum Temperature	75
Figure 6.5: BoB Post monsoon Average Minimum Temperature	76
Figure 6.6: Post-monsoon Average Maximum Temperature	77
Figure 6.7: Winter Average Minimum Temperature	78
Figure 6.8: Winter Average Maximum Temperature	79

Figure 6.9: Bay of Bengal region and season wise average Min and Max temperature variation	80
Figure 6.10: Bay of Bengal average Min and Max temperature from 1999 to 2018	81
Figure 6.11: Seasonal Min and Max temperature from 1999 to 2018	82
Figure 6.12: Seasonal Average temperature variation from 1999 to 2018	83

LIST OF MAPS

TITLE	PAGE
Map 3.1 Study Area	18
Map 6.1 Bay of Bengal Pre-monsoon Average Temperature from 1999 to 2018	84
Map 6.2 Bay of Bengal Monsoon Average Temperature from 1999 to 2018	85
Map 6.3 Bay of Bengal Post-monsoon Average Temperature from 1999 to 2018	86
Map 6.4 Bay of Bengal Winter Average Temperature from 1999 to 2018	87
Map 6.5 Bay of Bengal Yearly Average Temperature from 1999 to 2018	88
Map 6.6: Bay of Bengal Cyclone Location	90
Map 6.7: Bay of Bengal Cyclone Track from 2006 to 2018	83

LIST OF ABBREVIATIONS

SST : Sea Surface Temperature
AVHRR : Advanced Very High Resolution Radiometry
TM : Thematic Mapper
MSS : Multi-spectral scanner
MODIS : Moderate Resolution Imaging Spectroradiometer
IRS : Indian Remote Sensing Satellite
SPOT : Systeme Probatoire D'Observation De La Terre (France)
LIDAR : Laser Image Detection and Ranging
SAR : Synthetic Aperture Radar
UHF : ultra high frequency
BIL : band interleaved by line
BIP : band interleaved by pixel
BSQ : band sequential
BW : black and white
CIR : color infrared
DO(Q)Q : digital orthophoto (quarter) quad
EROS : Earth Resources Observation Systems
EDC : EROS Data Center
FOV : field-of-view
GPS : global positioning system
IFOV : instantaneous field-of-view
NASA : National Aeronautics and Space Administration
NOAA : National Oceanic and Atmospheric Administration
NIMA : national image and mapping agency
NLCD : national land cover data
LCCP : land cover characterization program
NALC : North American Landscape Characterization Project
GAP : National Gap Analysis Program
GSFC : Goddard Space Flight Center
GSTC : Geospatial Service and Technology Center
FAS : Foreign Agricultural service
NRI : national resource inventory
FGDC : federal geographic data committee
NRCS – : national resources conservation service (a USDI agency)
NAWQA :National Water Quality Assessment Program (a USGS program)
C-CAP : coastal change analysis program

ACKNOWLEDGEMENTS

At first, all praises belong to the almighty Allah, the most merciful, the most beneficent to man and his actions.

I feel very pleased to complete the study on **"An Assessment of SEA SURFACE TEMPERATURE IN THE BAY OF BENGAL"** Assessing the SST which is located in BAY OF BENGAL" for the degree of Bachelor of Science. This research work could not have been completed without the encouragement, suggestions and assistance I received from many people at different stages of this work. It gives me great pleasure to make this opportunity to show gratitude and thank them.

The author wishes to express sincere gratitude to his supervisor, Dr. Sheikh Tawhidul Islam, Professor,Department of Geography and Environment, Director, Institute of Remote Sensing and GIS (IRS), Jahangirnagar University, for his constant guidance, invaluable suggestions and advice, encouragement, sympathetic co-operation, generous help, persistent stimulating discussion and strong support towards the successful completion of the study at all stages of this research work. Without his affectionate guidance and valuable suggestions, it would have been impossible to carry out this study..

My great gratitude Mr. Md. Munir Mahmud and Krishna Proshad Mondal for their extraordinary support, Guidance and technical suggestion for my report perspectives.

I would like to thank to Mostak Arman Sakif, Hiru Mia and Saumic Samad for their support and nice cooperation during the time of my research.

I would feel debt free if this research could play meaningful role for the betterment of the helpless students of the study area.

ABSTRACT

The study was conducted to examine temporal and spatial variability of Sea Surface Temperature (SST) of the Bay of Bengal (BoB). Analysis of mean maximum and mean minimum temperatures was carried out on seasonal time-scales for examining the data from ten regions in the Bay of Bengal (BoB) for the period 1999 to 2018. The values of seasonal SST anomaly over this regions of the Bay of Bengal (BoB) are computed for the four meteorological seasons like, Pre-monsoon (March - May), Monsoon (June-September), Post-monsoon (October - November) and winter (December - February). ArcGIS & Erdas Imagine were used to produce maps for visualizing the spatial distribution SST. Annual mean minimum temperatures were found almost similar to the North Bay for all seasons within the period of 1999 to 2008 except in winter and mean maximum temperatures showed an increasing trend from the period of 2010 to 2015 in the North Bay except in the South Andaman in 2013. This showed a decreasing trend than other years. The spatial distribution of Sea surface temperature for all season shows increment of temperature overtime and maximum temperature was observed in the South Andaman which is about 30.5'C during pre-monsoon period in 2015.

CHAPTER ONE
INTRODUCTION

1.1 Introduction

Sea surface temperature (SST) may be a crucial variable for understanding, observing and anticipating fluxes of warm, energy and gasses at a assortment of scales that decide complex intelligent between the air and ocean. SST at the ocean atmosphere interface includes a critical societal affect, through, expansive sea gyres and climatic circulation cells impacting climate and climate, climate frameworks and serious storms and neighborhood scale marvels, such as the era of ocean breezes and convective clouds.

Mapping SST is now the responsibility of operational monitoring and forecasting agencies as accurate knowledge of global SST distribution and temporal variation is a key input to forecasting and prediction systems. SST fields constrain upper-ocean circulation and thermal structure on daily, seasonal, decadal and climatic timescales, for the exchange of energy between the ocean and atmosphere in coupled ocean-atmosphere models, and as boundary conditions for ocean, weather and seasonal forecasting models. Other applications include maritime safety, military operations, ecosystem assessment, supporting fisheries and tourism, transport and energy, human health, food security and environmental policy. Well-defined and error-quantified measurements of SST are also required in the form of climate data records to reveal the role of the ocean in short and long term climate variability.

A sustained operational stream of satellite SST measurements has been available since 1981, which together with in situ measurements collectively form the modern-era SST observing system. By 1998, SST data were a mature component of the observing system with demonstrated capability and data products. However, SST product availability was limited to a few data sets that were large, scientific in format and

difficult to exchange in near real time (NRT). Furthermore, product accuracy was insufficient for the emerging ocean modeling and data assimilation communities, while at the same time the number of applications requiring accurate spatial high-resolution SST was growing.

To address these issues, the Global Ocean Data Assimilation Experiment defined a minimum data specification for use in operational ocean models, requiring SST observations with global coverage, a spatial resolution of 10 km or higher, an accuracy of 0.2°C or better, and updated every 6h. The establishment of the Group for High Resolution Sea Surface Temperature, GHRSST (previously, GODAE High-Resolution Sea Surface Temperature Pilot Project) addressed these specifications. GHRSST is a self-organizing group of researchers and operational practitioners working together to improve the accuracy and availability of SST fields for all applications.

1.3 Aim of the Research

The aim of this research is to understand the characteristics (Pattern, Anomaly, Change) of sea surface temperature of Bay of Bengal.

1.4 The objectives of the research

- To identify the space borne satellite sensors as temperature data sources for the study and SST calculation assessment algorithm.
- To investigate the spatial and temporal distribution of sea surface temperature during last 20 years in the Bay of Bengal.

1.5 Scope of the Research

This research is prepared to highlight the pixel base SST database of newly Temperature change of Bay of Bengal.

This research may consider as essential for the policy maker to study on plot level and the methodology to be used in this research as state of the art like Arc GIS and remote sensing in conducting to achieve the specific objectives is innovative and dependable. Taking into consideration the above point of view this research work is very significant to carry out in assessing the scenario of the recently exchange heat and energy of sea surface in Bay of Bengal.

Google Earth platform and GIS (Geographic Information System) approaches have been used to analysis the erosion and accretion scenario of the study area.

1.6 Gaps and Limitations of the Research

1. Spatial Resolution are very low (Highest resolution is 10 km and Lowest Temperature is 45 km)
2. Temporal Resolution (Capturing data from 1978 but Resolution are very low)
3. Lacking's of Accuracy Assessment (User and Producer)
4. Field Data/Ground Data are not Available (Regional data are available)
5. Analysis data totally depend on secondary database

1.7 Organization of the research

This report is arranged in Eight different chapters with a number of sections and sub-sections, bibliography and appendix that's follow the chronological development of the study.

Chapter one gives an introductory description of the background, justification of the research, aim & objectives of the research, and the Organization of the research.

Chapter Two Literature Review

Chapter Three Data Sources and Methods

Chapter Four Study area

Chapter five Identify the space borne satellite sensors as temperature data sources for the study and SST calculation assessment algorithm.

Chapter six Investigate the spatial and temporal distribution of sea surface temperature during last 20 years in the Bay of Bengal.

Chapter Seven Conclusion and Reference

1.8 Conclusion

A well interpreted SST can be utilized to detect the surface temperature signature for forecasting cyclones. In general, cooling of SST is observed after the passing of a cyclone primarily as a result of surface heat losses. Using long-term observational data records and extensive experimentation with numerical models of various degrees of sophistication, and the complex interactions between the atmosphere and ocean in different geographical settings are now gradually unraveling. Therefore, SST anomaly may be useful in determining local as well as global weather conditions. But to forecast the effects and projections based on this criterion, it needs skilled interpretations and authentic data sources. A single study is not enough to understand such implications. So, further and continuous investigations in this very science are required.

CHAPTER TWO
LITERATURE REVIEW

2.1 Introduction

A literature review is an evaluative report of studies found in the literature related to the selected area. The review should describe, summarize, evaluate and clarify this literature. It should give a theoretical basis for the research and help to determine the nature of researchers own research. It is very essential part of research which helps to find out the relevant information regarding the research work. An extensive literature review is carried out to get the basic understanding and to acquire knowledge on Bay of Bengal Sea Surface Temperature system of a modern, efficient and sustainable ocean system as whole and basic elements of ocean environmental component[1].

Finally, in this chapter, a summary of former research works on Bay of Bengal Sea Surface Temperature variation from 1999 to 2018 and SST sensor use for SST measurement conducted in home and abroad are also discussed with relevant research approach and their findings and discussion on those works[2]. A brief review of historical and present development plans for Dhaka, urban planning legislations and policies in Bangladesh are also provided.

2.2 Literature Review

Literature is a body of text that aims to review the critical points of current knowledge on particular topics. Literature review means the directions of a new work which help to acquire the right result of a research[4].

A literature review goes beyond the search for information and includes the identification and articulation of relationships between the literature and field of research. While the form of the literature review may vary with different types of studies, the basic purposes remain constant

- Provide a background for the research
- Justify the research
- Ensure the individuality of the research
- Show where the research fits into the existing body of knowledge
    - Enable the researcher to learn from previous theory on the issue
    - Outline gaps in previous research
    - Show that the work is adding new to the understanding and knowledge of the field
    - Help refine, refocus or even change the topic

2.3 Remote Sensing

Remote sensing is the science or art of acquiring information about the Earth's surface and Sea Surface without actually being in contact with it. This is done by sensing and recording reflected or emitted energy and processing, analyzing, and applying that information. In much of remote sensing, the process involves an interaction between incident radiation and the targets of interest[10]. Remote sensing makes it possible to collect data on dangerous or inaccessible areas. Remote sensing applications include monitoring ocean in areas such as the land feature, Sea surface in world different regions, and depth sounding of coastal and ocean depths. Remote sensing also replaces costly and slow data collection on the ground, ensuring in the process that areas or objects are not disturbed. Remote sensing exceedingly influences everyday life, ranging from weather forecasts to reports on climate change or natural disasters. As an example, 80% of the German students use the services of Google Earth. (Wikipedia, 2012)

In recent time, with man's increasing interventions with the environment, the situation is aggravated. The quality of available data is extremely uneven. ocean planning based on unreliable data can lead to costly and gross errors.. Global extrapolation on the basis of few data collected by diverse and non-standardized methods can lead to gross errors and it can also lead to costly mistakes and misjudgments on critical policy issues. So, remote sensing provides convenient solution for this problem. Moreover, voluminous data gathered with the help of

remote sensing techniques are batter handled and utilized with the help of Geographical Information System (GIS) [3].

There are two different approaches that can be adopted for determining the characteristics of cyclone track from remote sensing data. The first approach determines more 'qualitative' characteristics such as number, distribution, type and character of ocean particle[13]. This can be achieved with either satellite or air borne imagery collected in the visible and infrared regions of the spectrum. The next approach complements the qualitative characterization, estimating dimensions (e.g. length, width, thickness and local slope, motion, and debris distribution) along and across the dust movement.

2.4 Satellite Sensor

Since the early days of satellite environmental remote sensing, efforts have been made to measure sea surface temperature (SST) from space with scientifically useful accuracy. The synoptic view from space allows SST to be mapped globally, including regions where ships and in situ measuring devices are sparse or nonexistent. Furthermore, satellites can provide frequent coverage, enabling the motions of current eddies and meanders to be studied in detail. During the past decade much progress has been made in satellite measurement of SST[14]. The satellite instruments and SST retrieval algorithms have improved considerably, scientific applications and requirements are much better understood, and the potential benefits of satellite observations are becoming widely recognized.

The physical basis for measurement of SST from space is the detection by a space borne microwave or infrared radiometer of the thermal energy emitted by the ocean surface[15]. The surface radiation is modified in its passage through the atmosphere to the radiometer by processes of atmospheric absorption, emission, and scattering, for which appropriate corrections must be made in order to obtain valid estimates of the surface radiance. The corrected radiances must be converted to surface temperature, which requires knowledge or measurement of the surface emissivity and corrections for reflected solar and atmospheric radiation. Infrared and microwave techniques provide these measurements and corrections in somewhat

different ways, each with unique advantages and disadvantages. Environmental satellites of the early 1970s carried infrared radiometers designed primarily for meteorological purposes (i.e. cloud imaging and atmospheric sounding), but which also included channels in spectral regions of low atmospheric absorption that could be used to observe the ocean surface and hence determine SST[17]. Beginning in late 1981 with the launch of the five-channel AVHRR instrument on the NOAA polar-orbiting satellites, an improved operational sea surface temperature product became available using a multichannel retrieval approach[17]. This multichannel SST (MCSST) product incorporated an improved atmospheric correction algorithm and cloud filtering procedure, and superseded the former less accurate GOSSTCOMP (Global Operational SST Computation) product that had been produced routinely by NOAA. These and other NOAA SST products were directed primarily towards meeting the needs of NOAA's operational users[18].

Following the launch of the NASA Seasat and Nimbus-7 satellites, and the NOAA Tiros-N generation of satellites, in late 1978, a number of other satellite instruments and retrieval methods were evaluated for research-oriented applications of SST. These instruments including the Scanning Multichannel Microwave Radiometer (SMMR) on the Seasat and Nimbus-7 satellites the High-resolution Infra-Red Sounder and Microwave Sounding Unit (HIRS/MSU) on the Tiros-N and NOAA satellites; and the Visible-Infrared Spin Scan Radiometer (VISSR) Atmospheric Sounder (VAS) on the NOAA GOES series of geostationary satellites[19]. Studies have shown that these instruments are capable of measuring SST to an rms accuracy of approximately 1°C and perhaps significantly better in some cases. Summary characteristics of these sensors are provided in Table 1.

In 2015, one of the most remarkable events in the space industry was when SpaceX realized the reusability of its rocket for the first time. Additionally, in June 2014, Russia used 1 rocket to launch 37 satellites at the same time[20]. At present, many countries have the capability to launch multiple satellites in one mission. For example, NASA and the US Air Force launched 29 satellites in a single mission in 2013. At that time, the mission represented the most satellites ever launched at one time [1]. In 2015 and 2016, China and India launched 20 satellites in single mission,

respectively. At present, six organizations have the capability to launch multiple satellites in a single mission: Russia, USA, China, India, Japan, and ESA [21]. This trend indicates that in the future, the cost of sending satellites to space will greatly decrease. More and more remote sensing resources are becoming available.

It is of great importance to have a comprehensive survey of the available remote sensing technology and to utilize inter- or trans-disciplinary knowledge and technology to create new applications.

Remote sensing is considered a primary means of acquiring spatial data. Remote sensing measures electromagnetic radiation that interacts with the atmosphere and objects. Interactions of electromagnetic radiation with the surface of the Earth can provide information not only on the distance between the sensor and the object but also on the direction, intensity, wavelength, and polarization of the electromagnetic radiation. These measurements can offer positional information about the objects and clues as to the characteristics of the surface materials[22].

Satellite remote sensing consists of one or multiple remote sensing instruments located on a satellite or satellite constellation collecting information about an object or phenomenon on the Earth surface without being in direct physical contact with the object or phenomenon. Compared to airborne and terrestrial platforms, space borne platforms are the most stable carrier. Satellites can be classified by their orbital geometry and timing[23]. Three types of orbits are typically used in remote sensing satellites, such as geostationary, equatorial, and sun-synchronous orbits. A geostationary satellite has a period of rotation equal to that of Earth (24 hours) so the satellite always stays over the same location on Earth.

Communications and weather satellites often use geostationary orbits with many of them located over the equator[24]. In an equatorial orbit, a satellite circles the Earth at a low inclination (the angle between the orbital plane and the equatorial plane). The Space Shuttle uses an equatorial orbit with an inclination of 57°. Sun-synchronous satellites have orbits with high inclination angles, passing nearly over the poles. Orbits are timed so that the satellite always passes over the equator at the same local sun time. In this way, these satellites maintain the same relative position with

the sun for all of its orbits[25]. Many remote sensing satellites are sun synchronous, which ensures repeatable sun illumination conditions during specific seasons. Because a sun-synchronous orbit does not pass directly over the poles, it is not always possible to acquire data for the extreme polar regions[26].

The frequency at which a satellite sensor can acquire data of the entire Earth depends on the sensor and orbital characteristics. For most remote sensing satellites, the total coverage frequency ranges from twice a day to once every 16 days. Another orbital characteristic is altitude[26]. The space shuttle has a low orbital altitude of 300 km, whereas other common remote sensing satellites typically maintain higher orbits ranging from 600 to 1000 km.

2.5 Space borne remote sensing

Although the term 'remote sensing' was introduced in 1960. However, in practice, remote sensing has a long history. In the 1600s, Galileo used optical enhancements to survey celestial bodies [10]. An early exploration of prisms was conducted by Sir Isaac Newton in 1666. Newton discovered that a prism dispersed light into a spectrum of red, orange, yellow, green, blue, indigo, and violet and recombined the spectrum into white light[27]. One hundred years later, in 1800, Sir William Herschel explored the thermal infrared electromagnetic radiation for the first time in the world. Herschel measured the temperature of light that had been split with a prism into the spectrum of visible colors.

In the following decades, some attempts were made with aerial photographs using cameras attached to balloons. However, the results were not satisfactory until 1858, when Gasper Felix Tourna chon took the first aerial photograph successfully from a captive balloon from an altitude of 1200 feet over Paris. Later, in 1889 in Labru guiere, France, Arthur Batut attached a camera and an altimeter to kites for the first time so that the image scale could be determined[28]. Therefore, he is considered to be the father of kite aerial photography.

Then, at the beginning of the twentieth century, the camera was able to be miniaturized so that it was easily carried by pigeons. The Bavarian Pigeon Corps took the first aerial photos using a camera attached to a pigeon in 1903. During the First

World War, the use of aerial photography grew. Later, in 1936, Albert W. Stevens took the first photograph of the actual curvature of the earth from a free balloon at an altitude of 72,000 feet[29].

2.6 Electromagnetic spectrum

Figure 2.1 contains the EMS range from gamma rays to radio waves. In remote sensing, typical applications include the visible light (380–780 nm), infrared (780 nm–0.1 mm), and microwave (0.1 mm–1 m) ranges. This paper treats the terahertz (0.1–1 mm) range as an independent spectral band separate from microwaves. Remote sensing sensors interact with objects remotely[30]. Between sensors and the earth surface, there is atmosphere. It is estimated that only 67% of sunlight directly heats the Earth. The remainder of the light is absorbed and reflected by the atmosphere. The Earth's atmosphere strongly absorbs infrared and UV radiation.

In visible light, typical remote sensing applications include the blue (450–495 nm), green (495–570 nm), and red (620–750 nm) spectral bands for panchromatic or multispectral or hyperspectral imaging. Current bathymetric and ice LIDAR generally uses green light (e.g., NASA's HSRL-1 LIDAR, with a spectrum of 532 nm) [31]. However, new experiments have shown that in the blue spectrum, such as at 440 nm, the absorption coefficient for water is approximately an order of magnitude smaller than at 532 nm, and 420–460 nm light can penetrate relatively clear water and ice much deeper, offering substantial improvements in sensing through water for the same optical power output, thus reducing power requirements.

The red spectrum together with near-infrared (NIR) is typically used for vegetation applications. For example, the Normalized Difference Vegetation Index (NDVI) is used to evaluate targets that may or may not contain live green vegetation. Infrared is invisible radiant energy. Usually, infrared is divided into different regions: near IR (NIR, 0.75–1.4 μm), shortwave IR (SWIR, 1.4–3 μm), mid-IR (MIR, 3–8 μm), longwave IR (LWIR, 8–15 μm), and far IR (FIR, 15–1000 μm). Alternatively, according to the ISO 20473 scheme, another division is proposed as NIR (0.78–3 μm), MIR (3–50 μm), and FIR (50–1000 μm).

Most of the infrared radiation in sunlight is in the NIR range. Most of the thermal radiation emitted by objects near room temperature is infrared [14]. In nature, on the surface of the Earth, almost all thermal radiation consists of infrared in the mid-infrared region, which is a much longer wavelength than that in sunlight[32]. Of these natural thermal radiation processes, only lightning and natural fires are hot enough to produce much visible energy, and fires produce far more infrared than visible light energy. NIR is mainly used in medical imaging and physiological diagnostics. One typical application of MIR and FIR is thermal imaging, for example, night vision devices. In the MIR and FIR spectrum bands, water shows high absorption, and biological systems are highly transmissive[33].

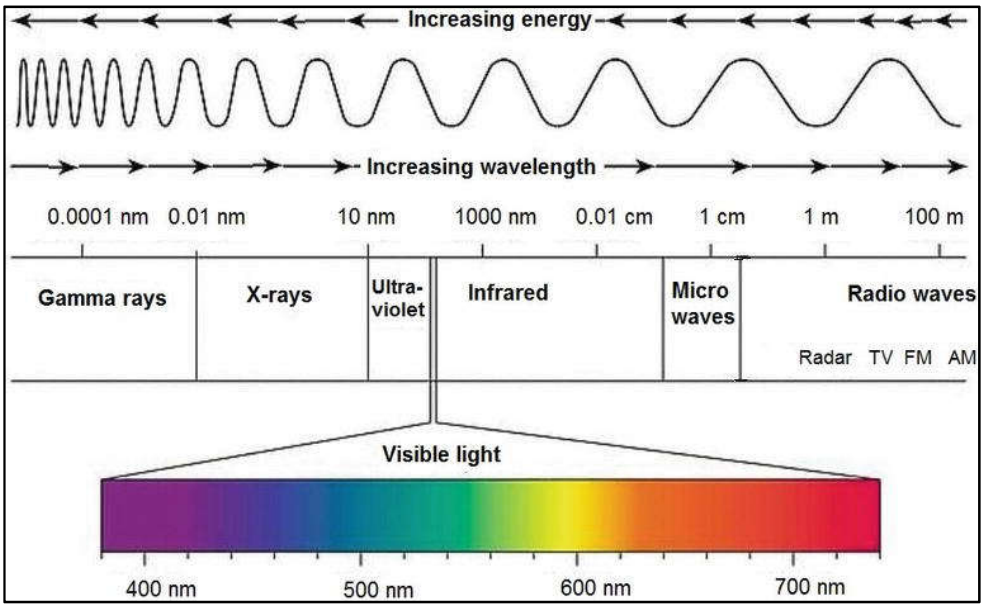


Figure 2.1 The electromagnetic spectrum. Image from UC Davis ChemWiki, CC-BY-NC-SA 3.0.

With regard to the terahertz spectrum band, terahertz frequencies are useful for investigating biological molecules. Unlike more commonly used forms of radiated energy, this range has rarely been studied, partly because no one knew how to make these frequencies bright enough and because practical applications have been impeded by the fact that ambient moisture interferes with wave transmission[34]. Nevertheless, terahertz light (also called T-rays) has remarkable properties. T-rays are safe, non-ionizing electromagnetic radiation. This light poses little or no health threat and can pass through clothing, paper, cardboard, wood, masonry, plastic, and ceramics. This light can also penetrate fog and clouds [35]. THz radiation transmits

through almost anything except for not metal and liquid (e.g., water). T-rays can be used to reveal explosives or other dangerous substances in packaging, corrugated cardboard, clothing, shoes, backpacks, and book bags. However, the technique cannot detect materials that might be concealed in body cavities.

2.7 Daytime SST Algorithm

The matchups of VIIRS BTs and in situ SST acquired from 15 April 2012 to 14 February 2013 (MDS 1) were used to calculate regression coefficients and LUTs of B and σ for all tested algorithms.

Table 2 shows average biases and SDs of TS T i for daytime algorithms arranged in the order of increasing SDs. The SD for NRL SST is much smaller than for other algorithms. This is the result of using TS0 as a regressor in equation (9). Recall that TS0 is obtained by blending satellite retrievals with in situ data and therefore may fit TSi more closely than satellite retrievals alone[38]. As a result, the NRL SST best coincides with in situ SST, but this is achieved at the expense of least sensitivity to true SST, as shown later in this section.

Out of all other algorithms, the lowest SD is produced by the OSI-SAF followed by the LATBAND and Pathfinder. The NAVO algorithm, whose equation (7) includes an adjustable offset at TS0, slightly outperforms ACSPO which exploits the standard NLSST equation (2) with first-guess SST in Celsius. The largest SD is delivered by the IDPS algorithm whose equation is similar to equations ((3a)–(3e)) but uses TS0 in kelvin rather than in Celsius[39].

2.8 Nighttime SST Algorithms

A procedure similar to the one described in the previous section was applied to the evaluation of nighttime algorithms, Omitting the intermediate steps for brevity, we present the main results of this analysis. Table 4 shows the overall statistics of T T i averaged over the 10 month MDS1. The algorithms are arranged in the order of decreasing SD. The smallest SDs are delivered by the OSI-SAF algorithm (5), which explicitly introduces the dependencies of regression coefficients on VZA, and by the LATBAND, which stratifies the coefficients of

equation (4) into latitudinal bands and months. The largest SD corresponds to the Pathfinder algorithm[35].

Interestingly, Pathfinder nighttime SD (0.54 K) is higher than daytime SD (0.48 K, according to Table 2). This fact has the following explanation. The matchups for the MDS used for algorithm evaluation were selected with the ACSPO Clear-Sky Mask, which is largely based on the analysis of retrieved SST. The nighttime ACSPO equation (1) exploits three bands at 3.7, 11, and 12 μm, and, therefore, is less sensitive to variations in TPW and vertical profiles of water vapor than the Pathfinder, which uses only two bands at 11 and 12 μm during both day and night. Consequently, the nighttime VIIRS MDS includes matchups, which would have been rejected during the daytime, when the ACSPO uses the NLSST algorithm.

This causes the increase of SD for the nighttime Pathfinder algorithm ((3a)–(3e)). This also confirms a known fact that at night, three-band algorithms are more efficient than split-window algorithms [e.g., Brisson et al., 1998]. Another observation from Table 4 is that three-band algorithms that use T3.7 as a standalone regressor (OSI-SAF, ACSPO) are more precise than the algorithms that use T3.7 only in the BT difference, ΔT3.7-12 (NAVO, IDPS). The LATBAND algorithm, which uses the same equation (4) as NAVO and IDPS algorithms, improves SD by using separate sets of coefficients for different latitudinal bands[39].

2.9 Sea Surface Temperature

Sea surface temperature (SST) is an important water environment parameter. It not only plays a vital role in aquatic ecosystems but also has a significant impact on the biogeochemical cycle process. Water is the carrier in aquatic ecosystems; thus, SST can greatly affect the reproduction of aquatic organisms and habitat of aquatic life[40]. In addition, observations of biological diversity under different SSTs have important reference value for the fishery industry. The spatial–temporal variation of SST is also a crucial factor for navigation and marine survey[41]. In general, SST variation is controlled by natural factors, such as seasons, ocean currents, and water depths.

However, water bodies suffer from the influence of rapid urbanization and industrialization. Human activities, such as industrial emissions and urban coastal construction, deeply alter SST in nearby areas, thereby affecting the aquatic ecological environment[41]. Therefore, the spatial temporal dynamics and short-term rapid change of SST caused by human pollution discharge and hydrological processes must be monitored using appropriate technology.

2.10 Applications of SST

Satellite derived SST products are used in applications encompassing a wide range of temporal (diurnal to decadal) and spatial (sub-km to global) scales and are required by many user communities with an interest in ocean processes. Daily global high-resolution (<10 km) products are now easily accessible in support of operational forecast systems[43]. The ability to resolve mesoscale and submesoscale features is facilitating new applications in coastal regions and frontal detection.

A full review of all applications of SST would be a review paper itself. So, in this section we first focus on two of the more established application areas of SST, in support of operational forecast systems and understanding changes to the Earth's climate over time. Then, we look at three evolving user-driven application areas, which are driving much of the required SST research and development activities for the next 10 years and where SST will play an increasingly more important role[44].

2.11 Special Variation

Spatial variability occurs when a quantity that is measured at different spatial locations exhibits values that differ across the locations. Spatial variability can be assessed using spatial descriptive statistics such as the range.

2.12 Temporal Variation

Temporal variations in nitrate concentrations in groundwater and springs reflect the interrelation of several important hydrogeologic, geochemical, land use, and climatic factors. The degree of temporal variation is related to the degree of karstification, mantle thickness, and the proportion of conduit to diffuse flow. For example, nitrate concentrations in groundwater generally increase following seasonal applications

of fertilizers and subsequent recharge of the groundwater system[44]. Large fluctuations in nitrate concentrations in springs have been observed during high discharge events related to annual variations in rainfall.

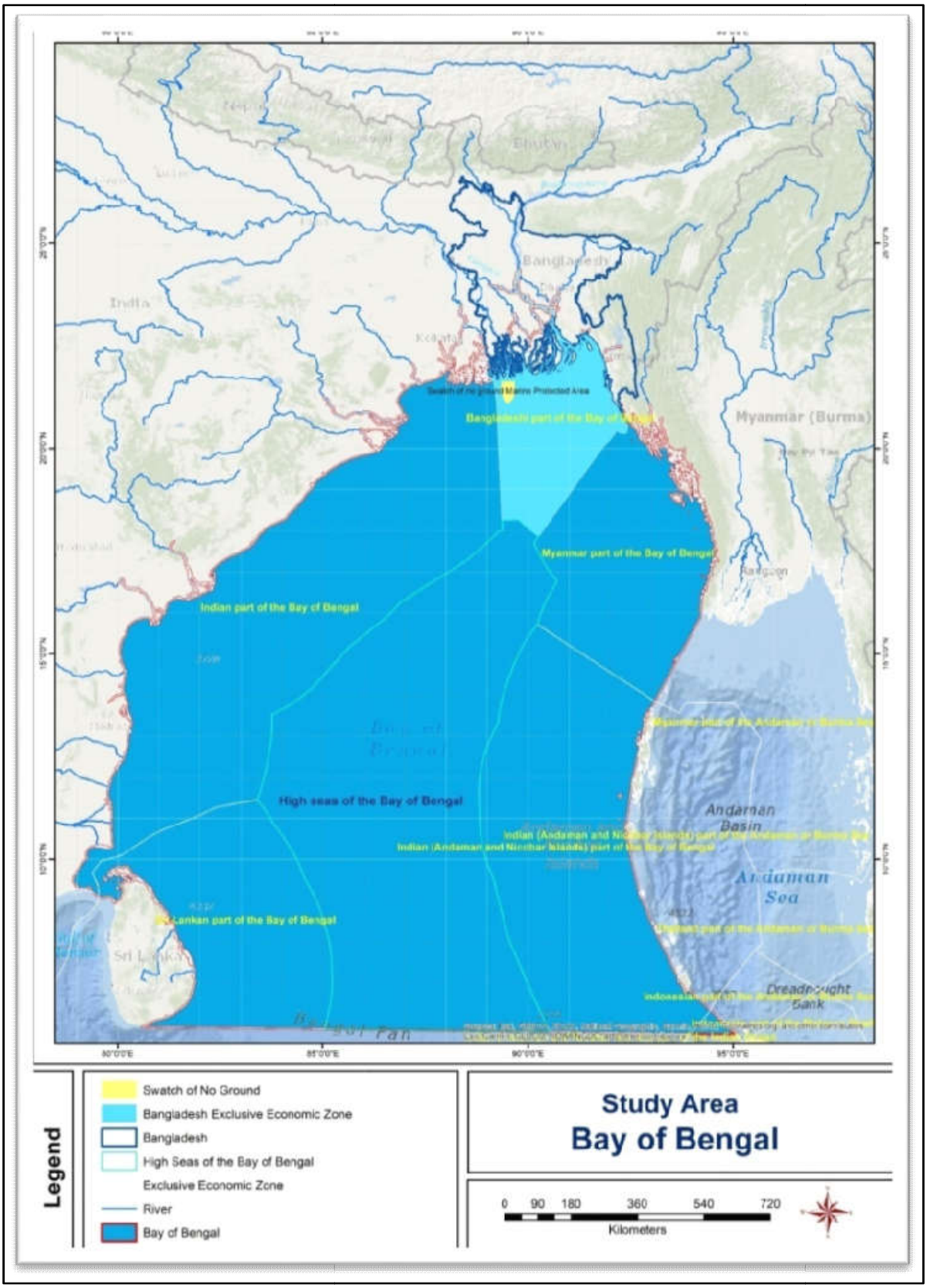
2.13 Conclusion

It overviews the current SST observing systems, describes progress and challenges over the past decade and into the next, and overviews the forward-looking vision over the next decade and beyond. User requirements for SST products in the next decade need a complementary blend of satellites and in situ measurements. The establishment of a framework for the exchange and management of international SST data has been successfully implemented and is operating on a daily basis coordinated by GHRSST[48]. A thriving user community has developed in which integrated SST data sets are being used at scientific institutions and operational agencies. Tools and data services have been developed and implemented to serve this user community. Through the activities of GHRSST, many lessons have been learned that provide the basis for an optimal configuration for the SST observing system in the next 10 years.

CHAPTR THREE
STUDY AREA

3.1 Introduction

Bay of Bengal, large but relatively shallow embayment of the northeastern Indian Ocean, occupying an area of about 839,000 square miles (2,173,000 square km). It lies roughly between latitudes 5° and 22° N and longitudes 80° and 90° E. It is bordered by Sri Lanka and India to the west, Bangladesh to the north, and Myanmar (Burma) and the northern part of the Malay Peninsula to the east. According to the definition of the International Hydrographic Bureau, the southern boundary extends from Dondra Head at the southern end of Sri Lanka in the west to the northern tip of the Indonesian island of Sumatra in the east. The bay is about 1,000 miles (1,600 km) wide, with an average depth of more than 8,500 feet (2,600 metres). The maximum depth is 15,400 feet (4,694 metres). A number of large rivers the Mahanadi, Godavari, Krishna, and Kaveri (Cauvery) on the west and the Ganges (Ganga) and Brahmaputra on the north flow into the Bay of Bengal. The Andaman and Nicobar groups, which are the only islands, separate the bay from the Andaman Sea.



Map 3.1 Study Area

3.2 Physical Features

3.2.1 Physiography

The Bay of Bengal is bordered to the north by a wide continental shelf that narrows to the south and by slopes of varying gradient on the northwest, north, and northeast, all cut by canyons from the rivers. Most important are the Ganges-Brahmaputra, Andhra, Mahadevan, Krishna, and Godavari canyons. These were former estuaries when the shoreline was at the margin of the continental shelf during the Pleistocene Epoch (about 2,600,000 to 11,700 years ago). The deep floor of the bay is occupied by a vast abyssal (deep-sea) plain that slopes to the south. The main submarine features include the beginning of the long, seismically active Java Trench near the Nicobar-Sumatra mainland and of the aseismic Ninetyeast Ridge. The fan of sediments of the Ganges River is the widest 5 to 7 miles (8 to 11 km) and thickest in the world. The bay itself was formed as the Indian subcontinent collided with Asia within roughly the past 50 million years.

3.2.2 Climate

The climate of the Bay of Bengal is dominated by the monsoons. From November through April a continental high-pressure system north of the bay produces northeast winds (the northeast monsoon) characteristic of the winter season. During the northern summer (June–September) the rain-bearing southwest monsoon prevails, as intense heat produces a low-pressure system over the continent and a subsequent air flow from the ocean.

Cyclones intense tropical storms of high winds and torrential rains occur in spring (April–May) and fall (October–November); these are the weeks preceeding the onset of monsoon rains and the weeks following their retreat. A cyclone in November 1970 in the Ganges River delta resulted in the deaths of an enormous number of people and livestock. A storm of comparable magnitude in April 1991 devastated the eastern shore of Bangladesh, and another powerful cyclone devastated the coastal Indian state

of Orissa in October 1999. Water spouts occur frequently in the bay during the summer months. Facts Matter. Support the truth and unlock all of Britannica's content.Special 30% off Holiday Sale!

3.2.3 Hydrology

A unique feature of the bay is the extreme variability of its physical properties. Temperature in the offshore areas, however, is warm and markedly uniform at all seasons, decreasing somewhat toward the north. Surface densities are considerably greater in spring than in fall, when river discharge is highest. Surface salinity, normally measuring 33 to 34 parts per thousand, can fall to nearly half that level and can extend well south of the bay during the fall. Below the surface layer is an oxygen-poor intermediate layer that has high salinity and undergoes only weak circulation. Weak upwelling occurs in the northeast during the northeast monsoon. The sea presents alternately slick and ruffled surfaces over shallow internal waves all along the east-coast shelf. Surface movements of the waters change direction with the season, the northeast monsoon giving them a clockwise circulation, the southeast monsoon a counterclockwise circulation. Severe storms occur at the change of monsoon, particularly to the south in October.

In addition to water-level changes resulting from waves and tide, the average sea level varies throughout the year. Because rainfall and riverine input exceed evaporation, the bay exhibits a net water gain annually. The bay is also subject to occasional tsunamis; one such event, caused by an undersea earthquake near the Indonesian island of Sumatra in December 2004, devastated extensive coastal areas of the bay, particularly in Sri Lanka and the Andaman and Nicobar Islands.

3.2.4 Bottom deposits

Sediments in the Bay of Bengal are dominated by terrigenous deposits from the rivers, derived mainly from the Indian subcontinent and from the Himalayas. Calcareous clays and oozes are found near the Andaman and Nicobar Islands and atop the Ninetyeast Ridge. The amount of organic matter present in the continental-shelf sediment of the

northern part of the east coast is poor compared with the world's average for nearshore sediments.

3.3 Economic Aspects

3.3.1 Resource exploitation

The Bay of Bengal has a distinct tropical marine ecosystem, and copious river drainage into the northern part of the bay and the profusion of wetlands, marshes, and mangroves increase productivity of nearshore fish species. The exploitation of these resources is carried out by small-scale fisheries; commercial fishing in deeper waters is done largely by countries bordering the bay and by Japan. The annual catch of prawns, the major export crop, has remained stable despite intensified harvesting. Several species of tuna found in the bay also are important. The tuna fishery is confined to the true oceanic sector of the bay, south of latitude 15°N, since fresh water runoff from the large rivers greatly influences the nearshore waters.

Petroleum and natural-gas discoveries have been made in the Bay of Bengal, notably offshore of the Godavari and Manandi deltas. The bay has a geologic setting similar to that of the Indus River basin and the western margin of the Indian Peninsula. Hydrocarbon resources in the Bay of Bengal generally are located in deep areas, as compared to those in the Arabian Sea. There are placer deposits of titanium off northeastern Sri Lanka and rare earths off northeastern India. Heavy mineral sands occur around Nagapatnam (in Tamil Nadu state) on the southeastern Indian coast, near Chennai (Madras), and in coastal areas around Vishakhapatnam. They consist of ilmenite, garnet, sillimanite, zircon, rutile, and manganite.

3.3.2 Transportation

The principal trade routes for large tankers en route from the Persian Gulf to the Strait of Malacca pass south of the Bay of Bengal. Hence, oceanic transportation is limited to carriage of cargoes to and from Sri Lanka, Bangladesh, and the east coast of India.

Principal ports in India are Kolkata (Calcutta), Haldia, Vishakhapatnam, Chennai, Cuddalore, and Paradeep. Sri Lankan ports of importance are Colombo and Trincomalee. Dhaka and Chittagong are noteworthy in Bangladesh, and Akyab (Sittwe) is Myanmar's chief port on the Bay of Bengal. Haldia, Vishakhapatnam, and Paradeep are well developed as iron ore terminals, reflecting India's profitable exportation of raw materials.

3.3.3 Study And Exploration

The Periplus Maris Erythraei, an early Greek manual of sailing directions written in the 1st century AD, described sailing routes from the Red Sea (Maris Erythraei) to coastal areas along the Arabian Sea and Bay of Bengal to eastern India north of the Ganges delta. During the 2nd century AD, Ptolemy described voyages from the Ganges across the Bay of Bengal to the Strait of Malacca. Based on these descriptions, it is presumed that Indian and Malayan navigators had been crossing the Bay of Bengal on trading voyages for some time. Colonizing voyages began in the 1st century AD and can be divided into two periods: gradual colonization between the 1st and 6th centuries and development journeys between the 7th and 10th centuries.

Chinese maritime dominance of the Bay of Bengal dates from the Nan (Southern) Song dynasty (1127–1279). In 1405–33 the renowned admiral Zheng He led voyages for the purpose of exacting tribute and extending Chinese political influence in the Indian Ocean. He crossed the bay and visited ports in Sri Lanka. The Portuguese explorer Vasco da Gama led the first European voyage into the bay, which after circumnavigating Africa reached Calicut (now Kozhikode, India) in 1498. By 1511 the Portuguese had reached and occupied Malacca (now Melaka, Malaysia). The other major European voyages of the 16th to 19th century passed well to the south of the bay.

Interest in the scientific study of the bay grew in the 20th century, especially after World War II. The postwar voyages of the research vessels *Galathea* of Denmark, *Vityaz* of the U.S.S.R., and *Pioneer* and *Anton Bruun* of the United States undertook significant work in the region; and a notable effort was the International Indian Ocean Expedition (1960–

65), during which a considerable amount of information was gathered. The National Institute of Oceanography, established in India in 1966, furthered this research, utilizing the vessels *Sagar Kanya* and *Gaveshani*. Indian Ocean fishery research and development programs have been carried out on a coordinated basis by Bangladesh, India, Myanmar, Sri Lanka, and several countries on the periphery of the Bay of Bengal, including Indonesia, Malaysia, Thailand, and Maldives.

3.8 Conclusion

Study area is an important factor in the case of research conduction. The study area of present research was a suitable for this study. As this research was about different aspects of types, uses, sources of water resources in the study area. People of the study area directly or indirectly are depended on these water resources in different way. There are some similarities between Jessore and Bhola Upazila but in context of geology, soil, landform, there are notable differences can be found. All maps in this chapter are generated by the author.

CHATPER FOUR
DATA SOURCES AND METHODS

4.1 Introduction

Methodology outlines here the techniques for the collection of data and the procedures applied for the execution of the study. It expresses a systematic way through which any study can be done in a fruitful way. This chapter outlines the overall design of the study and research methodologies that have been followed to achieve the objectives set out in Chapter 1. It also describes data collection procedures at different stage of the research work. Data analysis procedures and techniques are also presented here(Urban & Planning, 1996). Finally, the difficulties or problems faced during the data collection process and the limitation of the study has been illustrated.

4.2 Data Sources

There are two types of data sources. Such as; primary and secondary source. In this survey primary sources is field survey and secondary source is supplied maps and data. It is needed to develop a database to detect the land use change in two different years. For this purpose both primary and secondary data sources are used in this work. In addition, data should be obtained following good practice guidelines using appropriate method and for a reasonable length of time to allow long-term trends to be evaluated.

4.2.1 Secondary Sources

Secondary data, in a word is the storage of primary data. These data may be collected from any publication, journal, newspaper, survey report, annual report of any institution etc. Statistical data is the best example of secondary data. The past record of this study is mainly based on secondary information. Secondary data are collected from maps and publications and questionnaire survey.

4.3 Methodology of the Study

In this research, five data preprocesses were operated which were band combination, image clip, image enhancement, image classification and post classification. Through these preprocesses, the qualities of the original image data of year 1998, 2003, 2007, 2013 and 2017 were improved. After then, three major data processes should be completed. They were urban change detection. Through these processes, the final results could be obtained. Based on the introductions above, the methods used in this research can be divided into three subchapters. The first subchapter is data preprocessing which is explaining the detailed steps of each technique of preprocessing, classification and analysis with images. The second subchapter is image preparation which is the first major process in this thesis and post classification which is employed to improve the quality of classified images. The accuracy of results from post classification is estimated in next subchapter. In the final subchapter, the second major process which is change detection is introduced in three parts as mentioned before. Various secondary data was used for this research and several procedures have been maintained, such as; at first identification problem and topic selection, conceptualization, study the aim and objectives, collection of maps, Field survey, field observation etc. The whole methodology we depict through the following chart: Detail procedure and aspects of the data collection has been described.

Following processes/methods were applied for achieving the target which is setout as objective in the opening chapter.

- At the very outset of the research work, an extensive literature review has been carried out to know the conditions, types, nature, limitations, recommendations etc. of previous research, project reports conducted in home and abroad on Sea Surface and transportation system, transport operation and maintenance, institutional setup etc. in Bay of Bengal and to acquire knowledge for the basic understanding on that topics.
- Then objectives have been formulated related to the deficiencies of Bay of Bengal Sea Surface Temperature, Color, Height and its operation, maintenance

and management and organizational context as well as the area itself which has been described in the Chapter one.

- Existing and historical Sea Surface Temperature and ocean color and height situations have been assessed by collecting geographical information and base map (digital, hard, satellite) from secondary sources. In order to analyze the SST and to represent by visualizing the present and historical condition of the BoB, GIS base map has been collected, edited, manipulate and comprehensive GIS data base have been prepared.
- In order to evaluate the inherent weakness the Bay of Bengal related to SST, four Season have been identified i.e. Pre-monsoon, Monsoon, Post-monsoon and Winter etc. In this regard Secondary data have been collected.
- Secondary data have been analyzed and manipulated with a view to achieve the objective which is set out in the introductory chapter.
- Sector and zone wise comprehensive data and system analysis has been carried out to evaluate and point out the deficiencies of Temperature, Color, Height, Cyclone form.
- Finally, in line with research findings, the relevant guidelines, policies, regulations, have been proposed for realistic and affordable short and long term actions to improve the overall scenario in Bay of Bengal, which will fulfill the last objective of the study.

Objectives	Research Questions	Data Source	Methods	Analysis Tools
To identify the space borne satellite sensors as temperature data sources for the study and calculation assessment algorithm.	What types of satellites can be used to identify Sea Surface Temperature? How Sea Surface Temperature (SST) assessment algorithm can be calculated?	NOAA MODIS TRMM N2YO	Timeline infographics Geographic info graphics	SeaDAS Illustrator InDesign
To investigate the spatial and temporal distribution of sea surface temperature during last 20 years in the Bay of Bengal.	How was the spatial distribution of Sea Surface Temperature during last 20 years in the Bay of Bengal.	NOAA MODIS TRMM REMSS NESDIS EUMETSAT AMSR	Statistical analysis, (Excel) Programming(Google Earth Engine Cloud) Spatial Analysis (Arc Map)	SeaDAS Arc Map Google Earth Engine IllustratorExcel

Table 4.1 : Research Methods

4.4 Collection of Published Data

An extensive literature review has been done in search of relevant data. Purchasing of different books and reports containing the socio-economic data and along with these associated maps has been collected from different published sources such as

Different published source are

- ❖ REMSS
- ❖ NASA
- ❖ NOAA
- ❖ USGS
- ❖ Bangladesh Space Research and Remote Sensing Organization (SPARRSO)

4.5 Scanning and Digitization

After the collection of raw hard copy maps from different published sources the researcher have to scan each of the maps and then digitize them to convert in to a usable format (i.e., in digital format which has been converted in to GIS coverage).

4.6 Data analysis

Data analyses are one of the important parts of research work. We have got several types of data from the study area. Then we have made data table with each different field using Microsoft office excel. Using these data table we have made some maps on the basis of different database information's. In data table we have showed different parameter related to education sector and disaster oriented. In GIS there are a lot of ways to analyses data on the basis of spatial arrangements.

4.6.1 Data presentation

We have presented the latest vulnerability map using GIS and Remote Sensing techniques on the basis of information gathered from the field survey. Then we have analyzed the impact of natural disaster by composing maps and tables of Bay of

Bengal,. We have tried to find out the possible reasons behind it.

- Techniques of Analysis Geographic Information System (GIS) and Remote Sensing are used as tools for analyzing the land use, its pattern and land use change mapping. The Google Earth image is used for validation of the work.
- Statistical techniques will be performed by computer based programmed to show the chart and table. After collecting data, a various techniques will be processed manually and by using computer to manipulate the data accordance with the objectives and guidelines of the research.
- The maps also will be produced by using Arc Map, Erdas Imagine, Google Earth Engine and Google Earth Pro by the help of computer.

4.6.2 Geo- correction and Geo-referencing

This procedure is thus imperative to data modeling in the field of geographic information systems (GIS) and other cartographic methods. When data from different sources need to be combined and then used in a GIS application, it becomes essential to have a common referencing system. This is brought about by using various georeferencing techniques. Georeferencing tasks are undertaken to produce a map or because to link two or more different datasets together by virtue of the fact that they relate to the same geographic locations.

4.7 Data

The challenge was to find satellite data with the same temporal and spatial resolutions for SST and CHL-a, in our study area. Subsequently, the two parameters were first studied separately, using data at different spatial resolutions and over different periods. The purpose here is to decompose data and identify the mean patterns of variability for each parameter.

4.7.1 AVHRR Data

The Advanced Very High Resolution Radiometer (AVHRR) is a broad-band, four or five channel (depending on the model) scanner, sensing in the visible, near-infrared, and thermal infrared portions of the electromagnetic spectrum. This sensor is carried on the National Oceanic and Atmospheric Administration's (NOAA's) Polar Orbiting Environmental Satellites (POES), beginning with TIROS-N in 1978. ESA acquires and archives the 1km resolution AVHRR data over Europe.

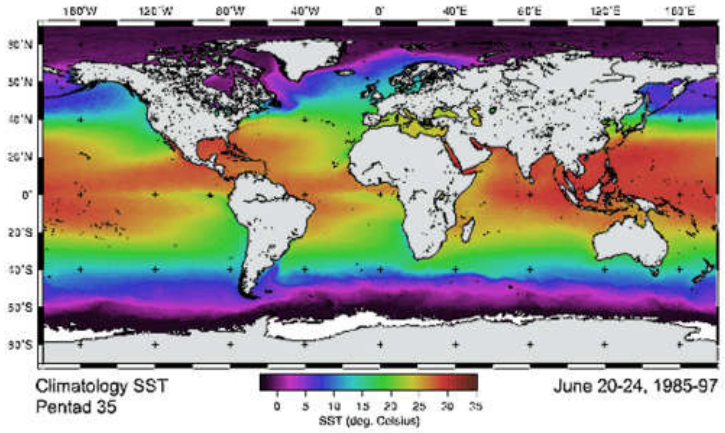


Figure 4.1 : AVHRR Temperature Data

4.7.1 TMI Data

The Tropical Rainfall Measuring Mission's (TRMM) Microwave Imager (TMI) is a passive microwave sensor designed to provide quantitative rainfall information over a wide swath under the TRMM satellite. By carefully measuring the minute amounts of microwave energy emitted by the Earth and its atmosphere, TMI is able to quantify the water vapor, the cloud water, and the rainfall intensity in the atmosphere. It is a relatively small instrument that consumes little power. This, combined with the wide

swath and the good, quantitative information regarding rainfall make TMI the "workhorse" of the rain-measuring package on Tropical Rainfall Measuring Mission.

4.8 Data on sea surface temperature

SST AVHRR_MetopA: For temporal and spatial variability analysis, we used the daily SST derived from the METOP/Advanced Very High Resolution Radiometer (AVHRR) for the period January 2008 to December 2012. These data were provided by the CERSAT. The data have spatial resolution of 0.05°× 0.05° which corresponds to approximately to 16 grid points in latitude direction and 20 grids points in longitude direction for the GOT, so we have 16×20 grid points and 225 observations (2008-2012), at each grid point to describe the state of GOT SST. Details on this product can be found in [15,16]. The validation of data for July 2007 to December 2013 at a global scale was made using the Matchup Data Base and also by comparison with data from the other sensors [17]. This indicates a negligible error of - 0.05 K and a standard deviation of 0.48 K for night time data against 0.9 K and 0.58 K for daytime data [18]. We used in this study only the night time data. To test the validity of these data in our area of study, we used in situdaily collected data using a temperature-conductivity sensor (Hobo U24) at near-surface (2 m depth) in the Gulf of Tadjourah from April to July 2013. The comparison of the SST AVHRR_MetopA daily-averaged data in the vicinity of the temperature-conductivity sensor showed that the two data evolve linearly during this short period. The mean difference was estimated at 0.6°C.

4.9 Ocean colour data

The CHL-a distribution in the GOT was analysed using the merged ocean colour product (Chlorophyll-a, case I water: CHL1) from the Moderate Resolution Imaging Spectroradiometer (MODIS) and Medium Resolution Imaging Spectrometer (MERIS) with

a 1 km by 1 km resolution. These data are 8-day composites and were provided by GlobColour/ST-ACRI (see: http://hermes.acri.fr/) from 2005 to 2011. Thus, in our area of

4.10 Temporal variability analysis

For each field, from each image, "sea pixels" were retrieved using land masking. Then time series was performed through a simple averaging of the "sea pixels" of each image. These time series can be presented as shown in (1): X is a time dependent physical variable, t is the equally spaced record time and N: the length of the sample. The objective here is to separate signals from noise as showed in (2). This was done using singular spectrum analysis decomposition.

Xm (t) = xt, xt+1, xt+2, ...xn (1)

X(t) = Signal(t) + □ (t) (2)

4.11 Singular spectrum analysis (SSA):

SSA is designed to extract useful information from short and noisy time series [21]. In simple terms, the SSA method can be visualised as a sliding window of length M, moving down a time series X(t) of length N. SSA decomposes time series into eigenvectors or temporal EOFs. The projection of these EOFs on the original time series yield temporal principal components or PCs Each PCs captures a type of variation representing trend, periodic oscillations, and structure less variations or noises [22-26].

4.12 Data source

The data source for AVHRR (Advanced Very High Resolution Radiometer) GAC SST is from National Oceanic and Atmospheric Administration (NOAA), National Environmental Satellite Data Information Service (NESDIS), Office of Satellite Data Processing and Distribution (OSDPD). Information on NOAA's POES Satellites can be found at poes website. The source data were derived by methods common to the

relevant scientific and technical communities. Information on the processing of AVHRR GAC SST can be found in the pre dissemination review and documentation from (Foley and Spence, 2005). The climatologically data were derived using methods described by Casey and Cornillon (1999). The SST anomaly product is used to show the difference between the sea surface temperature at a given time and the temperature that is normal for that time of year. The Bay of Bengal is a vast area to cover in a single short span study. Effort was optimal to cover the whole area to evaluate the anomalies.

4.13 Data mapping and visualization

The methods employed in the mapping and composite image generation were consistent with techniques suggested by Casey and Cornillon (1999). The data were mapped to an equal angle grid of 0.1 degrees longitude by 0.1 degrees latitude. The mapping was done using simple arithmetic means to produce individual and composite images of various durations (e.g., 1, 3, 8, 14-days, and monthly) following the recommendations of the International Ocean-Color Coordinating Group (Antonie et al., 2004). Graphics and products were generated using the Generic Mapping Tools Software (Wessel and Smith, 1998). The data visualization was done with open source GIS software SAGA-GIS. Further analysis was done using inbuilt statistical tools of the software.

4.14 Conclusion

The systematic data collection, the plan of research and the problems and prospects are the main subject matter of discussion in the methodology. The significance of the research rest upon the smooth expression and interpretation of the events .Data sources and methodology is the most essential and significance approach leading to penetrate in to the problem and solution in the entire research work. It is the structural framework of the study. It guides how to operate the study, interpret and analyze the research work from the beginning to ending. Research methodology provides the methods, systems and process of data collection, the logic behind the selection of the study area and some hypothetical assumptions to facilitate the study.

CHAPTER FIVE

SPACE BORNE SATELLITE SENSORS AS TEMPERATURE DATA SOURCES FOR THE STUDY OF SST ASSESSMENT ALGORITHM

5.1 Introduction

one of the most remarkable events in the space industry was when Space X realized the reusability of its rocket for the first time. Additionally, in June 2014, Russia used 1 rocket to launch 37 satellites at the same time. At present, many countries have the capability to launch multiple satellites in one mission. For example, NASA and the US Air Force launched 29 satellites in a single mission in 2013. At that time, the mission represented the most satellites ever launched at one time . In 2015 and 2016, China and India launched 20 satellites in single mission, respectively.

At present, six organizations have the capability to launch multiple satellites in a single mission: Russia, USA, China, India, Japan, and ESA. This trend indicates that in the future, the cost of sending satellites to space will greatly decrease. More and more remote sensing resources are becoming available. It is of great importance to have a comprehensive survey of the available remote sensing technology and to utilize inter- or trans-disciplinary knowledge and technology to create new applications.

Remote sensing is considered a primary means of acquiring spatial data. Remote sensing measures electromagnetic radiation that interacts with the atmosphere and objects. Interactions of electromagnetic radiation with the surface of the Earth can provide information not only on the distance between the sensor and the object but also on the direction, intensity, wavelength, and polarization of the electromagnetic radiation [2]. These measurements can offer positional information about the objects and clues as to the characteristics of the surface materials.

5.2 Remote Sensing

Remote sensing is the process of detecting and monitoring the physical characteristics of an area by measuring its reflected and emitted radiation at a distance (typically from satellite or aircraft). Special cameras collect remotely sensed images, which help researchers "sense" things about the Earth. Some examples are:

- Cameras on satellites and airplanes take images of large areas on the Earth's surface, allowing us to see much more than we can standing on the ground.
- Sonar systems on ships can be used to create images of the ocean floor without needing to travel to the bottom of the ocean.
- Cameras on satellites can be used to make images of temperature changes in the oceans.

Some specific uses of remotely sensed images of the Earth include:

- Large forest fires can be mapped from space, allowing rangers to see a much larger area than from the ground.
- Tracking clouds to help predict the weather or watching erupting volcanoes, and help watching for dust storms.
- Tracking the growth of a city and changes in farmland or forests over several years or decades.
- Discovery and mapping of the rugged topography of the ocean floor (e.g., huge mountain ranges, deep canyons, and the “magnetic striping” on the ocean floor).

5.3 Remote Sensors

Remote sensing instruments are of two primary types-

5.3.1 Active and passive

Active sensors, provide their own source of energy to illuminate the objects they observe. An active sensor emits radiation in the direction of the target to be investigated. The sensor then detects and measures the radiation that is reflected or backscattered from the target. Passive sensors, on the other hand, detect natural energy (radiation) that is emitted or reflected by the object or scene being observed. Reflected sunlight is the most common source of radiation measured by passive sensors.

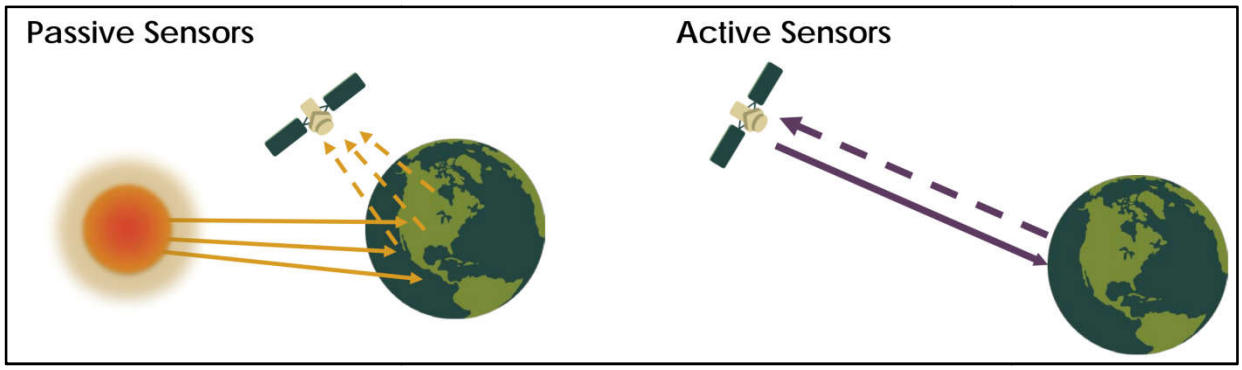


Figure 5.1 Active and Passive Sensor. **Source: Quora.com**

5.3.2 Active Sensors

The majority of active sensors operate in the microwave portion of the electromagnetic spectrum, which makes them able to penetrate the atmosphere under most conditions. An active technique views the target from either end of a baseline of known length. The change in apparent view direction (parallax) is related to the absolute distance between the instrument and target.

5.3.2.1 Laser altimeter

An instrument that uses LIDAR to measure the height of the platform (spacecraft or aircraft) above the surface. The height of the platform with respect to the mean Earth's surface is used to determine the topography of the underlying surface.

5.3.2.2 LIDAR

A light detection and ranging sensor that uses a laser (light amplification by stimulated emission of radiation) radar to transmit a light pulse and a receiver with sensitive detectors to measure the backscattered or reflected light. Distance to the object is determined by recording the time between transmitted and backscattered pulses and by using the speed of light to calculate the distance traveled.

5.3.2.3 Radar

An active radio detection and ranging sensor that provides its own source of electromagnetic energy. An active radar sensor, whether airborne or spaceborne, emits microwave radiation in a series of pulses from an antenna. When the energy reaches the target, some of the energy is reflected back toward the sensor. This backscattered

microwave radiation is detected, measured, and timed. The time required for the energy to travel to the target and return back to the sensor determines the distance or range to the target. By recording the range and magnitude of the energy reflected from all targets as the system passes by, a two-dimensional image of the surface can be produced.

5.3.2.4 Ranging Instrument

A device that measures the distance between the instrument and a target object. Radars and altimeters work by determining the time a transmitted pulse (microwaves or light) takes to reflect from a target and return to the instrument. Another technique employs identical microwave instruments on a pair of platforms. Signals are transmitted from each instrument to the other, with the distance between the two determined from the difference between the received signal phase and transmitted (reference) phase. These are examples of active techniques. An active technique views the target from either end of a baseline of known length. The change in apparent view direction (parallax) is related to the absolute distance between the instrument and target.

5.3.2.5 Scatterometer

A high-frequency microwave radar designed specifically to measure backscattered radiation. Over ocean surfaces, measurements of backscattered radiation in the microwave spectral region can be used to derive maps of surface wind speed and direction.

5.3.2.6 Sounder

An instrument that measures vertical distribution of precipitation and other atmospheric characteristics such as temperature, humidity, and cloud composition.

5.3.3 Passive Sensors

Passive sensors include different types of radiometers and spectrometers. Most passive systems used in remote sensing applications operate in the visible, infrared, thermal infrared, and microwave portions of the electromagnetic spectrum. Passive remote sensors include the following:

5.3.3.1 Accelerometer

An instrument that measures acceleration (change in velocity per unit time). There are two general types of accelerometers. One measures translational accelerations (changes in linear motions in one or more dimensions), and the other measures angular accelerations (changes in rotation rate per unit time).

5.3.3.2 Hyper spectral radiometer

An advanced multispectral sensor that detects hundreds of very narrow spectral bands throughout the visible, near-infrared, and mid-infrared portions of the electromagnetic spectrum. This sensor's very high spectral resolution facilitates fine discrimination between different targets based on their spectral response in each of the narrow bands.

5.3.3.3 Imaging radiometer

A radiometer that has a scanning capability to provide a two-dimensional array of pixels from which an image may be produced. Scanning can be performed mechanically or electronically by using an array of detectors.

5.3.3.4 Radiometer

An instrument that quantitatively measures the intensity of electromagnetic radiation in some bands within the spectrum. Usually, a radiometer is further identified by the portion of the spectrum it covers; for example, visible, infrared, or microwave.

5.3.3.5 Sounder

An instrument that measures vertical distributions of atmospheric parameters such as temperature, pressure, and composition from multispectral information.

5.3.3.6 Spectrometer

A device that is designed to detect, measure, and analyze the spectral content of incident electromagnetic radiation. Conventional imaging spectrometers use gratings or prisms to disperse the radiation for spectral discrimination.

5.3.3.7 Spectro radiometer

A radiometer that measures the intensity of radiation in multiple wavelength bands (i.e., multispectral). Many times the bands are of high-spectral resolution, designed for remotely sensing specific geophysical parameters.

5.4 Development in Space borne remote sensing

Although the term 'remote sensing' was introduced in 1960. However, in practice, remote sensing has a long history. In the 1600s, Galileo used optical enhancements to survey celestial bodies [10]. An early exploration of prisms was conducted by Sir Isaac Newton in 1666. Newton discovered that a prism dispersed light into a spectrum of red, orange, yellow, green, blue, indigo, and violet and recombined the spectrum into white light. One hundred years later, in 1800, Sir William Herschel explored the thermal infrared electromagnetic radiation for the first time in the world. Herschel measured the temperature of light that had been split with a prism into the spectrum of visible colors. In the following decades, some attempts were made with aerial photographs using cameras attached to balloons. However, the results were not satisfactory until 1858, when Gasper Felix Tournachon took the first aerial photograph successfully from a captive balloon from an altitude of 1200 feet over Paris. Later, in 1889 in Labruguiere, France, Arthur Batut attached a camera and an altimeter to kites for the first time so that the image scale could be determined.

Therefore, he is considered to be the father of kite aerial photography. Then, at the beginning of the twentieth century, the camera was able to be miniaturized (e.g., 70 g) so that it was easily carried by pigeons. The Bavarian Pigeon Corps took the first aerial photos using a camera attached to a pigeon in 1903. During the First World War, the use of aerial photography grew. Later, in 1936, Albert W. Stevens took the first photograph of the actual curvature of the earth from a free balloon at an altitude of 72,000 feet. The first space photograph from V-2 rockets was acquired in 1946. Table 1 addresses the evolution of the remote sensing, excluding the early development stage. The table starts with the use of aerial photographs for surveying and mapping as well for military use. The milestones in this evolution (see Table 1) were referenced to. Additionally, recent developments in microsatellites and satellite constellations are also listed in Table 5.1.

Phases	Time series	Remarks
Airborne remote sensing	During the First and Second World Wars	The use of photographs for surveying, mapping, reconnaissance and military surveillance
Rudimentary spaceborne satellite remote sensing	In the late 1950s	The launch of Sputnik 1 by Russia in 1957 and Explorer 1 by US in 1958
Spy satellite remote sensing	During the Cold War (1947–1991)	Remote sensing for military use spilled over into mapping and environment applications
Meteorological satellite sensor remote sensing	1960˜	The launch of the first meteorological satellite (TIROS-1) by the US in 1960. Since then, data in digital formats and the use of computer hardware and software
Landsat	1972˜	Landsat 1, 2, and 3 carrying a multispectral scanner; Landsat 4 and 5 carried a Thematic Mapper sensor; Landsat 7 carries an Enhanced Thematic Mapper; Landsat 8 carries the Operational Land Imager. Landsat satellites have high resolution and global coverage. Applications were initially local and have become global since then
European Space Agency's first Earth observing satellite program	1991˜	The European Space Agency launched the first satellite ERS-1 in 1991, which carried a variety of earth observation instruments: a radar altimeter, ATSR-1, SAR, wind scatterometer, and microwave radiometer. A successor, ERS-2, was launched in 1995
Earth observing system (EOS)	Since the launch of the Terra satellite in 1999	Terra/Aqua satellites carrying sensors, such as MODIS and taking measurements of pollution in the troposphere (MOPITT). Global coverage, frequent repeat coverage, a high level of processing, easy and mostly free access to data
New millennium	Around the same time as EOS	Next generation of satellites and sensors, such as Earth Observing-1, acquiring the first spaceborne hyperspectral data
Private industry/commercial satellite systems	2000˜	1. Very high-resolution data, such as IKONOS and Quickbird satellites 2. A revolutionary means of data acquisition: daily coverage of any spot on earth at a high resolution, such as Rapideye 3. Google streaming technology allows rapid data access to very high-resolution images 4. The launch of GeoEye-1 in 2008 for very high-resolution imagery (0.41 m)
Microsatellite era and satellite constellations	2008˜	1. Small satellites and satellite constellation (RapidEye and Terra Bella, formerly Skybox):

Phases	Time series	Remarks
		RapidEye was launched in August, 2008, with five EOS. These are the first commercial satellites to include the Red-Edge band, which is sensitive to changes in chlorophyll content. On March 8, 2016, Skybox imaging was renamed to Terra Bella. Satellites provided the ability to capture the first-ever commercial high-resolution video of Earth from a satellite and the ability to capture high-resolution color and near-infrared imagery 2. For the first time, Russia carried out a single mission to launch 37 satellites in June of 2014 3. ESA launched the first satellite of the Sentinel constellation in April of 2014. 4. SpaceX reusable rocket capacity since December of 2015 5. Current satellites in high revisiting period, large coverage, and high spatial resolution, up to 31 cm

Table 5.1 Evolution and advancement in remote sensing satellites and sensors.

5.5 Characteristics of materials in electromagnetic spectrum (EMS)

Remote sensors remotely interact with objects on the surface of the Earth. Objects on the surface of the Earth generally include terrain, buildings, road, vegetation, and water. The typical materials of these objects that interact with the EMS are categorized into groups: transparent and opaque (partly or fully absorbed).

5.6 Electromagnetic spectrum

Figure 5.1 contains the EMS range from gamma rays to radio waves. In remote sensing, typical applications include the visible light (380–780 nm), infrared (780 nm–0.1 mm), and microwave (0.1 mm–1 m) ranges. This paper treats the terahertz (0.1–1 mm) range as an independent spectral band separate from microwaves. Remote sensing sensors interact with objects remotely. Between sensors and the earth surface, there is atmosphere. It is estimated that only 67% of sunlight directly heats the Earth. The remainder of the light is absorbed and reflected by the atmosphere. The Earth's

atmosphere strongly absorbs infrared and UV radiation. In visible light, typical remote sensing applications include the blue (450–495 nm), green (495–570 nm), and red (620–750 nm) spectral bands for panchromatic or multispectral or hyperspectral imaging. Current bathymetric and ice LIDAR generally uses green light (e.g., NASA's HSRL-1 LIDAR, with a spectrum of 532 nm).

However, new experiments have shown that in the blue spectrum, such as at 440 nm, the absorption coefficient for water is approximately an order of magnitude smaller than at 532 nm, and 420–460 nm light can penetrate relatively clear water and ice much deeper, offering substantial improvements in sensing through water for the same optical power output, thus reducing power requirements. The red spectrum together with near-infrared (NIR) is typically used for vegetation applications. For example, the Normalized Difference Vegetation Index (NDVI) is used to evaluate targets that may or may not contain live green vegetation. Infrared is invisible radiant energy. Usually, infrared is divided into different regions: near IR (NIR, 0.75–1.4 μm), shortwave IR (SWIR, 1.4–3 μm), mid-IR (MIR, 3–8 μm), longwave IR (LWIR, 8–15 μm), and far IR (FIR, 15–1000 μm).

Alternatively, according to the ISO 20473 scheme, another division is proposed as NIR (0.78–3 μm), MIR (3–50 μm), and FIR (50–1000 μm). Most of the infrared radiation in sunlight is in the NIR range. Most of the thermal radiation emitted by objects near room temperature is infrared. In nature, on the surface of the Earth, almost all thermal radiation consists of infrared in the mid-infrared region, which is a much longer wavelength than that in sunlight. Of these natural thermal radiation processes, only lightning and natural fires are hot enough to produce much visible energy, and fires produce far more infrared than visible light energy.

NIR is mainly used in medical imaging and physiological diagnostics. One typical application of MIR and FIR is thermal imaging, for example, night vision devices. In the MIR and FIR spectrum bands, water shows high absorption, and biological systems are highly transmissive.

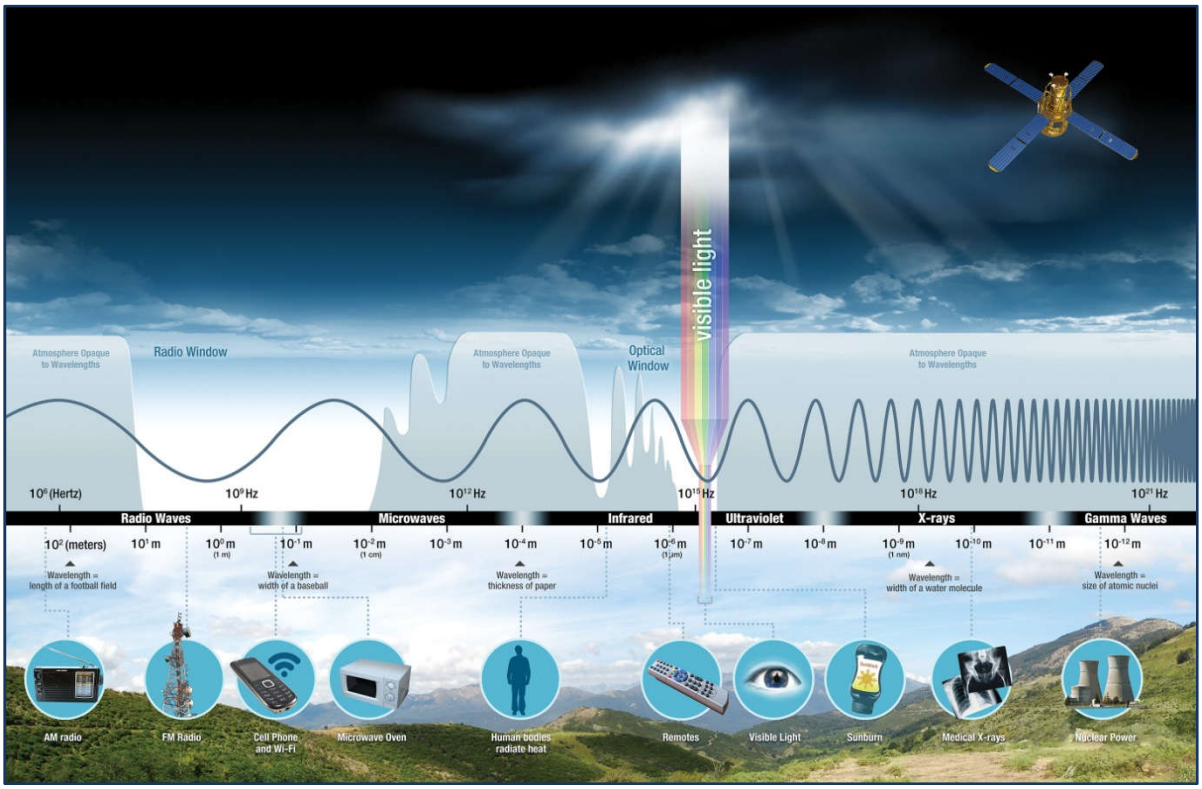


Figure 5.2 The electromagnetic spectrum. Source: Quora.com

With regard to the terahertz spectrum band, terahertz frequencies are useful for investigating biological molecules. Unlike more commonly used forms of radiated energy, this range has rarely been studied, partly because no one knew how to make these frequencies bright enough and because practical applications have been impeded by the fact that ambient moisture interferes with wave transmission. Nevertheless, terahertz light (also called T-rays) has remarkable properties. T-rays are safe, non-ionizing electromagnetic radiation.

This light poses little or no health threat and can pass through clothing, paper, cardboard, wood, masonry, plastic, and ceramics. This light can also penetrate fog and clouds. THz radiation transmits through almost anything except for not metal and liquid (e.g., water). T-rays can be used to reveal explosives or other dangerous substances in packaging, corrugated cardboard, clothing, shoes, backpacks, and book bags. However, the technique cannot detect materials that might be concealed in body cavities.

5.7 Objects and spectrum

When light encounters an object, they can interact in several different ways: transmission, reflection, and absorption. The interaction depends on the wavelength of the light and the nature of the material of the object.

Transparent material allows light to pass through the material without being scattered or absorbed. Typical transparent objects include plate glass and clean water. Figure 2 shows the transmission spectrum of soda-lime glass with a 2-mm thickness. Soda-lime glass is typically used in windows (also called flat glass) and glass containers. From Figure 2, it can be seen that soda-lime glass nearly blocks UV radiation. Nevertheless, it has high transmittance in the visible light and NIR wavelengths. It is easy to understand that when a laser scanner with a wavelength of 905, 1064, or 1550 nm hits a flat glass window or a glassy balcony, over 80% of the laser energy passes through the glass and hits the objects behind the window. Another typical example of transmissive material is clear water.

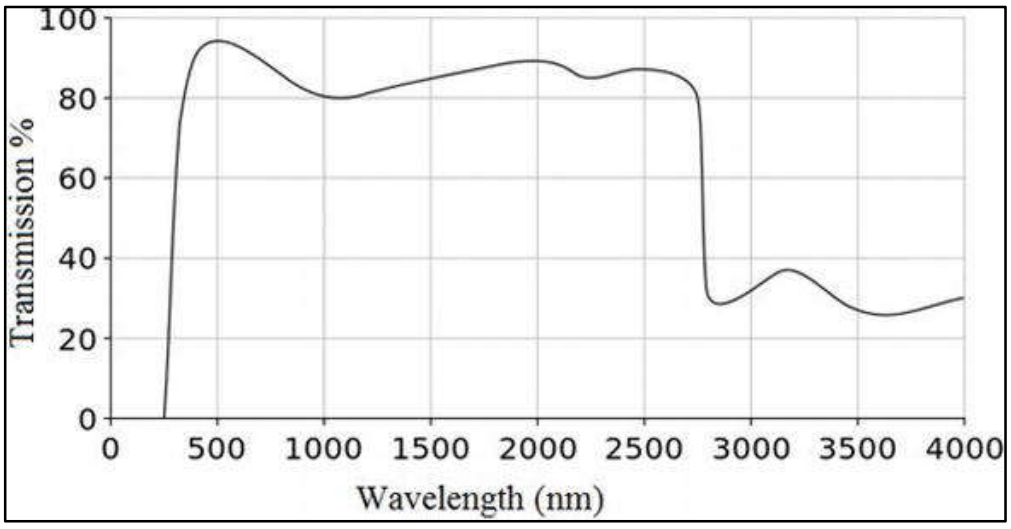


Figure 5.3 Transmission spectrum of soda-lime glass with a 2-mm thickness. Obtained from Wikipedia.

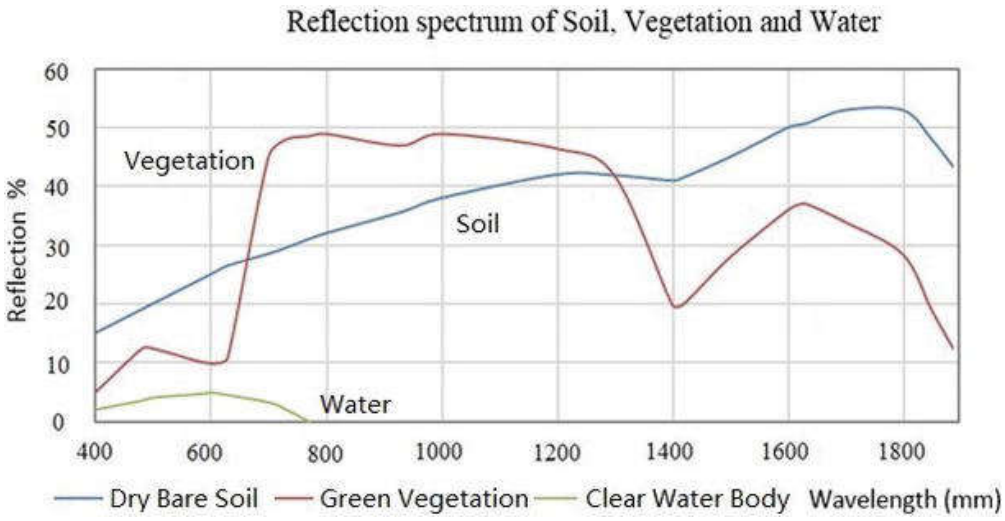
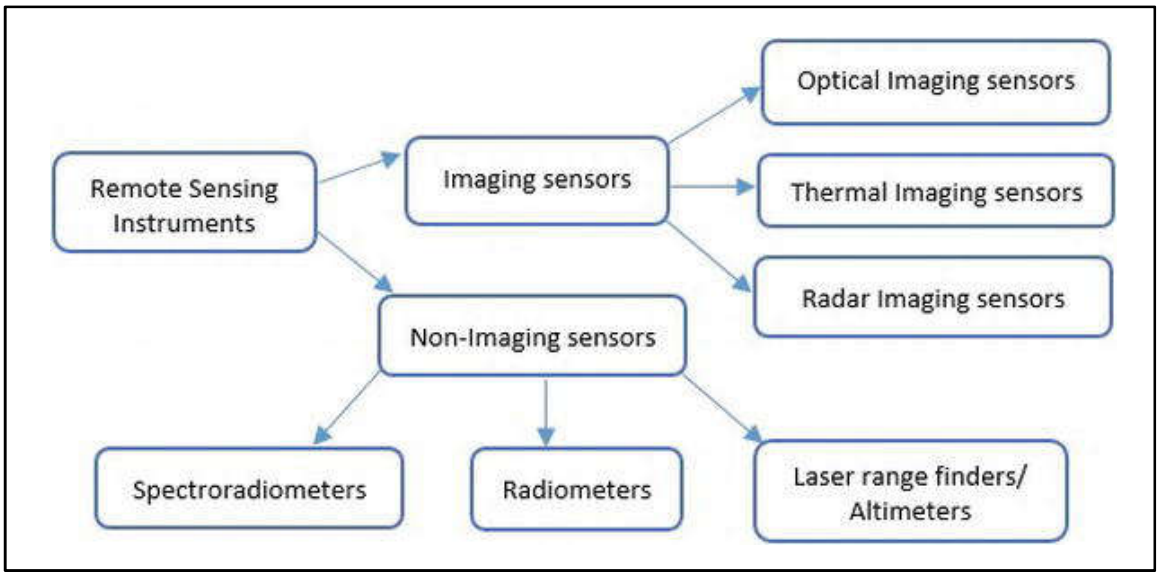


Figure 5.4 Examples of reflective materials. Image referenced from Wikimedia.

5.8 Space borne sensors

Space borne sensors have been developed for over 40 years. Currently, approximately 50 countries are operating remote sensing satellites. There are more than 1000 remote sensing satellites available in space, and among these, approximately 593 are from the USA, over 135 are from Russia, and approximately 192 are from China.

Conventionally, remote sensors are divided into two groups: passive sensors and active sensors, as we described in the first section. However, as sensor technology has advanced, nothing has been absolute. For example, an imaging camera is usually regarded as a passive sensor. However, in 2013, a new approach that integrates active and passive infrared imaging capability into a single chip was developed. This sensor enables lighter, simpler dual-mode active/passive cameras with lower power dissipation. Alternatively, remote sensing sensors can be classified into imaging sensors and non-imaging sensors. In terms of their spectral characteristics, the imaging sensors include optical imaging sensors, thermal imaging sensors, and radar imaging sensors. Figure 6 illustrates the category in terms of imaging sensors and non-imaging sensors.



5.5 Space borne remote sensing sensors.

5.9 Optical imaging sensor

Optical imaging sensors operate in the visible and reflective IR ranges. Typical optical imaging systems on space platform include panchromatic systems, multispectral systems, and hyperspectral systems. In a panchromatic system, the sensor is a monospectral channel detector that is sensitive to radiation within a broad wavelength range. The image is black and white or gray scale. A multispectral sensor is a multichannel detector with a few spectral bands. Each channel is sensitive to radiation within a narrow wavelength band. The resulting image is a multilayer image that contains both the brightness and spectral (color) information of the targets being observed. A hyperspectral sensor collects and processes information from 10 to 100 of spectral bands.

	Panchromatic systems	**Multispectral systems**	**Hyperspectral systems**
Spectral range (nm)	~430–720	~430–720 ~750–950	~470–2000
Satellites	QuickBird, SPOT, IKONOS	SPOT, QuickBird, IKONOS	TRW Lewis, EO-1

	Panchromatic systems	Multispectral systems	Hyperspectral systems
Spectral band	Monospectral, black and white, gray-scale image	Several spectral bands	10 to 100 of spectral bands
Spatial resolution	Submeter	Up to 1–2 m	Up to 2 m
Applications	Earth observation and reconnaissance applications	Red-green-blue (true color): visual analysis; Green-red-infrared: vegetation and camouflage detection; Blue-NIR-MIR: visualizing water depth, vegetation coverage, soil moisture content, and the presence of fires, all in a single image	(i) Agriculture; (ii) eye care; (iii) food processing; (iv) mineralogy; (v) surveillance; (vi) physics; (vii) astronomy; (viii) chemical imaging; (ix) environment
Advantages	High applicability in (i) imaging multiple targets; (ii) mosaic strips to large area; (iii) stereo and tristereo acquisition; (iv) linear feature acquisition, such as coastlines, pipelines, roads, and borders		
Disadvantages	Affected by sun illumination and cloud coverage. Polar areas with seasonal changes in sun illumination and the equatorial belt with persistent cloud coverage		

Table 5.3 Satellite optical imaging systems.

5.10 Thermal IR imaging sensors

A thermal sensor typically operates in the electromagnetic spectrum between the mid-to-far-infrared and microwave ranges, roughly between 9 and 14 μm. Any object with a temperature above zero can emit infrared radiation and produce a thermal image. A warm object emits more thermal energy than a cooler object. Therefore, the object becomes more visible in an image. This is especially useful in tracking a living creature, including animals and the human body, and detecting volcanos and forest fires because a thermal image is independent from the lights in a scene and is available whether it is daytime or nighttime. Commonly used thermal imaging sensors include

IR imaging radiometers, imaging spectroradiometers, and IR imaging cameras. Currently, the satellite IR sensors in use include ASTER, MODIS, ASAA, and IRIS. Table 3lists the thermal IR sensors and their applications.

Sensor	Operational wave band	Definition	Satellites sensors	Applications
IR imaging radiometer	UV, mid-to-far-infrared, or microwave	Measures the intensity of electromagnetic radiation	ASTER	Volcanological, mineralogical, and hydrothermal studies, forest fires, glacier, limnological and climatological studies and DEM
Imaging spectroradiometer	Infrared	Measure the intensity of radiation in multiple spectrums	MODIS, ASAS, IRIS	Sea surface temperature, cloud characteristics, ocean color, vegetation, trace chemical species in the atmosphere
Infrared imaging camera	Mid-far infrared	Measure reflected energy from the surface		Volcanology, determining thunderstorm intensity, identifying fog and low clouds

Table 5.5 Thermal IR sensors.

5.11 Radar imaging sensors

A radar (microwave) imaging sensor is usually an active sensor, operating in an electromagnetic spectrum range of 1 mm–1 m. The sensor transmits light to the ground, and the energy is reflected from the target to the radar antenna to produce an image at microwave wavelengths. The radar moves along a flight path, and the area illuminated by the radar, or footprint, is moved along the surface in a swath. Each pixel in the radar image represents the radar backscatter for that area on the ground. A microwave instrument can operate in cloudy or foggy weather and can also penetrate sand, water, and walls. Unlike infrared data that help us identify different minerals and

vegetation types from reflected sunlight, radar only shows the difference in the surface roughness and geometry and the moisture content of the ground (the complex dielectric constant). Radar and infrared sensors are complimentary instruments and are often used together to study the same types of Earth surfaces [30]. Frequently used microwave spectrum bands for remote sensing include the X-band, C-band, S-band, L-band, and P-band. Specific characteristics of each band can be found in Table 5.6

.Band	Frequency (GHz)	Wavelength (cm)	Key characteristics
Ka	40–27	0.75–1.11	Usually for astronomical observations
K	27–18	1.11–1.67	Used for radar, satellite communications, astronomical observations, automotive radar
Ku	18–12	1.67–2.5	Typically used for satellite communications
X	12.5–8	2.4–3.75	Widely used for military reconnaissance, mapping and surveillance
C	4–8	3.75–7.5	Penetration capability of vegetation or solids is limited and restricted to the top layers. Useful for sea-ice surveillance
S	4–2	7.5–15	Used for medium-range meteorological applications, for example, rainfall measurement, airport surveillance
L	2–1	15–30	Penetrates vegetation to support observation applications over vegetated surfaces and for monitoring ice sheet and glacier dynamics
P	1–0.3	30–100	So far, only for research and experimental applications. Significant penetration capabilities regarding vegetation canopy, sea ice, soil, and glaciers

Table 5.6. Commonly used frequency and spectrum bands of radar imaging sensors.

Conventional passive microwave imaging instruments (such as cameras or imaging radiometers) provide imagery with a relatively coarse spatial resolution when compared to an optical instrument. The diffraction-limited angular resolution of a camera aperture is directly proportional to the wavelength and inversely proportional to the aperture dimension. To achieve a similar spatial resolution as optical instruments, a large antenna aperture (e.g., tens of kilometers) is needed. Clearly, it is

not feasible to carry such a large antenna on a space platform. SAR is an active microwave instrument that resolves the above problem. SAR utilizes the motion of the spacecraft to emulate a large antenna from the small craft itself. The longer the antenna is, the narrower the beam is. A fine ground resolution usually results from a narrow beam width. At present, a synthesized aperture can be several orders of magnitude larger than the transmitter and receiver antenna. It has become possible to produce an SAR image with a half meter of accuracy.

5.12 Non-imaging sensors

A non-imaging sensor measures a signal based on the intensity of the whole field of view, mainly as a profile recorder. In contrast with imaging sensors, this type of sensor does not record how the input varies across the field of view. In the remote sensing field, the commonly used non-imaging sensors include radiometers, altimeters, spectrometers, spectro radiometers, and LIDAR. Table 5 provides detailed information about conventional non-imaging sensors. In the remote sensing field, non-imaging sensors typically work in the visible, IR, and microwave spectral bands. The applications for non-imaging sensors mainly focus on height, temperature, wind speed, and other atmospheric parameter measurements.

Sensor	Operational wave band	Definition	Application
Radiometer	Ultraviolet, IR, microwave	To measure the amount of electromagnetic energy present within a specific wavelength range	Calculating various surface and atmospheric parameters
Altimeter	IR, microwave/radiowave, sonic	To measure the altitude of an object above a fixed level	Mapping ocean-surface topography and the hills and valleys of the sea surface
Spectrometer	Visible, IR, microwave	To measure the spectral content of the incident electromagnetic radiation	Multispectral and hyperspectral imaging

Sensor	Operational wave band	Definition	Application
Spectro-radiometer	Visible, IR, microwave	To measure the intensity of radiation in multiple spectrums	Monitoring sea surface temperature, cloud characteristics, ocean color, vegetation, trace chemical species in the atmosphere
LIDAR	Ultraviolet, visible, NIR	To measure distance and intensity	Ocean, land, 3D topographic mapping
		Doppler LIDAR: measure the wave number for speed; Polarization effects of LIDAR: shape	Meteorology, cloud measurements, wind profiling and air quality monitoring
Sonar	Acoustic	Measure the distance to an object; determine the depth of water beneath ships and boats	Navigation, communication and security (e.g., vessels) and underwater object detection. For example, handheld sonar for a diver
Sodar	Acoustic	As a wind profiler, sodar systems measure wind speeds at various heights above the ground and the thermodynamic structure of the lower layer of the atmosphere	Meteorology: atmospheric research, wind monitoring (typically in a range from 50 to 200 m above ground level)
A radio acoustic sounding system (RASS)	Radio wave and acoustic wave	Measuring the atmospheric lapse rate using backscattering of radio waves from an acoustic wave front to measure the speed of sound at various heights above the ground	Is added to a radar wind profiler or to a sodar system

Table 5.7 Non-imaging sensors.

Lasers have been applied in measuring the distance and height of targets in the remote sensing field. We generally call a laser scanning system as LIDAR (light detection and ranging) system.

Laser types	Pump source	Typical applications
Gas laser	Electrical discharge	Interferometry, holography, spectroscopy, material processing
Chemical laser	Chemical reaction	Military use
Dye laser	Other laser, flashlamp	Research, laser medicine
Metal-vapor laser	Electrical discharge	Printing and typesetting applications, fluorescence excitation examination, scientific research
Solid-state laser	Flashlamp, laser diode, Fiber laser, Nd: YAG.	Material processing, rangefinding, laser target designation
Semiconductor laser	Electrical current	Telecommunications, holography, printing, weapons, machining

Table 5.8 Typical laser sources.

In general, at a wavelength of 1064 nm, vegetation has stronger reflectance than soil, while at a wavelength of 1550 nm, soil shows greater a reflectance than vegetation. Taking measurements with different wavelengths is beneficial for object classification. Green lasers with a wavelength of 532 nm are usually pumped by a solid-state laser (Nd:YAG). This type of laser is widely used for bathymetric measurement. Table 7 lists the typical applications of different laser light wavelengths.

Name	wavelength (nm)	Laser sources	Typical applications
UV laser	355	Gas laser	Cutting and drilling
Violet laser	405	Semiconductor laser or solid-state laser	Laser printing, data recording, laser microscopy, laser projection displays, spectroscopic measurements
Blue laser	488	Solid-state laser	Environmental monitoring, medical diagnostics, handheld projectors and displays, telecommunications
Green laser	532	Solid-state laser (Nd:YAG)	Bathymetric measurement
Red laser	640	Semiconductor laser	Vegetation measurement
NIR	1064	Semiconductor	Airborne laser scanning

Name	wavelength (nm)	Laser sources	Typical applications
laser		laser or solid-state laser (fiber laser)	
NIR laser	1550	Semiconductor laser or solid-state laser (fiber laser)	Airborne laser scanning

Table 5.9. Commonly used laser wavelength.

5.13 Commonly used remote sensing satellites

So far, more than 1000 remote sensing satellites have been launched. These satellites have been updated with new generation satellites. The few spectral sensors from the earliest missions have been upgraded to hyperspectral sensors with hundreds of spectral bands. The spatial and spectral resolutions have been improved on the order of 100-fold. Revisit times have been shortened from months to daily. In addition, more and more remote sensing data are available as open data sources. Table 8 gives an overview of the commonly used remote sensing satellites and their parameters.

Mission	Country	Launch year	Sensors	Height of orbit (km)	Swath (km)	Revisit (day)	Channels	Spatial resolution
Landsat	USA	1972, 1975, 1978,1982, 1984,1993, 1999,2013, 2020	Panchromatic and multispectral sensor	705	185, 183	16	7–11	120 m, 100 m, 60 m, 30 m, 15 m
SPOT	USA	1986, 1990, 1993, 1998, 2002, 2012	Imaging spectroradiometer	694	60	1–3	Panchromatic, B, G, R, NIR	2.5 m, 5 m, 10 m, 20 m
ERS	ESA	1991, 1995	IR radiometer,	782–785	5–100 km (AMI) -	3, 35, 336	SAR	26 m across track and

Mission	Country	Launch year	Sensors	Height of orbit (km)	Swath (km)	Revisit (day)	Channels	Spatial resolution
			microwave sounder, Radiometer, SAR		500 km (ATSR)			6–30 m along track
RADARSAT	Canada	1995, 2007, 2018	SAR	793–821, 798, 592.7	45–100, 18–500, 5–500	1	SAR	8–100 m, 3–100 m, 3–100 m
MODIS	USA	1999, 2002	Imaging spectroradiometer	705	2330	1	36	1000 m, 500 m, 250 m
IKONOS	USA	1999	Imaging spectroradiometer	681	11.3	3	Panchromatic, B, G, R, NIR	Panchromatic:80 cm B, G, R, NIR:3.2 m
QuickBird	USA	2000, 2001	Imaging spectroradiometer	482, 450	16.8–18	2.4–5.9	Panchromatic, B, G, R, NIR	Panchromatic:65 cm /61 cm B, G, R, NIR:2.62 m/2.44 m
Envisat	ESA	2002	ASAR, MERIS, AATSR, RA-2, MWR, GOMOS, MIPAS, SCIAMACHY, DORIS, LRR	790	1150 km, 100 km, 400 km	35 days	15 bands (VIS, NIR), C-band	300 m, 30–150 m
GeoEye	USA	2008	Imaging spectroradiometer	681	15.2	8.3	Panchromatic, B, G, R, NIR	Panchromatic:41 cm B, G, R, NIR: 1.65 m
WorldView	USA	2007 2009 2014	Imaging spectroradiometer,	496, 770, 617,	17.6 km 16.4 km 13.1 km	1.7 1.1 <1	Panchromatic; Panchrom	Panchromatic 0.5 m; Panchrom

Mission	Country	Launch year	Sensors	Height of orbit (km)	Swath (km)	Revisit (day)	Channels	Spatial resolution
		2016.9	Laser altimeter	681	14.5 km	3	atic and eight multispectrum; Panchromatic and eight multispectrum; Panchromatic, B, G, R, NIR	atic and stereo images:0.46 m multispectral: 1.84 m; Panchromatic 0.34 m and multispectral 1.36 m
Sentinel 1–6	ESA	2014, 2015, 2016, 2017, 2021	Radar and super-spectral imaging	693, 786, 814	250 km 290 km, 250 km,	12, 10, 27	C-SAR, 12 bands (VIS, NIR, SWIR), 21 bands (VIS, NIR), S-band & X-band	5–20 m, 5–40 m, 10 m & 20 m & 60 m

Table 5.10 Remote sensing satellites.

5.14 Types of Ocean Satellite and their Sensor



Figure 5.6 Types of Ocean Satellite and their Sensor

5.15 Ocean Satellite and Sensor

	Applications	Satellite and Sensor
1	Sea Surface Temperature	AVHRR, TMI, AMSR E, GMI, Windsat, AMSR-1 etc.
2	Front Circulation	AVHRR, GEOS, JASON, POES
3	Ocean Current	AVHRR, GEOS, JASON, POES
4	Wave Height	GEOSAT, ASAR (ENVI SAT)
5	Chronological Contents (Phytoplankton)	SeaWiFs, IKONOS, ASTER
6	High Potential and Fishing Zone	NOAA AVHRR, OCM
7	Sea surface Height	Topex, ERS-1, ERS-2
8	Total Suspended Solid (Hydrodynamic Solid)	Landsat, ASTER
9	Sea Surface Salinity	SPURS, Aquarius (SSS)
10	Ocean Color	CZCS, OCTS, OCI, OCM, MODIS, GLI, SeaWiFs, MISR

Table 5.11 Ocean satellites and Sensors.

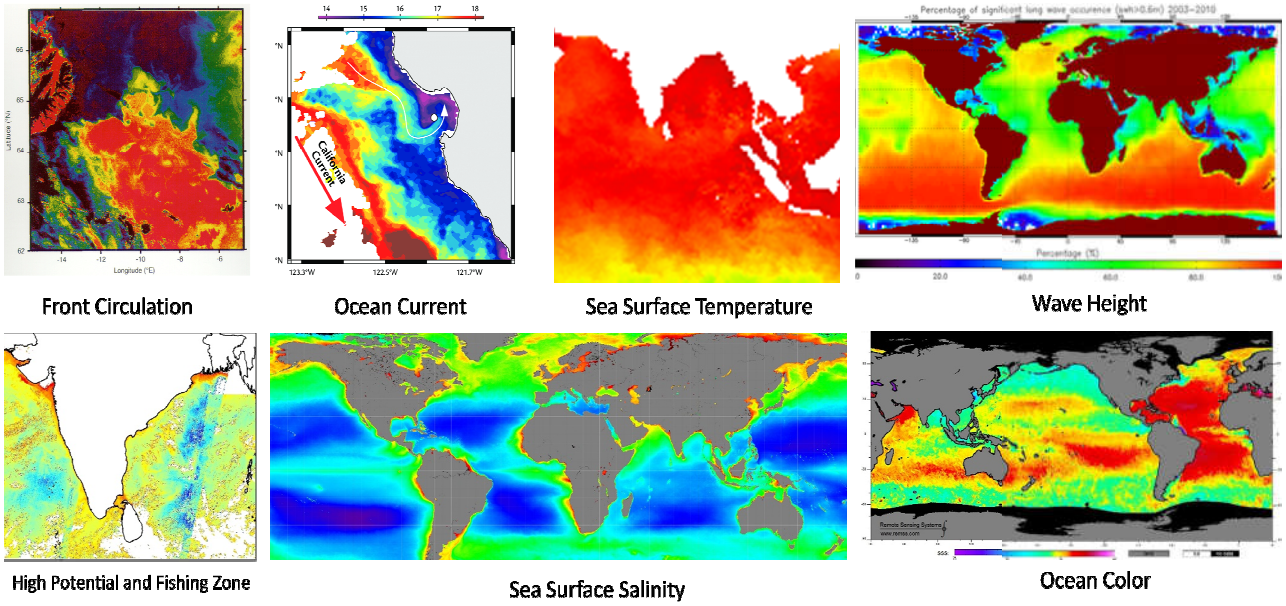


Figure 5.7 Ocean Sensor Applications

5.16 Ocean Microwave Satellite Sensor

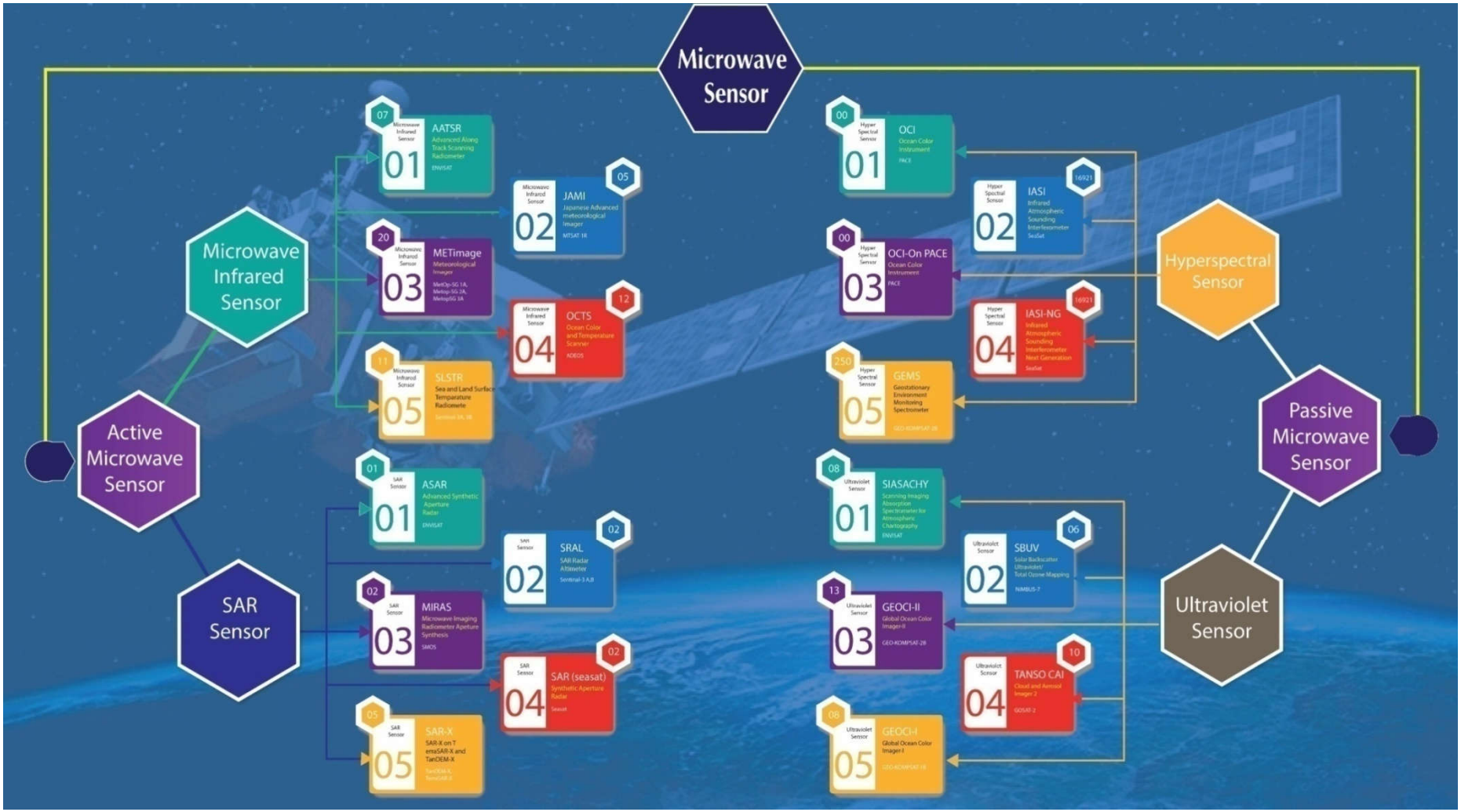


Figure 5.8 Types of Ocean Microwave Sensor

5.17 Ocean Optical Satellite Sensor

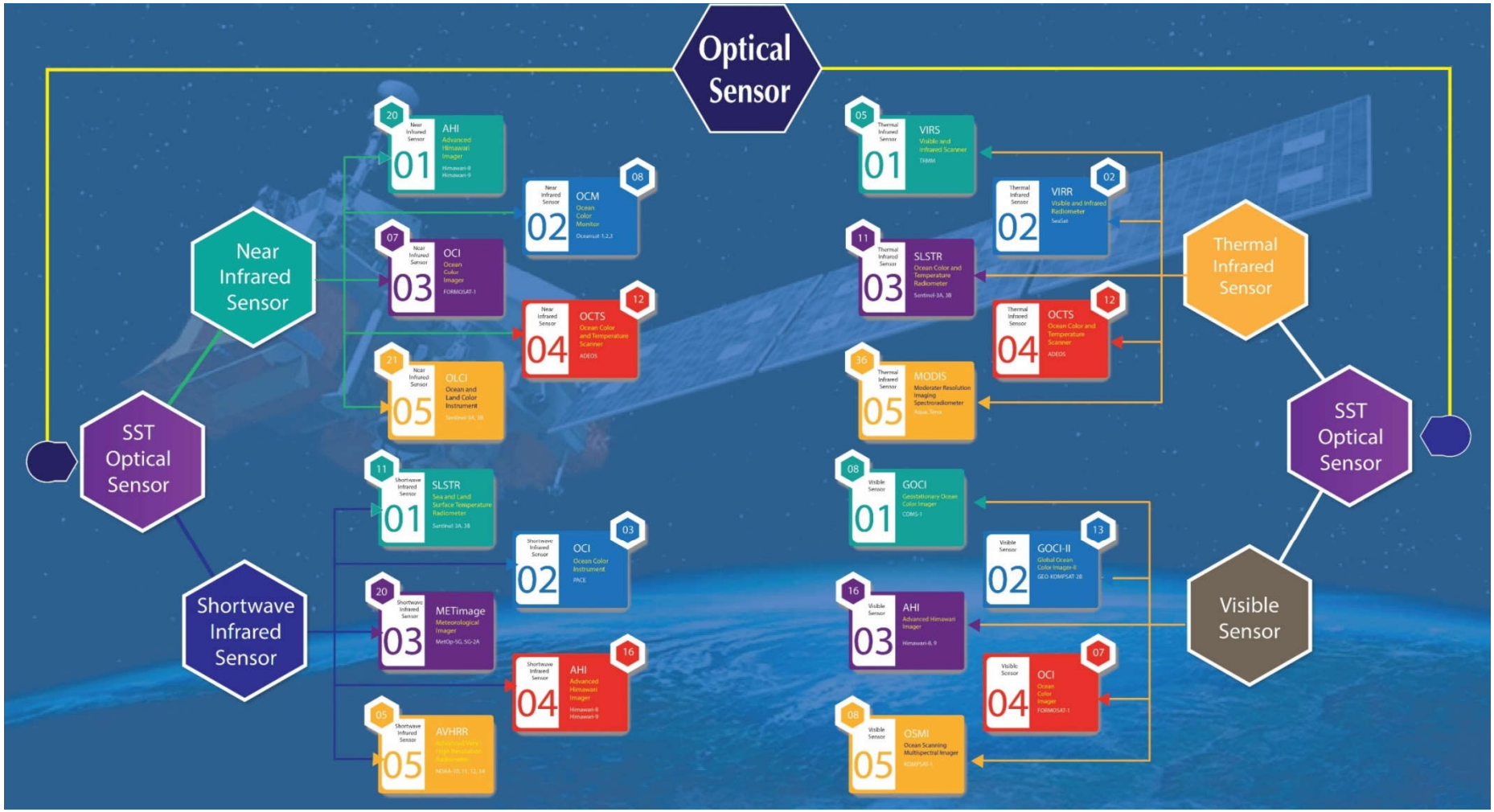


Figure 5.9 Types of Ocean Satellite Sensor

5.18 Ocean Sensor, Mission, Band, Swatch Area and their resolution.

S.N	Sensor	Mission	No of Band	Swatch (km)	Resolution (M)
1	Advanced Microwave Radiometer	Jason-2, Jason-3	3	1336	
2	Advanced Microwave Scanning Radiometer	ADEOS-II	8	1445	
3	Multifrequency Scanning Microwave Radiometer	OceanSat-2	4	1420	
4	Microwave Radiometer	Sentinel-3A, Sentinel-3B, Sentinel-3C, 3D	2		
5	TRMM Microwave Imager	TRMM	5	860	
6	Seasat-A Satellite Scatterometer	Seasat	1		
7	Advanced Himawari Imager	Himawari-8, Himawari-9	16		
8	Japanese Advanced meteorological Imager	MTSAT-1R	5		
9	Moderate Resolution Imaging Spectroradiometer	Terra, Aqua	36		
10	Ocean Color and Temperature scanner	ADEOS	12		
11	Sea and Land Surface Temparature Radiometer	Sentinel-3A, Sentinel-3B, Sentinel-3C, 3D	11	1270	
12	Visible and Infrared scanner	TRMM	5	833	2400
13	Global Ocean Color Imager-II	GEO-KOMPSAT-2B	13		
14	Scanning Imaging Absorption Spectrometer	ENVISAT (Atmospheric Chartography)	8		
15	Advanced Synthetic Aperture Radar	ENVISAT	1		
16	SAR Radar Altimeter	Sentinel-3A, Sentinel-3B, Sentinel-3C, 3D	21	1270	
17	Microwave Imaging Radiometer Apeture Synthesis	SMOS	1		
18	Advanced Along Track Scanning Radiometer	ENVISAT	7		

S.N	Sensor	Mission	No of Band	Swatch (km)	Resolution (M)
19	Advanced Meteorological Imager	GEO-KOMPSAT-2A	16		
20	Advanced Very High Resolution Radiometer	NOAA-10,11,12,14,15, 17, 18, 19 Metop-A, B, C	6		
21	Geostationary Ocean Color Imager	COMS-1	8		
22	Global Ocean Color Imager-II	GEO-KOMPSAT-2B	13		
23	Ocean Color Imager	FORMOSAT-1	7		
24	Ocean and Land Color Instrument	Sentinel-3A, Sentinel-3B, Sentinel-3C, 3D	21	1270	
25	Ocean Scanning Multispectral Imager	KOMPSAT-1	8		
26	Sea viewing Wide Field Sensor	Orbview-2	8		
27	Sea and Land Surface Temparature Radiometer	Sentinel-3A, Sentinel-3B, Sentinel-3C, 3D	11	1270	
28	Meteorological Imager	MetOp-SG 1A, MetopSG 2A, Metop-SG 3A	20		
29	Prism spectrometer	PRISMA	240		
30	Wide Field Sensor	IRS-1C, IRS-1D, IRS-P3	8	2806	1100
31	Coastal Zone Color Scanner	NIMBUS-7	6	1556	825
32	Visible and IR Radiometer	Seasat	2		
33	Infrared Atmospheric Sounding Interferometer	MetOp-SG 1A, Metop-SG 2A, Metop-SG 3A	16921	823	

Table 5.12 List of ocean satellites, Sensors, Band, Mission, Swatch, Resolution .

5.19 Sea Surface Temperature Measurement Algorithm

Given the desire to combine the high accuracy and resolution of the thermal infrared SST measurements with the better temporal and spatial coverage of passive microwave SST measurements (due to cloud transparency), efforts are being made to create a blended product which combines these strengths. One such project is the international Global Ocean Data Assimilation Experiment (GODAE) High-Resolution SST Pilot Project (GHRSST-PP). In the effort to combine these two kinds of SST products, careful consideration must be made to correct for differences due to diurnal heating and evaporative cooling as well as biases introduced by high wind speeds, water vapor and other atmospheric conditions. Models are being tested for each of these considerations. Algorithms which incorporate these models still use *in situ* measurements, as well, to quality assure and to adjust the final product. Here is an example of a blended SST algorithm being developed in Japan:

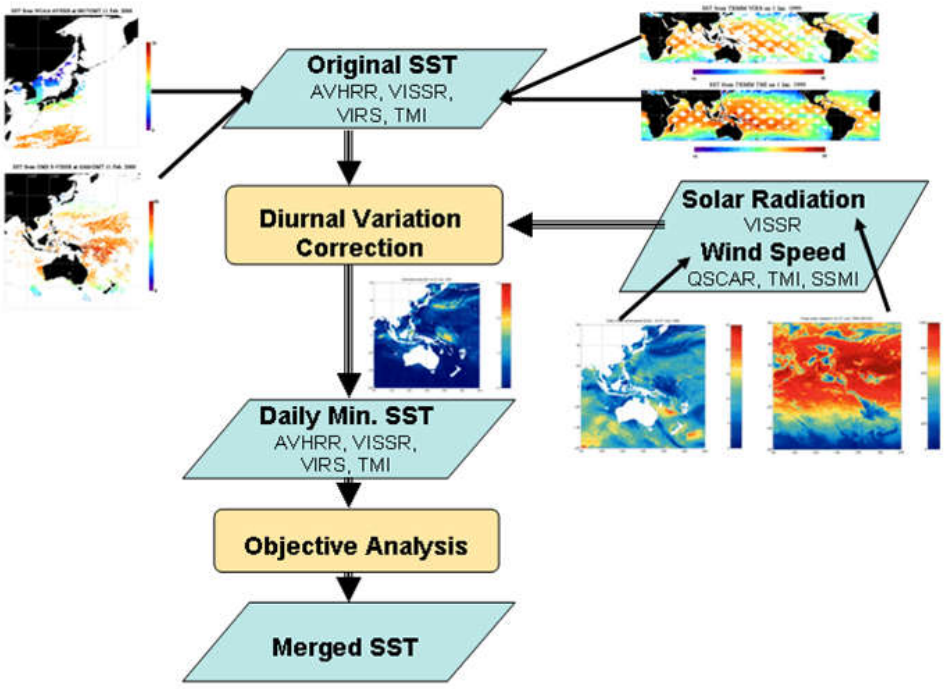


Figure 5.10 SST Algorithm Model.

5.20 AVHRR SST Algorithms

AVHRR data that have been scaled to 8-bit depth cannot be used to compute SSTs because NOAA does not modify the calibration coefficients stored in the file's Level 1B header. ENVI computes SST images in degrees Celsius, using AVHRR bands 3, 4, and 5. Currently, it does not use a cloud or land mask in the sea surface temperature calculation. It uses the Multi-Channel Sea Surface Temperature (MCSST) algorithms: one for daytime data and three for nighttime data:

- Day MCSST Split
- Night MCSST Split
- Night MCSST Dual
- Night MCSST Triple

These algorithms differ by which bands are used to correct for the atmosphere. Split-window uses bands 4 and 5, dual-window uses bands 3 and 4, and triple-window uses

5.21.1 SST equations for NOAA-12, -14, and -15:

Day MCSST Split

$T_s = a_0 + a_1*band4 + a_2(band4 - band5) + a_3(band4 - band5)(sec(f) -1)$

Night MCSST Split

$T_s = a_0 + a_1*band4 + a_2(band4 - band5) + a_3(band4 - band5)(sec(f)-1)$

Night MCSST Dual

$T_s = a_0 + a_1*band4 + a_2(band3 - band4) + a_3(sec(f) -1)$

Night MCSST Triple

$T_s = a_0 + a_1*band4 + a_2(band3 - band5) + a_3(sec(f)-1)$

5.21.2 ENVI uses the following SST equations for NOAA-16 through NOAA-18:

Day MCSST Split

$T_s = a_0 + a_1*band4 + a_2*band5 + a_3(band4 - band5)(sec(f) -1)$

Night MCSST Split

$T_s = a_0 + a_1*band4 + a_2*band5 + a_3(band4 - band5)(sec(f) -1)$

Night MCSST Dual

$T_s = a_0 + a_1*band4 + a_2(band3 - band4) + a_3(sec(f) -1)$

Night MCSST Triple

$T_s = a_0 + a_1*band3 + a_2*band4 + a_3*band5 + a_4(band3 - band5)(sec(f) -1)$

5.21.3 ENVI uses the following SST equations for NOAA-19:

Day MCSST Split

$T_s = a_0 + a_1*band4 + a_2(band4 - band5) + a_3(band4 - band5)(sec(f) -1)$

Night MCSST Split

$T_s = a_0 + a_1*band4 + a_2(band4 - band5) + a_3(band4 - band5)(sec(f) -1)$

Night MCSST Dual

$T_s = a_0 + a_1*band4 + a_2(band3 - band4) + a_3(sec(f) -1)$

Night MCSST Triple

$T_s = a_0 + a_1*band4 + a_2(band3 - band5) + a_3(band3 - band5)(sec(f) -1)$

5.21.4 ENVI uses the following SST equations for NOAA MetOp-A FRAC data:

Day MCSST Split

$T_s = a_0 + a_1*band4 + a_2(band4 - band5) + a_3(band4 - band5)(sec(f) -1)$

Night MCSST Split

$T_s = a_0 + a_1*band4 + a_2(band4 - band5) + a_3(band4 - band5)(sec(f) -1)$

Night MCSST Dual

$T_s = a_0 + a_1*band4 + a_2(band3 - band4) + a_3(sec(f) -1)$

Night MCSST Triple

$T_s = a_0 + a_1*band4 + a_2(band3 - band5) + a_3*(band3 - band5)(sec(f) -1)$

Sec (f) is the secant of the satellite zenith angle (f), and bands 3 through 5 are the calibrated brightness temperatures of NOAA AVHRR bands (in Kelvins). The "a" coefficients are derived from a regression model based on drifting buoy and tropical Pacific fixed-buoy data. The coefficient values depend on which NOAA satellite was used to collect the AVHRR image. ENVI uses published MCSST coefficients for NOAA-12 through NOAA-17. The following tables show the "a" coefficients for the various NOAA sensors, for each algorithm that is computed.

5.21.5 Day MCSST Split

Satellite	a0	a1	a2	a3
NOAA-12	-263.006	0.963563	2.579211	0.242598
NOAA-14	-278.43	1.017342	2.139588	0.779706
NOAA-15	-261.029735	0.959456	2.663579879	0.570613
NOAA-16	-273.77	3.301267	-2.30195	0.628966
NOAA-17	-271.206	0.992818	-2.49916	0.915103
NOAA-18	-280.43	1.02453	2.10044	0.784059
NOAA-19	-278.74596	1.01922	1.72270	0.80263
MetOp-A FRAC	-273.816	1.00255	2.39451	0.903773

Table: 5.13 Day time MC SST Split Algorithm data

5.21.6 Night MCSST Split

Satellite	a0	a1	a2	a3
NOAA-12	-263.94	0.967077	2.384376	0.480788
NOAA-14	-282.24	1.029088	2.275385	0.752567
NOAA-15	-271.3969724	0.993892	2.7523466369	0.662999
NOAA-16	-273.15	-2.53655	3.5316	0.753291
NOAA-17	-276.59	1.01015	-2.5815	1.000541
NOAA-18	-276.075	1.00841	2.23459	0.736946
NOAA-19	-277.71304	1.01432	1.91798	0.72064
MetOp-A FRAC	-277.447	1.01377	2.52362	1.03056

Table: 5.14 Night time MC SST Split Algorithm data

5.21.7 Night MCSST Dual

Satellite	a0	a1	a2	a3
NOAA-12	-279.846	1.031355	1.288548	2.265075
NOAA-14	-273.914	1.008751	1.409936	1.975581
NOAA-15	-283.5117285	1.041037	1.5875819344	1.67743
NOAA-16	-273.082	1.50825	1.00413	1.52452

Satellite	a0	a1	a2	a3
NOAA-17	-276.603	1.01805	1.49789	1.96181
NOAA-18	-275.493	1.01463	1.42759	1.68783
NOAA-19	-276.61174	1.01873	1.47374	1.88560
MetOp-A FRAC	-273.235	1.00711	1.49927	1.88373

Table: 5.15 Day time MC SST Dual Algorithm data

5.21.8 Night MCSST Triple

Satellite	a0	a1	a2	a3	a4
NOAA-12	-271.971	1.000281	0.911173	1.710028	
NOAA-14	-275.364	1.010037	0.920822	1.760411	
NOAA-15	-276.7558563	1.015354	1.0635723508	1.294955	
NOAA-16	-271.763	0.733532	1.01684	0.344182	-0.753123
NOAA-17	-274.622	1.00903	0.913248	0.440015	
NOAA-18	-274.398	1.00820	0.841674	0.377061	
NOAA-19	-275.24563	1.01084	0.81643	0.43235	
MetOp-A FRAC	-273.044	1.00424	0.894349	0.508159	

Table: 5.16 Night time MC SST Dual Algorithm data

5.22 Fittest Algorithm

Fittest Algorithm The “fittest” algorithm takes the form:

$$SST = c_0 + c_1 T_{11} + c_2 (T_{11} - T_{12}) T_4 + \frac{c_3 (T_{11} - T_{12})}{\cos(1.13 \times \theta_s)} + c_4 \times \cos(1.0078 \times \theta_a - 0.7099)$$

where: Ti is the brightness temperature at "= i #m !s is the satellite zenith angle !a is the angle on the mirror (a feature of the MODIS paddle-wheel mirror design) Which looks similar to the NLSST:

5.23 Variants of the new algorithms

* Terra SST4:

$$SST = c_0 + c_1 T_{4.0} + c_2 (T_{3.9} - T_{4.0}) T_{3.9} + \frac{c_3 (T_{3.9} - T_{4.0})}{cos(1.13 \times \theta_s)} + c_4 \times cos(1.0078 \times \theta_a - 0.7099)$$

* Terra SSTnight, SSTday, SST:

$$SST = c_0 + c_1 T_{11} + c_2 (T_{11} - T_{12}) + \frac{c_3 (T_{11} - T_{12})}{cos(1.13 \times \theta_s)} + c_4 \times cos(1.0078 \times \theta_a - 0.7099)$$

* Terra newSSTnight:

$$SST = c_0 + c_1 T_{3.9} + c_2 (T_{3.9} - T_{4.0}) + \frac{c_3 (T_{3.9} - T_{4.0})}{cos(1.13 \times \theta_s)} + c_4 \times cos(1.0078 \times \theta_a - 0.7099)$$

* Aqua SST4:

$$SST = c_0 + c_1 T_{3.9} + c_2 (T_{3.9} - T_{4.0}) T_{3.9} + \frac{c_3 (T_{3.9} - T_{4.0})}{cos(1.13 \times \theta_s)} + c_4 \times cos(1.0078 \times \theta_a - 0.7099)$$

* Aqua SSTnight, SSTday, SST:

$$SST = c_0 + c_1 T_{11} + c_2 (T_{11} - T_{12}) + \frac{c_3 (T_{11} - T_{12})}{cos(1.13 \times \theta_s)} + c_4 \times cos(1.0078 \times \theta_a - 0.7099)$$

* Aqua newSSTnight:

$$SST = c_0 + c_1 T_{3.8} + c_2 (T_{11} - T_{12}) T_{3.9} + \frac{c_3 (T_{11} - T_{12})}{cos(1.13 \times \theta_s)} + c_4 \times cos(1.0078 \times \theta_a - 0.7099)$$

5.23 Conclusion

Sea-surface temperature (SST) was one of the first ocean variables to be studied from earth observation satellites. Pioneering images from infrared scanning radiometers revealed the complexity of the surface temperature fields, but these were derived from radiance measurements at orbital heights and included the effects of the intervening atmosphere. Corrections for the effects of the atmosphere to make quantitative

estimates of the SST became possible when radiometers with multiple infrared channels were deployed in 1979. At the same time, imaging microwave radiometers with SST capabilities were also flown. Since then, SST has been derived from infrared and microwave radiometers on polar orbiting satellites and from infrared radiometers on geostationary spacecraft. As the performances of satellite radiometers and SST retrieval algorithms improved, accurate, global, high resolution, frequently sampled SST fields became fundamental to many research and operational activities.

Here we provide an overview of the physics of the derivation of SST and the history of the development of satellite instruments over half a century. As demonstrated accuracies increased, they stimulated scientific research into the oceans, the coupled ocean-atmosphere system and the climate. We provide brief overviews of the development of some applications, including the feasibility of generating Climate Data Records. We summarize the important role of the Group for High Resolution SST (GHRSST) in providing a forum for scientists and operational practitioners to discuss problems and results, and to help coordinate activities world-wide, including alignment of data formatting and protocols and research.

CHAPTER SIX

SPATIAL AND TEMPORAL DISTRIBUTION OF SEA SURFACE TEMPERATURE DURING THE LAST 20 YEARS IN THE BAY OF BENGAL

6.1 Introduction

Bangladesh is one of the most disaster-prone countries in the world and is a victim of frequent natural calamities like tropical cyclones, tornadoes, floods, storm surges and droughts. In most cases of cyclones and tornadoes, the Bay of Bengal plays an important role. The Bay of Bengal (BoB) forms the North-Eastern part of the Indian Ocean, opened to the Ocean to the South only, and in other directions, it is surrounded by land. The landmasses around the Bay have a profound effect on the weather regimes of the area and knowledge of the relevant physical features of these landmasses is essential to an understanding of the meteorological phenomenaaffecting the Bay of Bengal. Monsoon (June to September) rainfall is directly linked to the economic development and disaster management of the country. Sea Surface Temperature (SST) of the Bay of Bengal (BoB) has been linked to rainfall patterns in Bangladesh. Despite the recent advances in research and development and strategic shifts in agricultural methods, the summer monsoon variability over the Asian continent is still an important limiting factor for stable food production and thus for social and economic development in these regions.

6.2 Temporal distribution of SST

The temporal distribution of SST in four sampling seasons is summarized in table 6.1 There observed an increasingtrend of SST in the North region, temperature rise more in the North Andaman ranging between 28.24°C-30.33°C, 27.44°C - 29.43°C, 27.85°C - 29.86°C and26.40°C -28.36°C during pre-monsoon, monsoon, monsoon and winter

respectively. The SST for South Andaman of the south region also demonstrated increasingtrend ranging between 28.76°C-30.49°C, 27.77°C-29.50°C, 27.77°C-29.50°C and 27.38°C-28.92°C during pre-monsoon, monsoon, post-monsoon and winter respectively (Table 6.2) Similarly, there revealed an increasing-trend of SST over the Bay of Bengal ranging between 28.12°C - 30.09°C, 28.07°C - 29.81°C, 27.71°C- *29.43°*and *26.4TC-27.8TC* during pre-monsoon, monsoon, post-monsoon and winter respectively and found significant in the normal test. In the East Central Bay, the temperature ranged from 27.78°C-29.79°C and25.74°C - 27.53°C which found quite lower than that of the South East and the South West Bay in pre-monsoonand winter respectively, while in monsoon and post-monsoon, the temperature ranged from 27.94°C - 29.48°C,27.65°C - 29.63°C respectively. This seemed quite higher than that of the South East and the South West Bay.

The SST for West Central Bay, the temperature in pre-monsoon and winter ranged from 27.87°C - 29.96 °C and25.91°C - 27.59 °C and seemed quite higher than that of the West Bay and the North East Bay while in monsoon and post-monsoon the temperature ranged from 28.20°C - 29.60°C and 27.47°C-29.48°C respectively which seemed quite lower than that of the North West Bay and the North East Bay. The inter-annual variability of SST anomaly over the Bay of Bengal for the four seasons viz, winter (Dec-Feb), Pre-monsoon (Mar-May),SW Monsoon (Jun-Sep) and Post-monsoon (Oct-No v) respectively, for the period 1999-2018. The inter-annual variability of SST anomaly over the South Bay of Bengal for the four seasons is characterized by high degree variability

6.2.1 Pre-monsoon Average Minimum Temperature

BoB is being divided into six regions. A table showing the variation of Pre-monsoon average minimum temperature over the bay regions in the past twenty years is given below.

Pre-monsoon Average Minimum Temperature					
Region	1999	2003	2008	2013	2018
North West Bay	27.95	26.65	25.24	25.18	26.95
North East Bay	27.47	26.29	24.97	24.88	26.58
South West Bay	27.95	27.15	27.95	26.26	27.57
South East Bay	28.27	27.09	27.68	27.65	27.96
West Central Bay	27.62	27.46	26.58	25.52	27.07
East Central Bay	27.58	26.46	26.15	25.45	26.61

Table 6.1 BoB Pre-monsoon Average Minimum Temperature

Analyzing the variation average minimum temperature in the Bay of Bengal regions we can see the successive decrease of temperature in the North West ba, North East, West Central and East Central Bay from 1999 but increase in 2018. While in the regions of South East Bay, the temperature decreased up to 2003 but started to increase after then. On the contrary, the variation of temperature in the South West Bay is has shifted a couple of times.

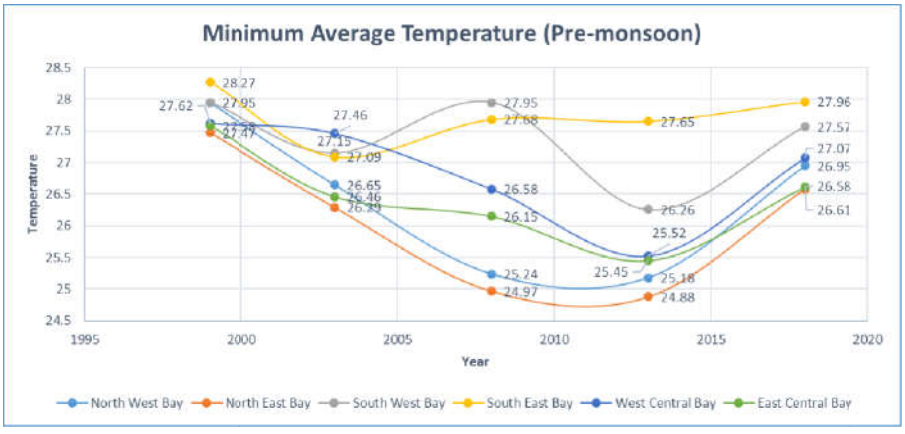


Figure 6.1 BoBPre-monsoon Average Minimum Temperature

6.2.2 Pre-monsoon Average Maximum Temperature

BoB is being divided into six regions. A table showing the variation of pre-monsoon average maximum temperature over the bay regions in the past twenty years is given below.

Pre-monsoon Maximum Average Temperature					
Region	1999	2003	2008	2013	2018
North West Bay	30.31	30.6	30.33	30.24	30.3
North East Bay	30.67	30.2	30.26	30.5	30.82
South West Bay	30.31	30.15	30.17	28.69	31.16
South East Bay	30.38	30.52	29.56	31.04	30.64
West Central Bay	30.35	30.19	30.68	31.02	31.21
East Central Bay	30.55	30.31	29.67	31.02	30.85

Table 6.2: BoB Pre-monsoon Average Maximum Temperature

Analyzing the Pre-monsoon maximum average temperature anomaly in the regions of BoB, we can see the increase of temperature in the West Central and the North East Bay. While in the East Central and the South East Bay, the maximum average temperature shifted a couple of times in the past twenty years. In the South West Bay regions, the temperature has not changed much up to 2008 but critically decreased in 2013 and then gradually increased.

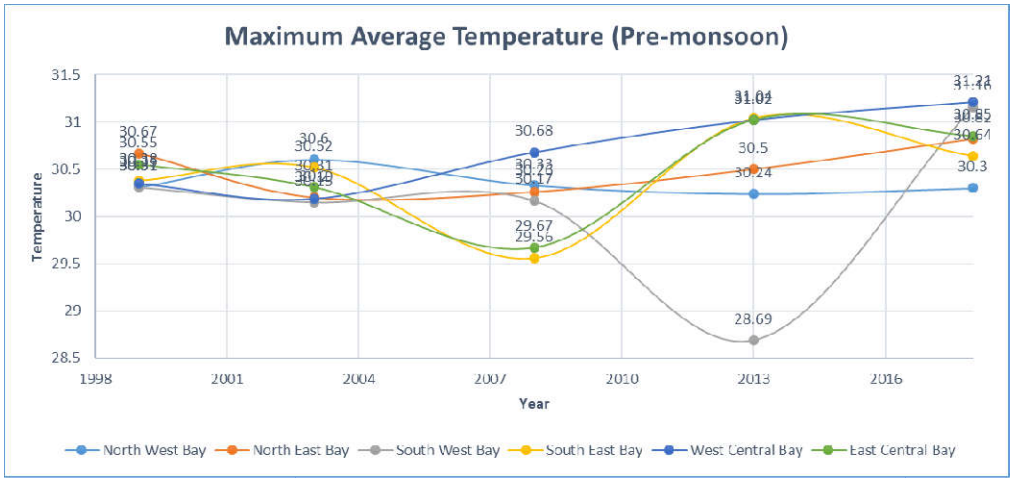


Figure 6.2: BoBPre-monsoon Average Maximum Temperature

6.2.3MonsoonAverageMinimum Temperature

BoB is being divided into six regions. A table showing the variation of monsoon average minimum temperature over the bay regions in the past twenty years is given below

Monsoon Average Minimum Temperature					
Region	1999	2003	2008	2013	2018
North West Bay	26.71	27.57	26.85	27.7	28.01
North East Bay	26.77	27.81	27.3	28.14	27.81
South West Bay	26.71	28.15	27.16	27.04	27.26
South East Bay	26.93	28.02	27.21	27.73	27.72
West Central Bay	26.6	27.62	26.08	27.52	27.95
East Central Bay	26.72	27.65	26.55	27.73	27.58

Table 6.3: BoB Monsoon Average Minimum Temperature

Analyzing the monsoon minimum average temperature anomaly in the BoB regions over the past twenty years we can see, the temperature has shifted a couple of times similarly in the North East, North West, South East, East Central and West Central Bay regions. But the maximum average temperature in the South West Bay regions has shifted once and then gradually increased.

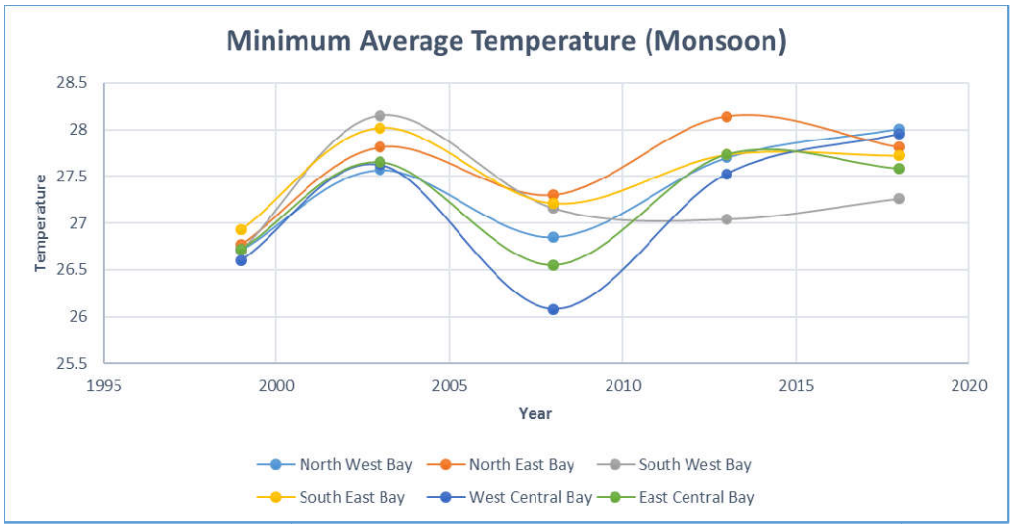


Figure 6.3 BoB Monsoon Average Minimum Temperature

6.2.4 Monsoon Average Maximum Temperature

BoB is being divided into six regions for better understanding. A table showing the variation of monsoon average maximum temperature over the bay regions in the past twenty years is given below.

Monsoon Average Maximum Temperature					
Region	1999	2003	2008	2013	2018
North West Bay	29.19	29.68	30.43	30.53	31.5
North East Bay	30	29.62	30.38	30.04	31.15
South West Bay	29.19	29.84	29.98	29.89	30.71
South East Bay	29.06	29.68	29.49	29.61	30.18
West Central Bay	29.7	29.67	30.43	30.25	30.83
East Central Bay	29.32	29.69	30.15	29.69	30.58

Table 6.4: BoB Monsoon Average Maximum Temperature

Analyzing the monsoon average temperature anomaly in the Bay regions of BoB, we can a slight increase in temperature in the past twenty years. Of all the six Bay regions comparatively, the South East Bay region has the least increase in temperature.

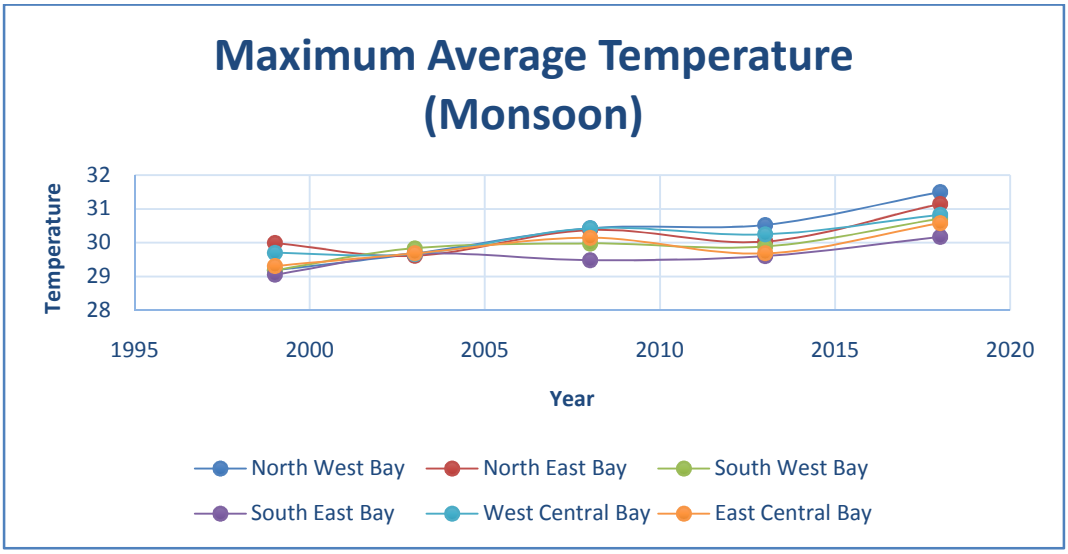


Figure 6.4: BoB Monsoon Average Maximum Temperature

6.2.5 Post-monsoon Average Minimum Temperature

BoB is being divided into six regions. A table showing the variation of Post-monsoonAverage Minimum Temperatureover the bay regions in the past twenty years is given below.

Post-monsoonAverageMinimum Temperature					
Region	1999	2003	2008	2013	2018
North West Bay	26.99	27.71	27.9	27.29	27.28
North East Bay	27.67	27.46	28.06	27.45	27.15
South West Bay	26.99	27.22	27.79	27.63	27.98
South East Bay	27.27	27.7	27.82	27.42	28.15
West Central Bay	26.88	27.71	27.93	27.56	28.17
East Central Bay	26.94	27.57	27.96	27.58	27.95

Table 6.5: Post-monsoon Average Minimum Temperature

Analyzing the Post-monsoon Average Minimum Temperature over twenty years we can see that, the gradual increase in temperature in all the Bay regions up to 2008 and a gradual decrease in 2013. Then the temperature gradually increased in the East Central, West Central, South West and South East Bay regions in 2018. On the contrary, the temperature tends to gradually decrease in the North East and The North East Bay regions.

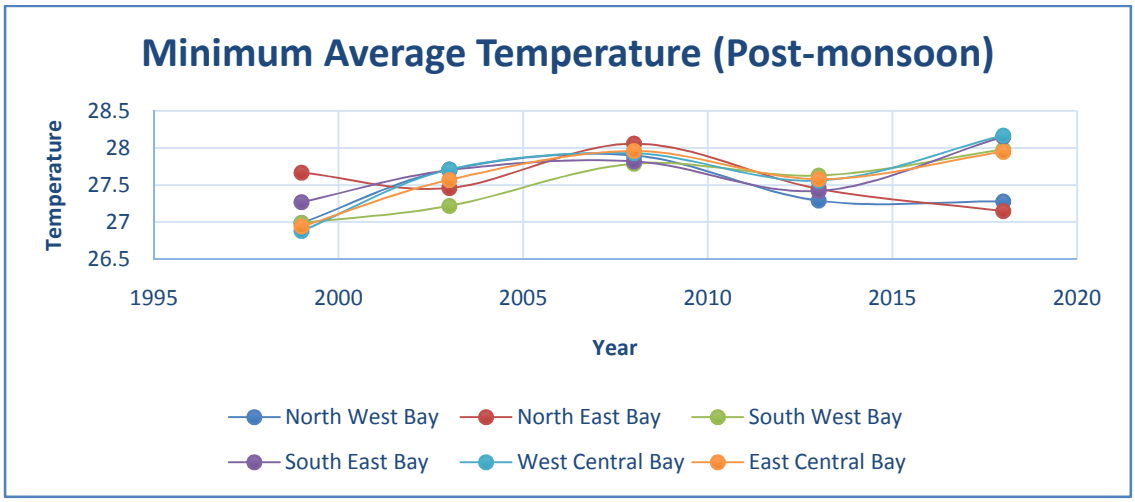


Figure 6.5: BoB Post monsoon Average Minimum Temperature

6.2.6 Post-monsoon Average Maximum Temperature

BoB is being divided into six regions for better understanding. A table showing the variation of Post-monsoon Average Maximum Temperatureover the bay regions in the past twenty years is given below.

Post-monsoon Average Maximum Temperature					
Region	1999	2003	2008	2013	2018
North West Bay	29.44	29.59	29.83	30	31.5
North East Bay	29.76	29.95	29.73	29.46	30.89
South West Bay	29.44	29.67	29.68	29.36	30.21
South East Bay	29.07	29.54	29.9	29.49	30.38
West Central Bay	29.41	29.75	30.13	29.96	31.02
East Central Bay	29.42	29.8	29.8	29.57	31.23

Table 6.6 Post-monsoon Average Maximum Temperature

Analyzing the Post-monsoon Average Maximum Temperature anomalyin the regions of BoB, we can see the gradual increase in temperature until 2013 but a sudden increase in temperature in 2018.

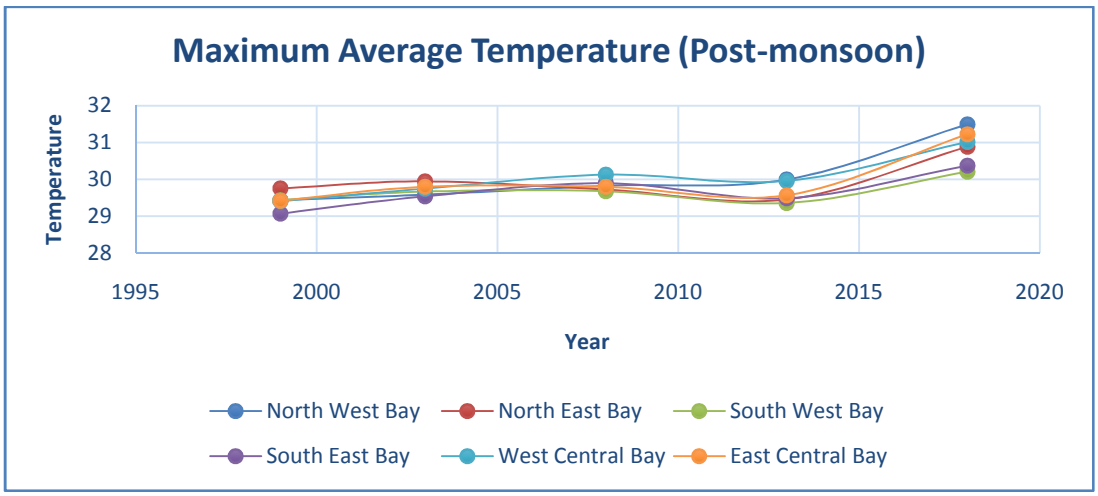


Figure 6.6: Post-monsoon Average Maximum Temperature

6.2.7 Winter Average Minimum Temperature

BoB is being divided into six regions. A table showing the variation of Winter Average Minimum Temperatureover the bay regions in the past twenty years is given below.

Winter Average Minimum Temperature					
Region	1999	2003	2008	2013	2018
North West Bay	26.42	24.46	23.44	23.26	24.21
North East Bay	24.03	23.34	23.22	22.44	23.92
South West Bay	26.42	27.07	26.83	26.26	26.15
South East Bay	27.05	27.32	27.1	26.61	27.13
West Central Bay	25.72	25.7	25.35	25.23	25.38
East Central Bay	25.84	25.58	25.13	24.16	25.01

Table 6.7: Winter Average Minimum Temperature

Analyzing the variation of Winter Average Minimum Temperatureover the bay regions we can see a gradual change in temperature over the past twenty years. Of all the regions, the temperature significantly decreased in the North West Bay.

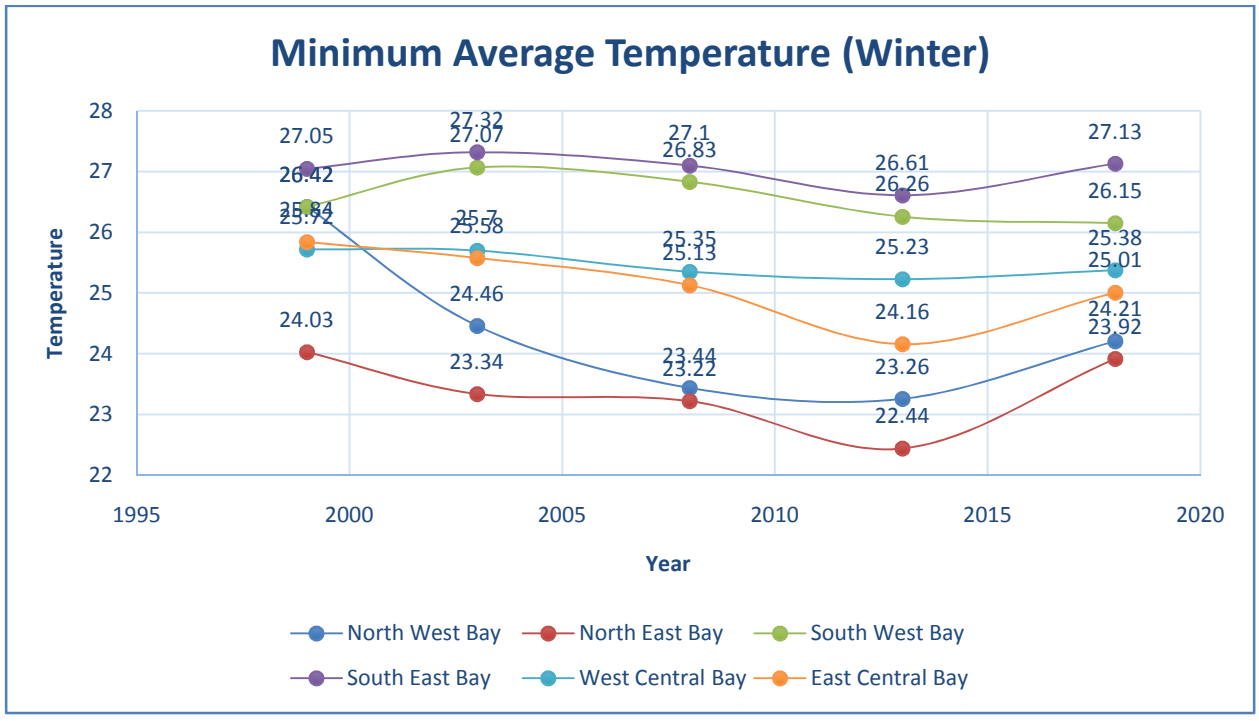


Figure 6.7: Winter Average Minimum Temperature

6.2.8 Winter Average Maximum Temperature

BoB is being divided into six regions. A table showing the variation of Winter Average Maximum Temperatureover the bay regions in the past twenty years is given below.

Winter Average Maximum Temperature					
Region	1999	2003	2008	2013	2018
North West Bay	28.6	27.82	27.99	27.94	27.73
North East Bay	28.27	28.02	28.1	28.06	28.46
South West Bay	28.6	29.1	29.21	28.69	29.32
South East Bay	28.99	29.56	29.35	29.17	29.69
West Central Bay	28.67	28.44	28.48	28.2	28.59
East Central Bay	28.59	28.78	28.6	28.63	28.82

Table 6.8: Winter Average Maximum Temperature

Analyzing the variation of Winter Average Maximum Temperature anomaly we see the gradual change of temperature over the past twenty years where the maximum temperature rose in South East Bay and the least temperature in the West Central Bay region.

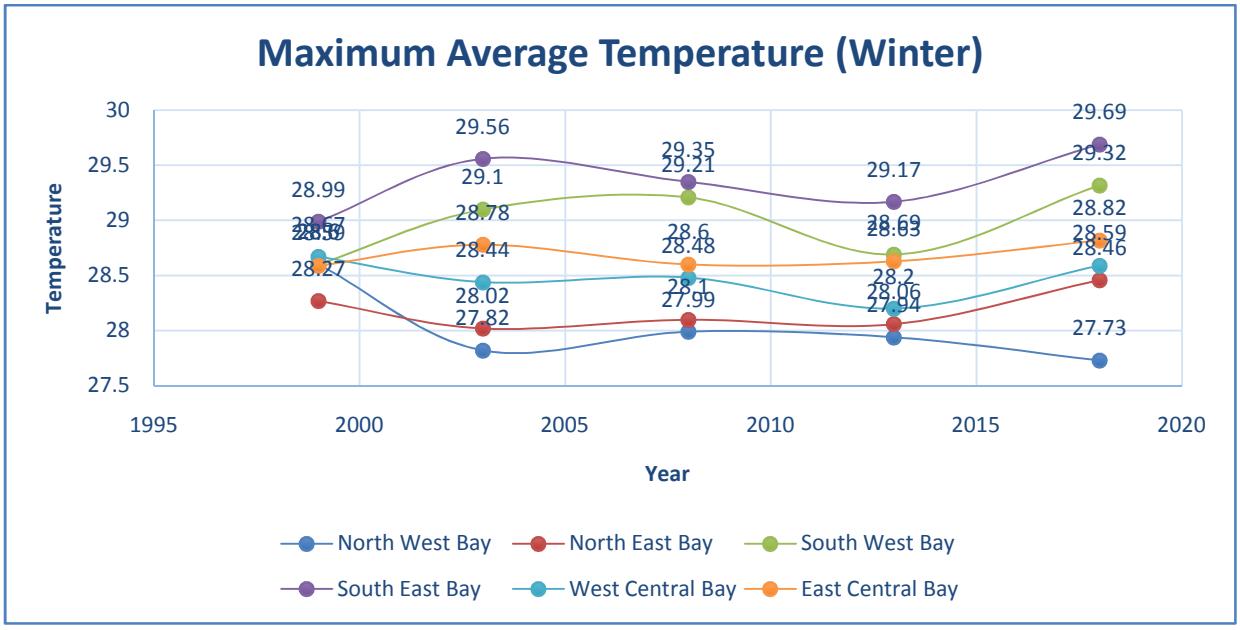


Figure 6.8: Winter Average Maximum Temperature

6.2.9 Bay of Bengal region and season wise average Min and Max temperature variation from 1999 to 2018

A comparable minimum and maximum variation of temperature in the Pre-monsoon, Monsoon, Post-monsoon, and Winter season is shown in a table below:

Season	Pre-monsoon		Monsoon		Post-monsoon		Winter	
Region/Value	Min_Var	Max_Var	Min_Var	Max_Var	Min_Var	Max_Var	Min_Var	Max_Var
North West Bay	-0.05	-0.0005	0.065	0.1155	0.0145	0.103	-0.1105	-0.0435
North East Bay	-0.0445	0.0075	0.052	0.0575	-0.026	0.0565	-0.0055	0.0095
South West Bay	-0.019	0.0425	0.0275	0.076	0.0495	0.0385	-0.0135	0.036
South East Bay	-0.0155	0.013	0.0395	0.056	0.044	0.0655	0.004	0.035
West Central Bay	-0.0275	0.043	0.0675	0.0565	0.0645	0.0805	-0.017	-0.004
East Central Bay	-0.0485	0.015	0.043	0.063	0.0505	0.0905	-0.0415	0.0115

Table 6.9: Bay of Bengal region and season wise average Min and Max temperature variation

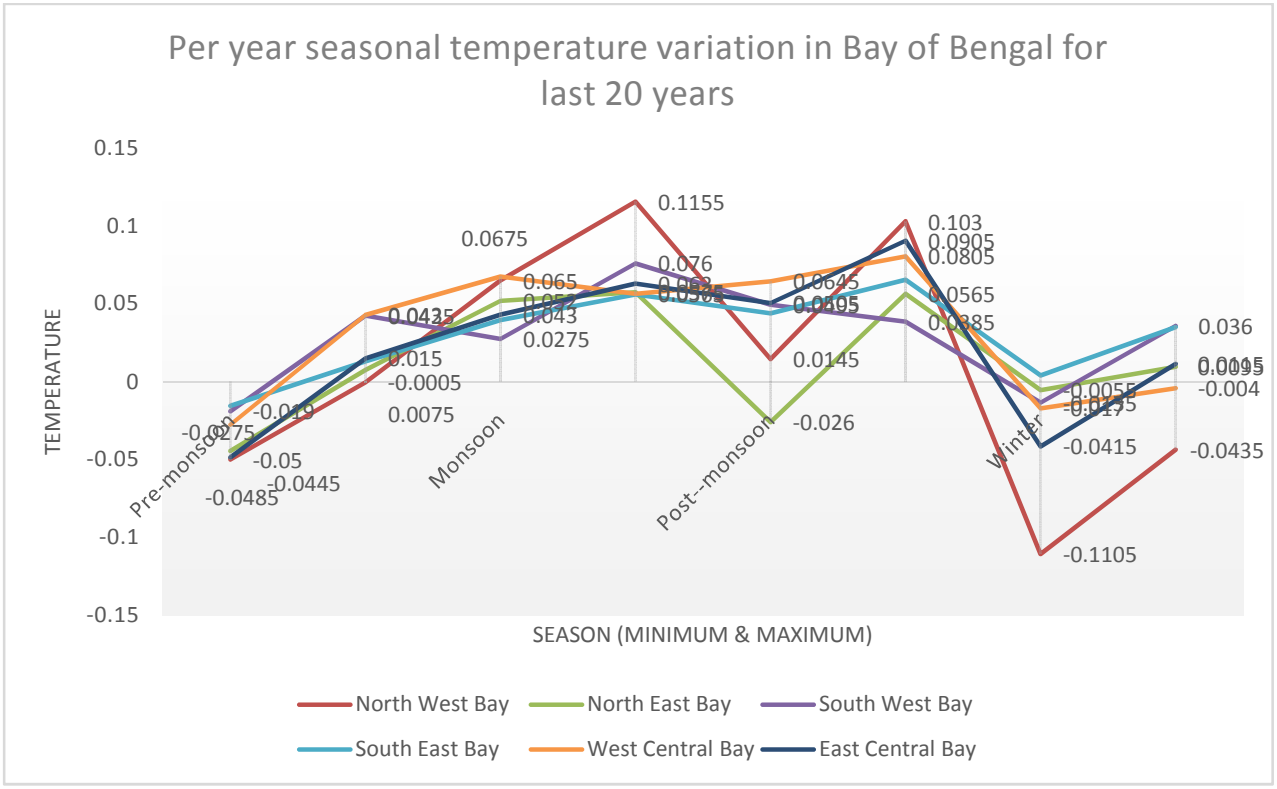


Figure 6.9: Bay of Bengal region and season wise average Min and Max temperature variation

6.2.10 Bay of Bengal average Min and Max temperature from 1999 to 2018

A graph showing the variation of Minimum and Maximum Average Temperature in context to linear momentum over the past twenty years from 1999 to 2018 in the Bay of Bengal where the maximum temperature anomaly has increased progressively and the minimum temperature anomaly has reduced regressively is specified below:

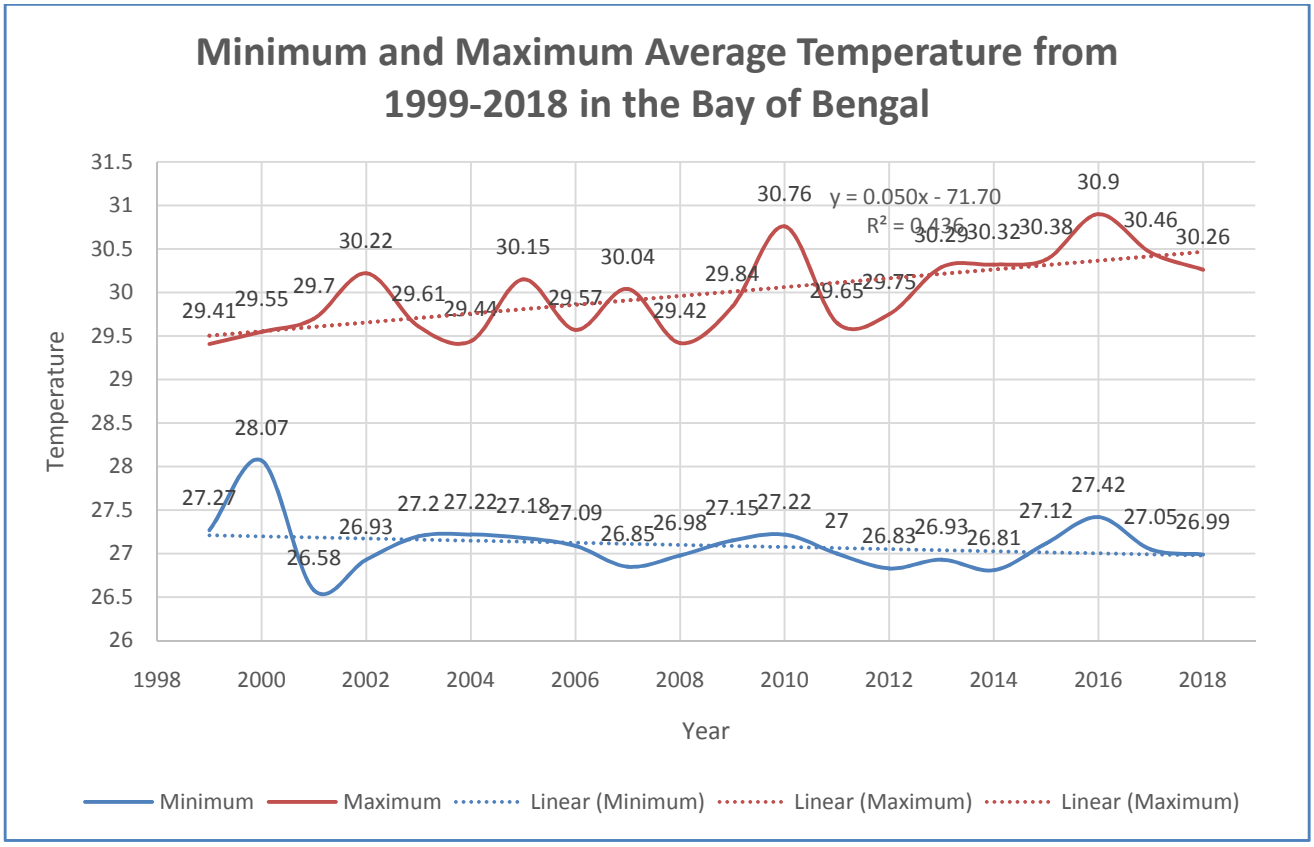


Figure 6.10: Bay of Bengal average Min and Max temperature from 1999 to 2018

The variation of yearly minimum and maximum temperature anomaly over the past twenty years from 1999 to 2018 has been stated in a chart below:

Year	Minimum	Maximum			
1999	27.27	29.41	2009	27.15	29.84
2000	28.07	29.55	2010	27.22	30.76
2001	26.58	29.7	2011	27	29.65
2002	26.93	30.22	2012	26.83	29.75
2003	27.2	29.61	2013	26.93	30.29
2004	27.22	29.44	2014	26.81	30.32
2005	27.18	30.15	2015	27.12	30.38
2006	27.09	29.57	2016	27.42	30.9
2007	26.85	30.04	2017	27.05	30.46
2008	26.98	29.42	2018	26.99	30.26

6.2.11 Seasonal Min and Max temperature from 1999 to 2018

The temperature variation in the regions of the Bay of Bengal is not absolute. From the analogous seasonal minimum and maximum temperature anomaly over the past twenty years in the Bay regions of Bay of Bengal, we see both the maximum and minimum temperature variation is found in the regions of North West Bay. A comparative seasonal temperature variation in the regions of Bay of Bengal from 1999 to 2018 is presented in the graph below.

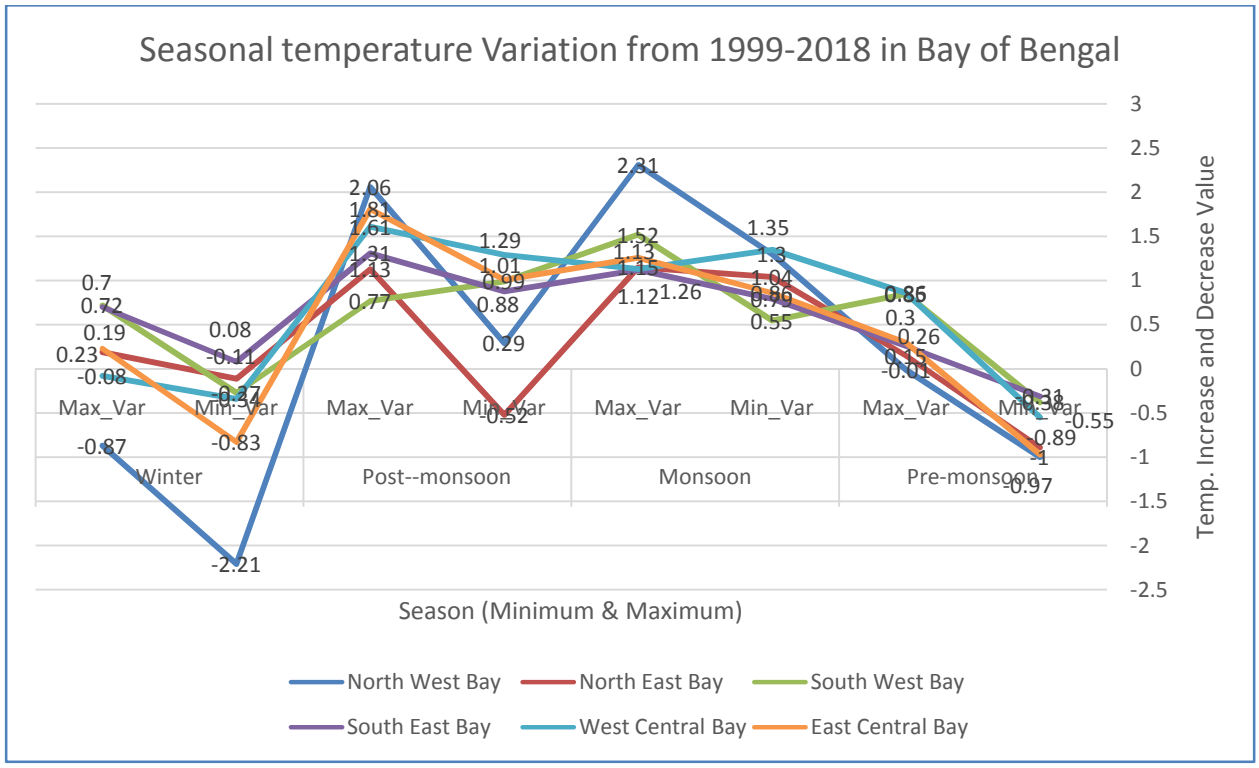


Figure 6.11: Seasonal Min and Max temperature from 1999 to 2018

6.2.12 Seasonal Averagetemperature variationfrom 1999 to 2018

The Seasonal Average temperature variation in correspondent to their value from 1999 to 2018 is shown in the table below:

Region/Value	Pre-monsoon		Monsoon		Post--monsoon		Winter	
	Min	Max	Min	Max	Min	Max	Min	Max
Average	-0.68333	0.401667	0.981667	1.415	0.656667	1.448333	-0.61333	0.148333

Table 6.11: Seasonal Average temperature variation from 1999 to 2018

From the seasonal average temperature variation from 1999 to 2018 in the Bay of Bengal we can see the heighest temperature in Post-monsoon and the least temperature in winter.

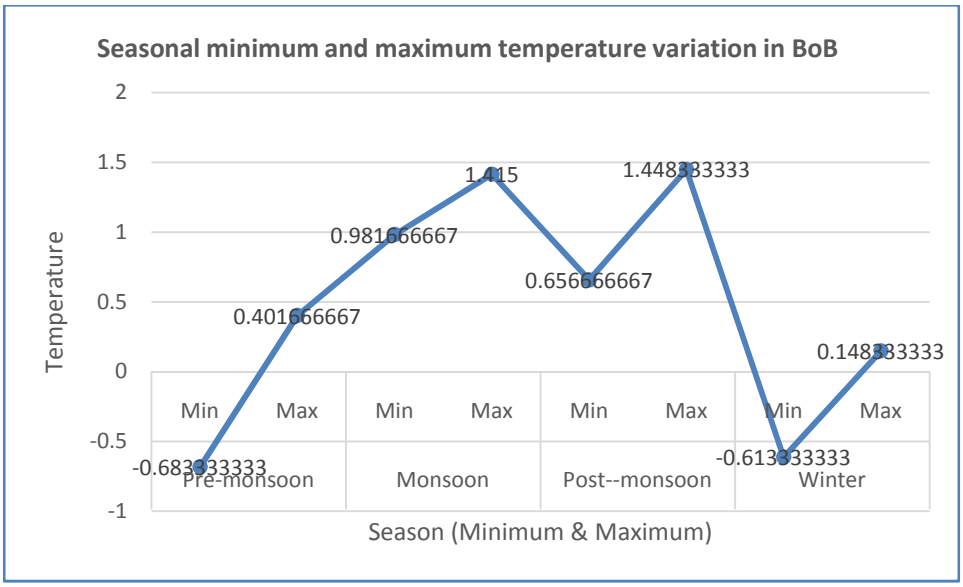
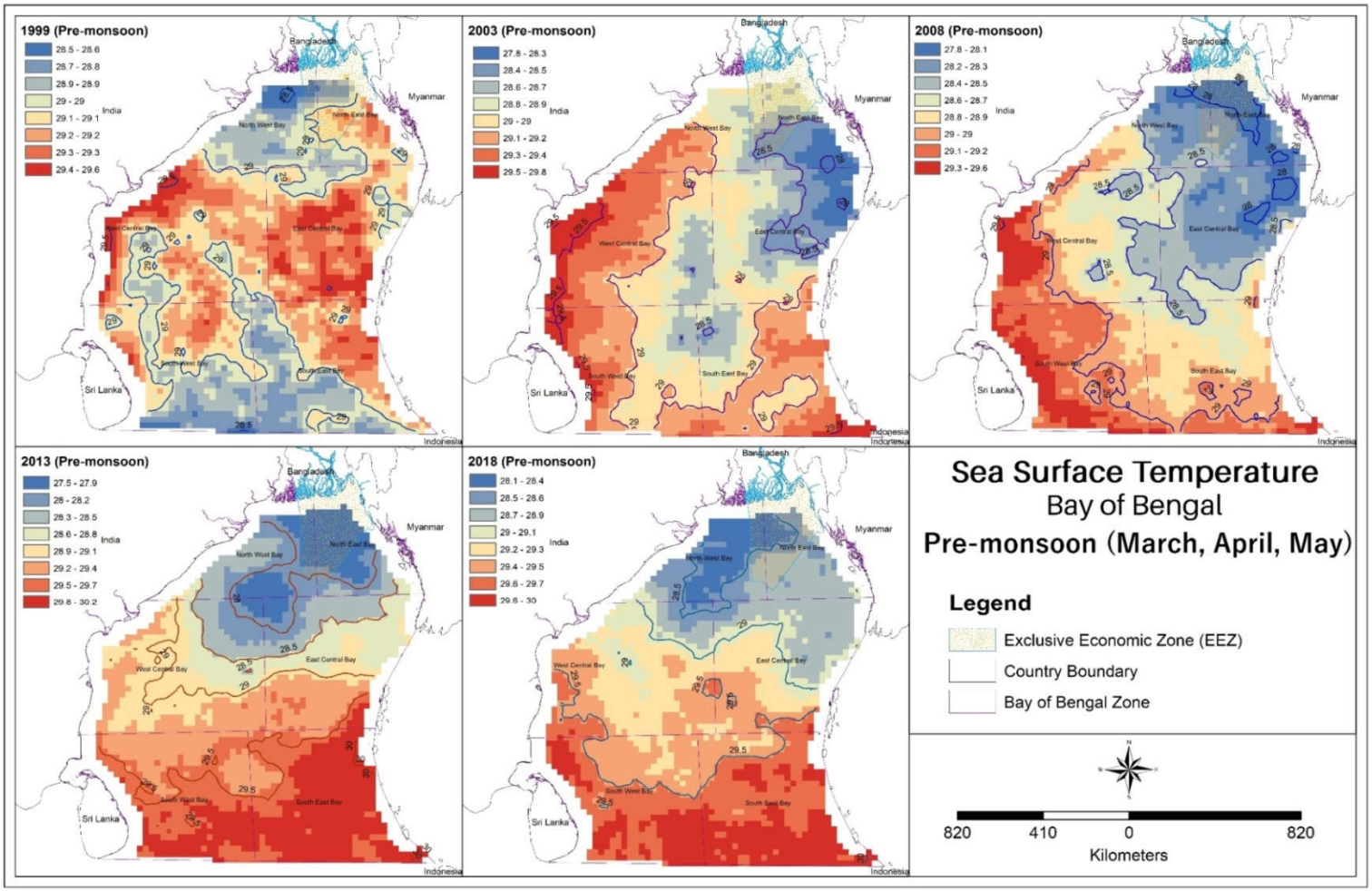


Figure 6.12: Seasonal Average temperature variation from 1999 to 2018

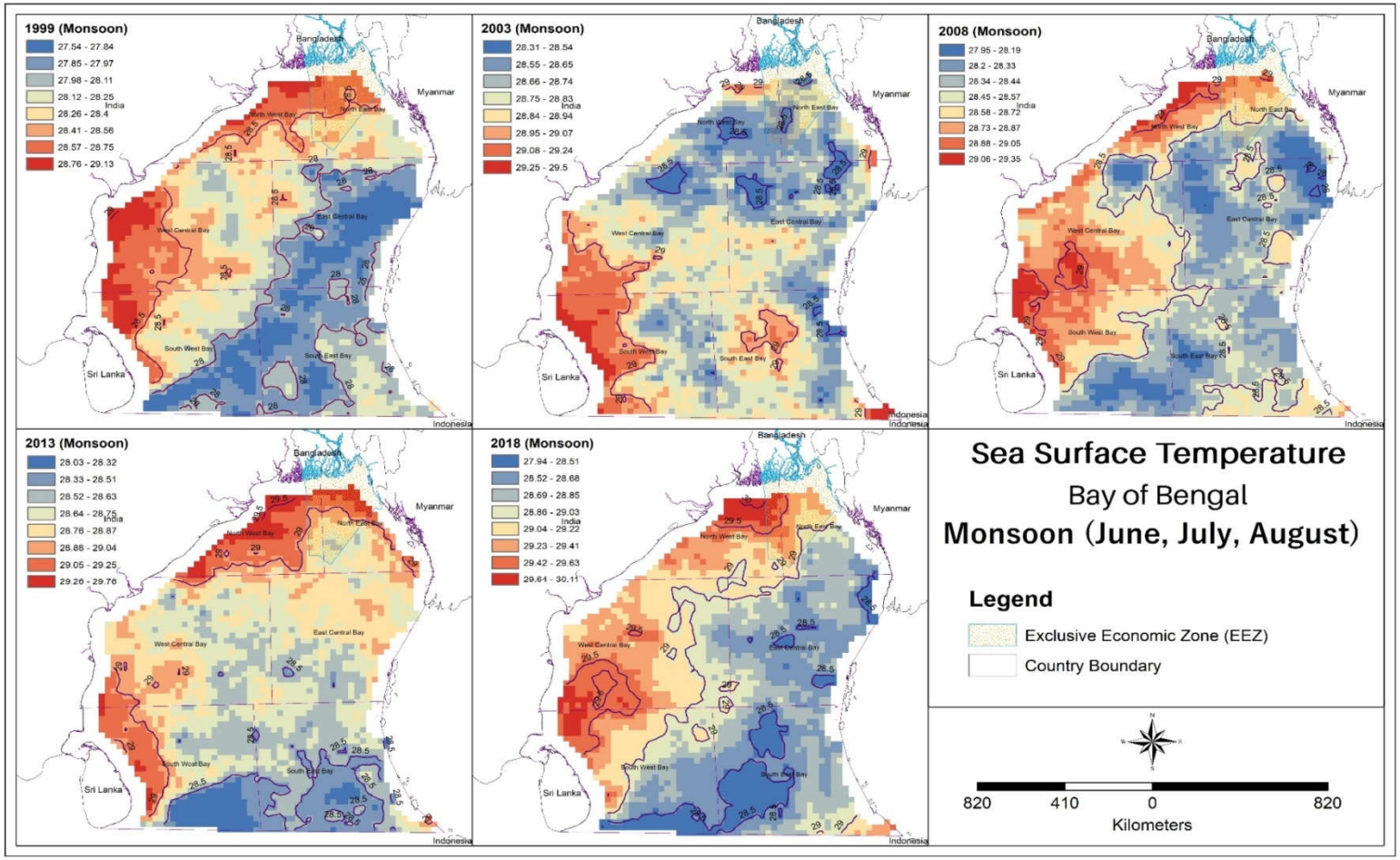
6.2.13 Bay of Bengal Pre-monsoon Average Temperature from 1999 to 2018

The average SST anomaly in the Pre-monsoon season over the past twenty years from 1999 to 2018 is shown in the map below



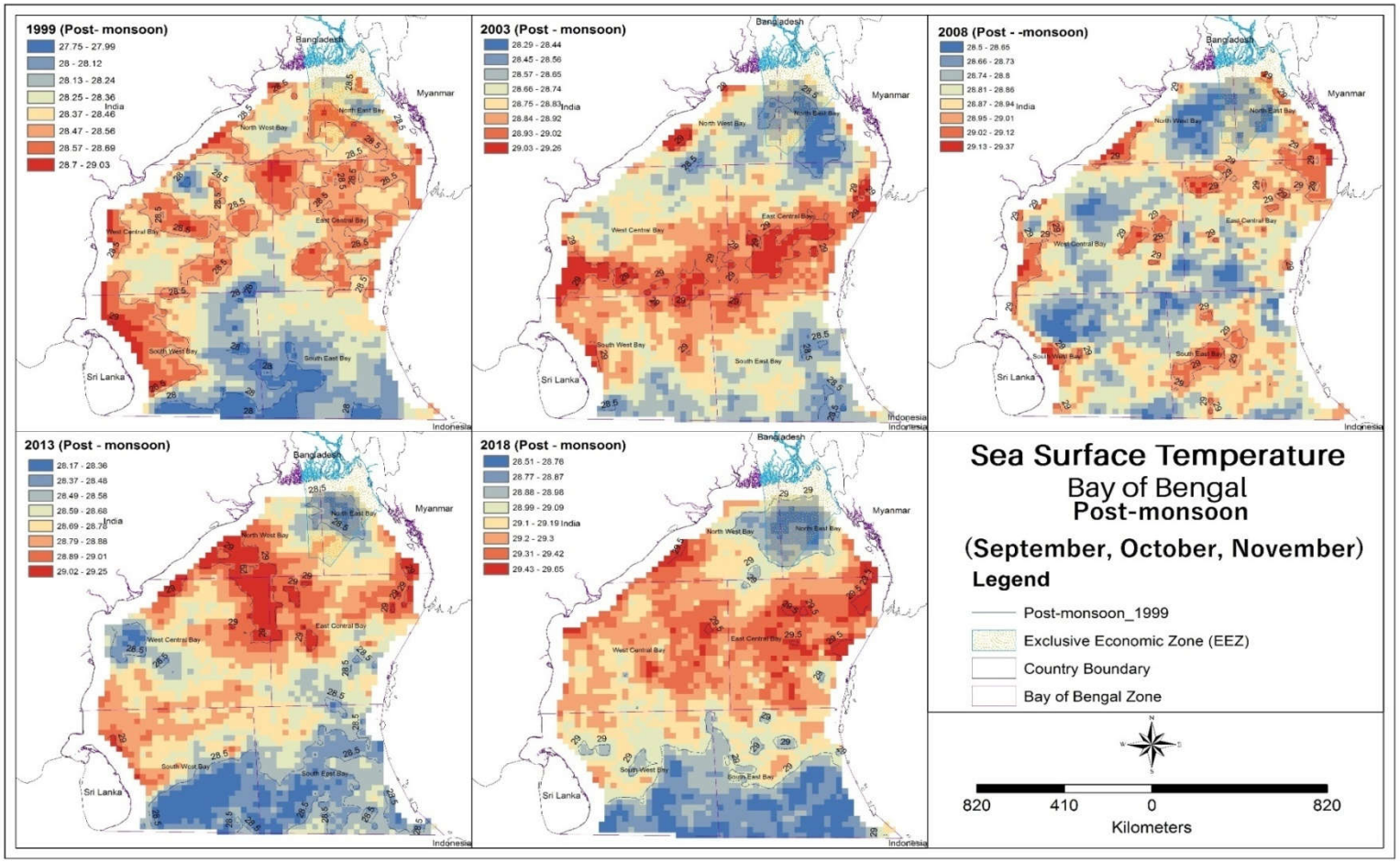
6.2.14 Bay of Bengal Monsoon Average Temperature from 1999 to 2018

The average SST anomaly in the Monsoon season over the past twenty years from 1999 to 2018 is presented in the map below



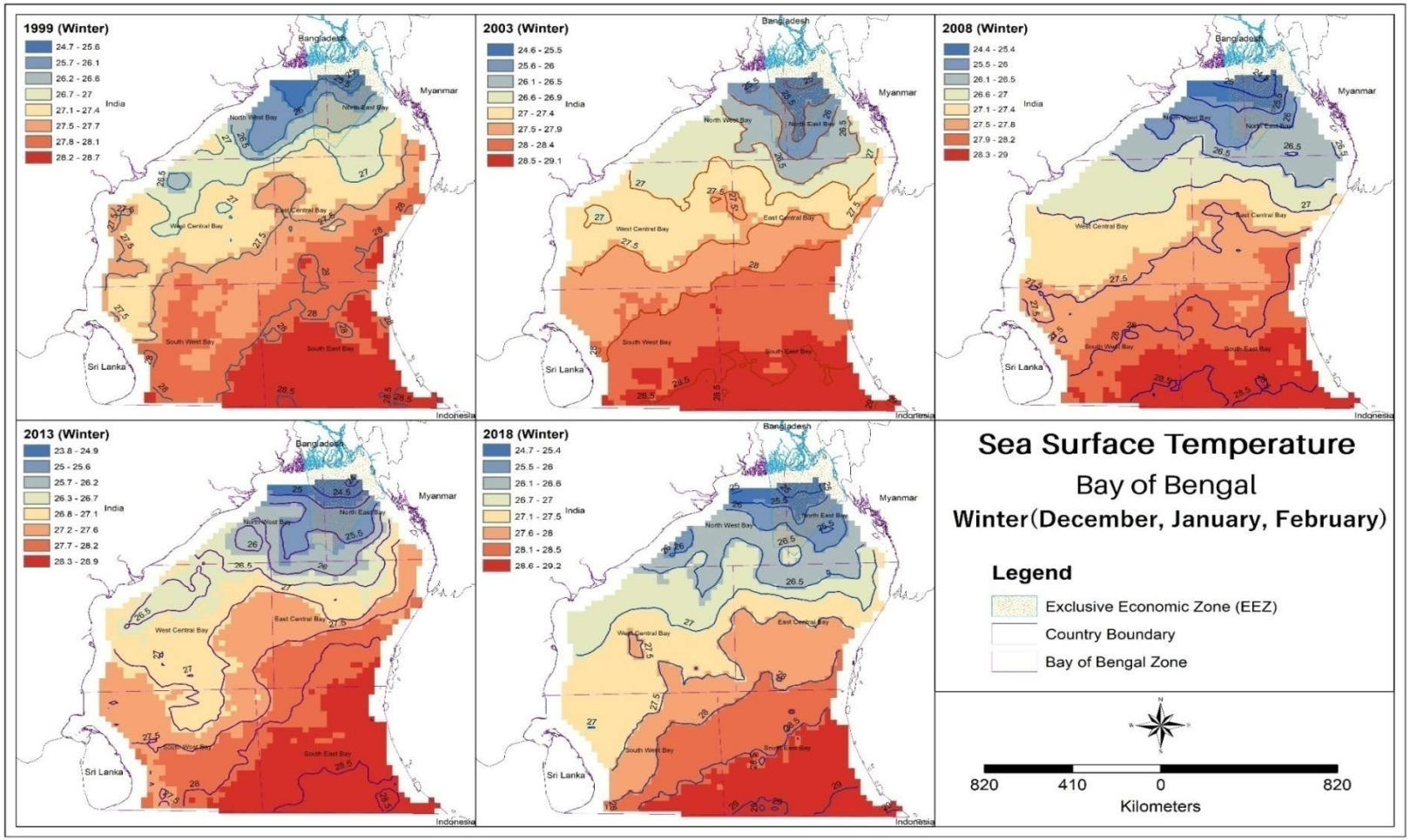
6.2.15 Bay of Bengal Post-monsoon Average Temperature from 1999 to 2018

The average SST anomaly in the Post-monsoon season over the past twenty years from 1999 to 2018 is presented in the map below



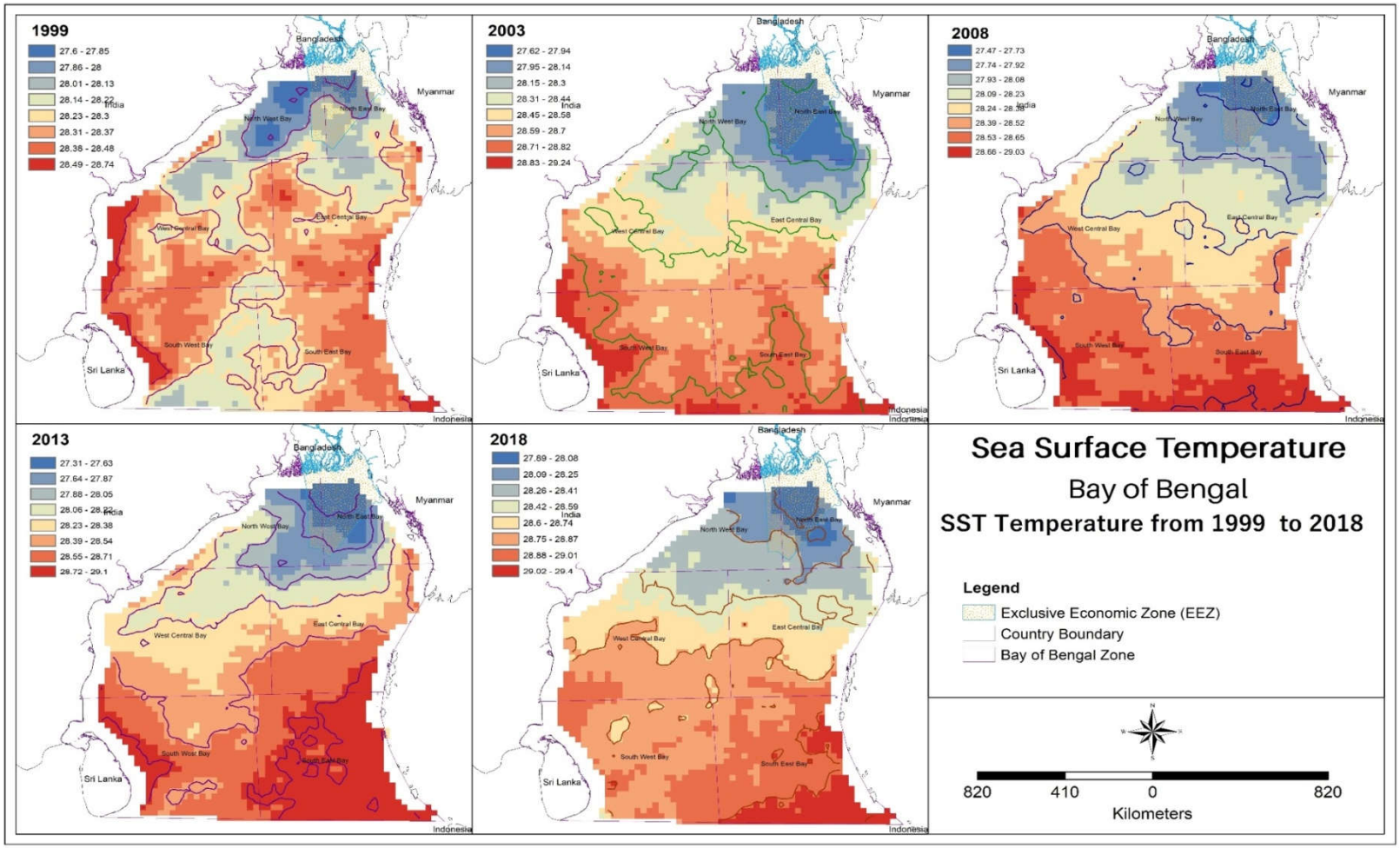
6.2.16 Bay of Bengal Winter Average Temperature from 1999 to 2018

The average SST anomaly in the Winter season over the past twenty years from 1999 to 2018 is presented in the map below



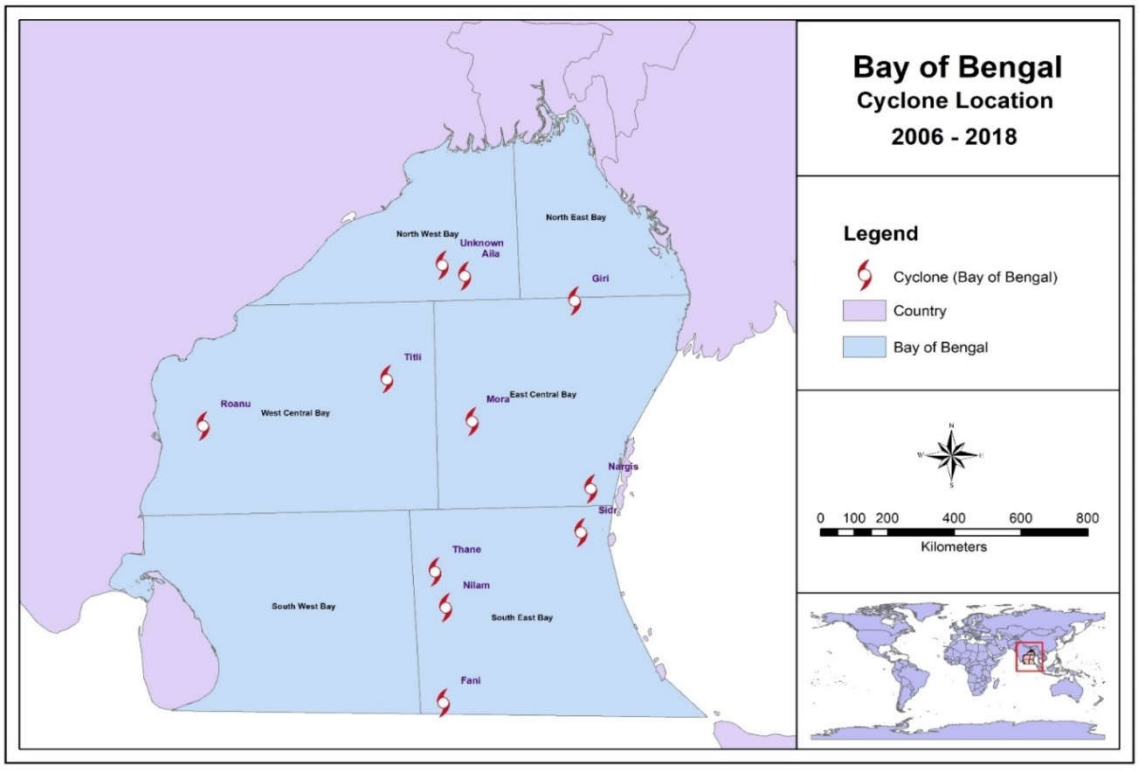
6.2.17 Bay of Bengal Yearly Average Temperature from 1999 to 2018

The yearly average SST anomaly in over the past twenty years from 1999 to 2018 is presented in the map below



6.3 Sea Surface Temperature and Tropical Cyclone Intensity

In most cyclone prediction models, sea surface temperature (SST) is the only oceanographic input, even though storms are known to be impacted by the thermal energy available through oceanic heat content, not just by SST alone. In the tropical Indian Ocean (TIO 30° S -30° N, 30-120° E), there are no studies that examine the relationship between instantaneous cyclone intensity (CI) and SST as a function of time. Here, we explore that relationship using SST data from the Tropical Rainfall Measuring Mission Microwave Imager and CI data (maximum sustained winds) from the Joint Typhoon Warning Centre. We find that out of 75 TIO cyclones studied during 1998-2011, more than 50% of the cyclones have no significant correlation between CI and SST. The numbers having significant negative (positive) correlations are 31 (3), 13 (10), and 17 (14) with SST leading CI by one, two, and three days, respectively. These results demonstrate that SST is not a useful indicator of CI in the TIO.



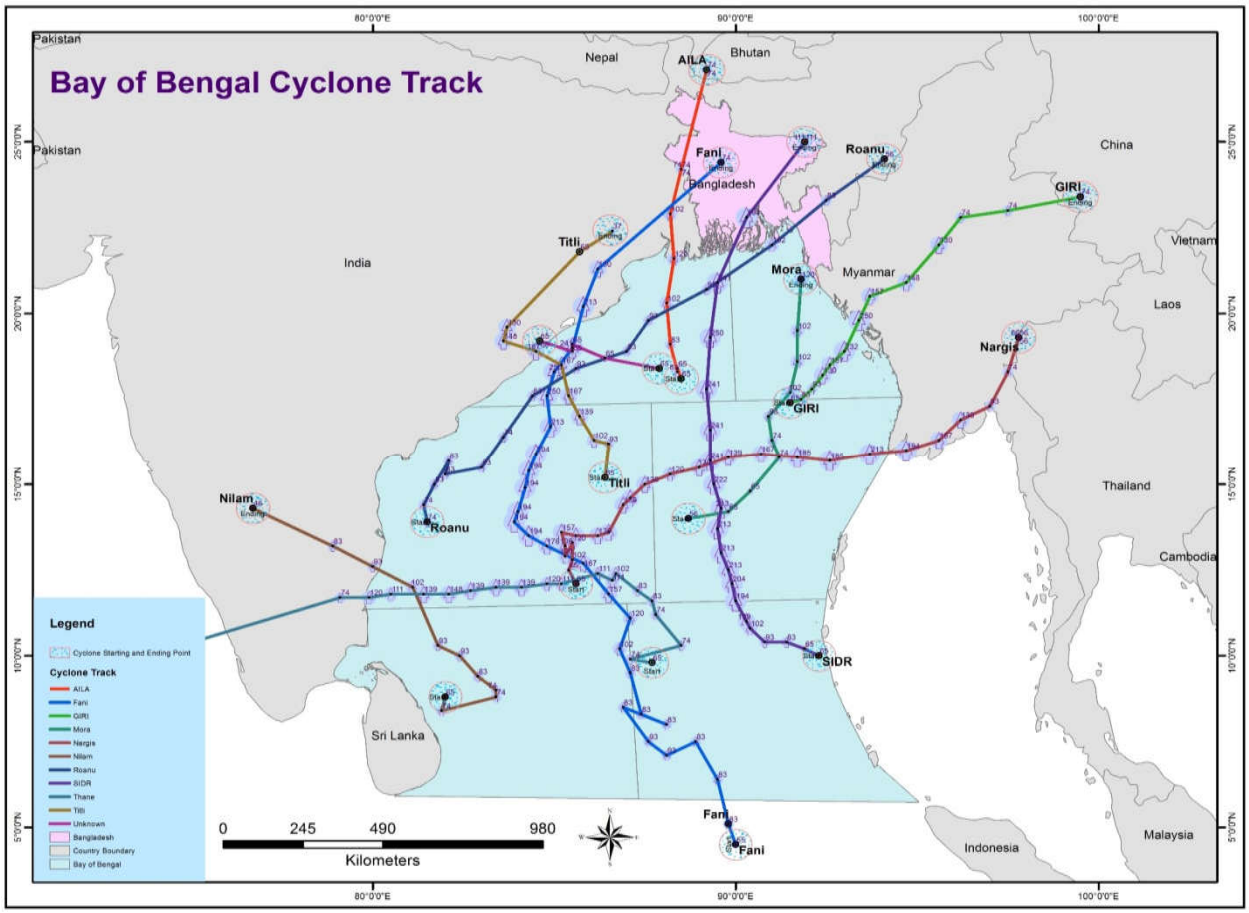
Map 6.1: Bay of Bengal Cyclone Location

A set of data comprising of the names of Cyclones, date, year and season of occurrence, region, wind speed, and level of cyclone is stated in a chart below.

Year	Date	Season	Temp.	Name	Region	Wind.S (Kts)	Wind.S (Kmph)	Levels
2006	28-Sep	Post-monsoon	28.45	Unknown	North West Bay	<64	118.4	Violent storm
2007	11-Nov	Post-monsoon	28.16	Sidr	South East Bay	>=96	177.6	Hurricane
2008	28-Apr	Pre-monsoon	29.46	Nargis	East Central Bay	>=96	177.6	Hurricane
2009	24-May	Pre-monsoon	27.87	Aila	North West Bay	>64	118.4	Hurricane
2010	21-Oct	Post-monsoon	28.1	Giri	North East Bay	>=96	177.6	Hurricane
2011	25-Dec	Winter	27.19	Thane	South East Bay	>64	118.4	Hurricane
2012	29-Oct	Post-monsoon	28.79	Nilam	South East Bay	<64	118.4	Violent storm
2016	18-May	Pre-monsoon	29.59	Roanu	West Central Bay	<64	118.4	Violent storm
2017	27-May	Pre-monsoon	30.62	Mora	East Central Bay	>64	118.4	Hurricane
2018	10-Sep	Post-monsoon	28.86	Titli	West Central Bay	>64	118.4	Hurricane
2019	27-Apr	Pre-monsoon	29.8	Fani	South East Bay	>=96	177.6	Hurricane

Table 6.12: Bay of Bengal Cyclone track, data, season, temperature, region, intensity and Levels.

6.4 Bay of Bengal Cyclone Track from 2006 to 2018



Map 6.2: Bay of Bengal Cyclone Track from 2006 to 2018

6.5 Conclusion

The results of the present study reveals that the sea surface warming trend is more distinct in the winter in the Southern Bay which is .45°C higher than the past and in other season this variation is more less. This result indicates that the Sea Surface Temperature shows increasing trend overtime which is significant to cause sea level rise. Further analyses with observational and model data for climatic variable are needed. A well interpreted Sea Surface Temperature (SST) can be utilized to detect the surface temperature signature for forecasting cyclones. Using long - term observational data records and extensive experimentation with numerical models of various degrees of sophistication and the complex interactions between the atmosphere and ocean in different geographical settings are now gradually unraveling. Overall, the combined impact of global ocean warming results in increasing winter time Sea Surface Temperature (SST) variability in Bay of Bengal and marine ecosystem.

CHAPTER SEVEN

CONCLUSION

7.1 Conclusion

The results of the present study reveals that the sea surface warming trend is more distinct in the winter in the Southern Bay which is.45°C higher than the past and in other season this variation is more less. This result indicates that the Sea Surface Temperature shows increasing trend overtime which is significant to cause sea level rise. Further analyses with observational and model data for climatic variable are needed. A well interpreted Sea Surface Temperature (SST) can be utilized to detect the surface temperature signature for forecasting cyclones. Using long - term observational data records and extensive experimentation with numerical models of various degrees of sophistication and the complex interactions between the atmosphere and ocean in different geographical settings are now gradually unraveling. Overall, the combined impact of global ocean warming results in increasing winter time Sea Surface Temperature (SST) variability in Bay of Bengal and marine ecosystem.

Reference

1. Aiki H, Takahashi K, Yamagata T (2006) The Red Sea outflow regulated by the Indian monsoon. Continental Shelf Research 26: 1448-1468.
2. Al Saafani MA, ShenoiSSC (2006) Seasonal and interannual variability of eddy field and surface circulation in the Gulf of Aden.
3. Ali M.M., Swain D., Kashyap T., McCreary J.P., Nagamani P.V. 2013b. Relationship between cyclone intensities and sea surface temperature in the tropical Indian Ocean. IEEE Geoscience and Remote Sensing Letters.
4. Allen M, Smith LA (1996) Monte Carlo SSA: Detecting irregular oscillations in the Presence of colourednoise.J Clim93373-3404.
5. Almogi-Labina A, Schmiedl G, Hemleben C, Siman-Tov R, Segl M, et al. (2000) The influence of the NE winter monsoon on productivity changes in the Gulf of Aden, NW Arabian Sea, during the last 530 ka as recorded by foraminifera. Marine Micropaleontology 40: 295-319.
6. Ashok K., Guan Z., Saji N.H., Yamagata T. 2004. Individual and combined influences of ENSO and the Indian Ocean Dipole on the Indian Summer Monsoon. J Clim.
7. Ashok, K., Z. Guan, and T. Yamagata, 2001. Impact of the Indian Ocean Dipole on the relationship between the Indian Monsoon rainfall and ENSO. Geophys. Res. Lett., BMJ Volume- 1, Issue- 1 ISSN 2519-597224
8. Australian Tropical Cyclones. International Journal of Environmental Science and Development, Vol. 4, No. 6.
9. Awaleh MO, Hoch FB, Okieh BH, Ahmed SI, SoubanehYD,et al. (2015) Impact of Human Activity on Marine and Coastal Environment in the Gulf of Tadjourah. J Marine Sci Res Dev 5: 2-11.
10. Baars MA, Schalk PH, Veldhuis MJW (1998) In: Sherman K, Okemwa EN, Ntiba MJ (eds.) Seasonal fluctuations in plankton biomass and productivity in the ecosystems of the Somali Current. Gulf of Aden and Southern Red Sea. Large Marine Ecosystems of the Indian Ocean – Assessment, Sustainability and Management. Blackwell Science, Cambridge, U.S. 143-174.
11. Bauer S, Hitchcock GL, Olson DB (1991) Influence of monsoonally-forced Ekman dynamics upon surface layer depth and plankton biomass distribution in the Arabian Sea. Deep-Sea Research 38: 531-553.

12. Bentamy A, Grodsky SA, Katsaros K, Mestas-NunezAM(2013) Improvement in air-sea flux estimates derived from satellite observations. International Journal of Remote Sensing 34: 5243-5261.
13. Bonatti E, Cipriani A, Lupi L (2015) The Red Sea: birth of ocean. In The Red Sea: The Formation, Morphology, Oceanography and Environment of a young ocean basin.
14. Bosworth W, Huchon P, McClay K (2005) The Red Sea and Gulf of Aden basins. Journal of African Earth Sciences 43: 334-378.
15. Bouhlel M (1988) Poissons de Djibouti. RDA International, Inc. Placerville, CA 95667, Etats-Unis.416 pages.
16. Broomhead DS, King GP (1986b) "On the qualitative analysis of experimentaldynamical systems". Nonlinear Phenomena and Chaos, Sarkar S (Ed.), Adam Hilger, Bristol pp: 113-144.
17. BroomheadDS, King GP (1986a) "Extracting qualitative dynamics fromexperimental data", Physica D,20: 217-236.
18. Campbell J (1995) The lognormal distribution as a model for bio-optical variability in the sea. J Geophys Res 100: 13237-13254.
19. Carter, R. W. G. and Woodroffe, C., 1994: Coastal Evolution, Pub!. Cambridge University Press, 39.
20. Cattell RB (1966) The screen test for the number of factors. Multivariate Behavioral Research 1: 245-276.
21. Charney J.G, Shukla J. 1981. Predictability of monsoons. In Monsoon Dynamics, Lighthill J, Pearce RP (eds). Cambridge University Press: London; .
22. Chowdhury A. M. 1994. Bangladesh floods, cyclones and ENSO. Paper presented at the International Conference on Monsoon Variability and Prediction. International Centre for Theoretical Physics (ICTP), Italy.
23. Doney SC, Ruckelshaus M, Duffy JE, Barry JP, Chan F, et al. (2012) Climate Change Impacts on Marine Ecosystems. Annual Review of MarineScience4: 11-37.
24. Donguy JR (1970) Surface observations along the shipping lines in the partWestIndianOcean. CahOckznogr22 : 353-366.
25. Donguy JR (1972) Surface data comparisonwiththose of artificial satellites in the western part of the IndianOcean. Cah O.R.S.T.O.M., sér.Océunogr X: 99-104.
26. Donguy JR (1974) A year of surface observations in the monsoon zone ofwestern part of the IndianOcean. Cah. O.R.S.T.O.M., sér. Océanogr. XII: 117-128.
27. Eastwood S, Andersen S (2007) Masking of Sea Ice for METOP SST retrieval. OSI.

28. Emanuel, K.A., 1987: The dependence of hurricane intensity. Nature, 326 (6112),483 - 485.
29. Evan, A.T. and Camargo, S.T., 2011: A climatology of Arabian Sea cyclonic storms. J. Clim. 24 (1),140- 158.
30. Ferranti, L., J. M. Slingo, et al. 1997. Relations between interannual and intraseasonal monsoon variability as diagnosed from AMIP integrations. Quarterly Journal of the Royal Meteorological Society, Berkshire, England.
31. Fraedrich K (1986) Estimating dimensions of weather and climate attractors. J AtmosSci43: 419-432.
32. Frankignoul C, Czaja A, L Heveder B (1998) Air-sea feedback in the North Atlantic and surface boundary conditions for ocean models. J Clim 11: 2310-2324.
33. Gadgil, S. and Gadgil, S., 2006: The Indian Monsoon, GDP and agriculture. Econom. Pol. Weekly 41(47),4887 - 4895.
34. Gadgil, S. and Kumar, K.R., 2006: The Asian monsoon - agriculture and economy in The Asian Monsoon. Bin Wang (ed.) Springer: Berlin, p. 651 - 683.
35. Gentemann, C. L., F. J. Wentz, C. A. Mears, and D. K. Smith. 2004. In situ validation of Tropical Rainfall Measuring Mission microwave sea surface temperatures. J. Geophys.
36. Golyandina N, Nekrutkin V, and Zhigljavsky A (2001) Analysis of Time Series Structure: SSA and related techniques.
37. Golyandina N, Osipov E (2007) "The 'Caterpillar'-SSA method for analysis of time series with missing values".J Stat Plan Inference 137: 2642-2653.
38. Golyandina N, Zhigljavsky A (2013) Singular Spectrum Analysis for time series. Springer Briefs in Statistics, Springer.
39. Goswami, B. N. and R. Mohan . 2001. Intraseasonal oscillations and interannual variability of the Indian summer monsoon. Journal of Climate, Boston, MA Kamal Kumar Saha and Saleh A. 2013. Wasimi, Interrelationship between Indian Ocean Dipole (IOD) and
40. Hassani H (2007) Singular Spectrum Analysis: Methodology and Comparison. Journal of Data Science. 5: 239-257.
41. Hassani H, Mahmoudvand R (2013) Multivariate Singular Spectrum Analysis: A General View and New Vector Forecasting Approach. Int J Energy Stat 1: 55-83.
42. Khan, T.M.A., Quadir, D.A., Murty, T. and Sarker, M.A., 2004: Seasonal and inter-annual sea surface temperature variability in the coastal cities of Arabian Sea and Bay of Benga!. Nat. Hazards, 31 (2),549- 560.

43. Kripalani R. H., Inamdar S. and Sontakke N. A. 1996. Rainfall Variability over Bangladesh and Nepal: Comparison and corrections with features over India. Int. J. Climatol., vol. 16: 689-703.
44. Krishnamurthy V., Kirtman B.P. 2008. Relation between Indian monsoon variability and SST. Technical Report No.261, Centre for Ocean-Land-Atmopshere Studies (COLA).
45. Krishnamurthy V., Shukla J. 2000. Intraseasonal and interannual variability of rainfall over India. J Clim.
46. Kummerow, C., W. Barnes, T. Kozu, J. Shiue, and J. Simpson. 1998. The Tropical Rainfall Measuring Mission (TRMM) sensor package. J. Atmos. Oceanic Technol., 15: 809–817.
47. Künzel T, Darar A, Vakily JM (1996) Composition, Biomasses et Possibilitésd'Exploitation des RessourcesHalieutiquesDjiboutiennes. Tome 2 Données. Ministèredel'Agriculture et de l'Hydraulique, Djibouti / GTZ, Allemagne. 114.
48. Le Borgne P, Legendre G, Marsouin A, Péré S (2008) Operational SST retrieval from METOP/AVHRR, Validation Report.
49. Levitus S, Antonov JI, Boyer TP, Baranova OK, Garcia HE, et al. (2012) World Ocean heat content and thermosteric sea level change (0-2000 m) 1955-2010. GeophysRes Lett 39: L10603.
50. Li T., Zhang Y., Chang C-P., Wang B. 2001. On the relationship between Indian Ocean sea surface temperature and Asian Summer Monsoon. Geophys Res Lett. Md. Mizanur Rahman, M. Rafiuddin and Md. Mahbub Alam. 2013. Teleconnections between Bangladesh Summer Monsoon Rainfall and Sea Surface Temperature in the Indian Ocean, International Journal of Ocean and Climate Systems, Volume 4(4).
51. Marsouin A, Le Borgne P, Legendre G,Péré S (2010) Homogeneous validation scheme of the OSI SAF Sea surface temperature products, proceedings of the 2010 EUMETSAT conference, Cordoba, Spain, September 2010.
52. McClanahan, T. R., Ateweberhan, M. C., Muhando, A., Maina, J.and Mohammed, M. S., 2007.Effects of climate and seawater temperature variation on coral bleaching and mortality. Ecological Monographs, 77, 503-525.
53. Merchant CJ, Le Borgne P, Roquet H, Marsouin A (2009B) Sea surface temperature from a geostationary satellite by optimal estimation. Remote Sensing of Environment 113: 445-457.
54. Mitchell, J. and Manabe, S., 1990.Equilibrium Climate Change and its Implications for the Future.

55. Namias J., Canyan D.R. 1981. Large air–sea interaction and short period climatic fluctuations. Science.
56. Nandkeolyar (2013) Comparative Analysis of Sea Surface Temperature Pattern in the Eastern and Western Gulfs of Arabian Sea and the Red Sea in Recent Past Using Satellite Data.
57. North GR, Bell TL, Cahalan RF, Moeng FJ (1982) Sampling error in the estimation of empirical orthogonal functions. MonWea Rev 110:699-706.
58. Perez R, et J-PBraud (1978) Possibility of a culture of the industrialsearch rouge EucheumaSpinusum in the Gulf of Tadjourah. Science et Pêche Bull Inst Pêchesmarit 285.
59. References

    Rahman, M.M., Ferdousi, N., Abdullah, A.M., Yasuo, S., Kusunoki, S. and Akio, k., 2011. Inter - annual and Decadal Variability of Sea Surface Temperature over Bay of Bengal. Nepal Journal of Science and Technology, 12,296-303.
60. Reynolds RW, Rayner A, Smith TM, Stokes DC, Wang W. 2002. An improved in situ and satellite SST analysis for climate. Journal of Climate 15: 1609-1625.